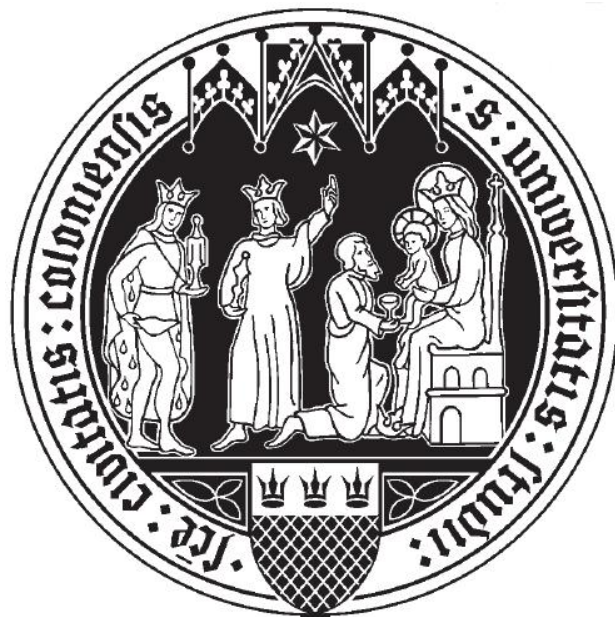


**The effect of Dietary Restriction on the
Microbiome and the Adaptive Immune System in
Mouse Ageing**

Inaugural-Dissertation
zur
Erlangung des Doktorgrades
der Mathematisch-Naturwissenschaftlichen Fakultät
der Universität zu Köln



vorgelegt von
Carolina Monzó Cataluña
aus Valencia, Spanien

Köln, 2022

Gutachter: Prof. Dr. Linda Partridge

Prof. Dr. Filipe Cabreiro

Tag der mündlichen Prüfung: 17th of October 2022

Per a Pepe Abuelo, Salva i el Abuelo Arturo

I. Table of contents

<i>I. Table of contents</i>	5
<i>II. Acknowledgements</i>	7
<i>III. Abbreviations</i>	9
<i>IV. Aim of the thesis</i>	11
IV.I Summary	11
IV.II Zusammenfassung	13
<i>1. Methods</i>	15
1.1 Mice	15
1.1.1 Mouse husbandry and DR treatment	15
1.1.2 <i>Irs1</i> ^{-/-} and Rapamycin-treated mice	15
1.2 Biochemistry and molecular-biology methods	17
1.2.1 Microbiome metabolomics and sequencing	17
1.2.2 B-cell receptor repertoire sequencing	21
1.3 Computational and biostatistical methods	24
1.3.1 Morbidity Index	24
1.3.2 Microbiome 16S rRNA-Sequencing	24
1.3.3 Whole microbiome shotgun metagenomic sequencing	31
1.3.4 Faecal metabolomics	32
1.3.5 BCR-Sequencing	33
<i>2. The effect of dietary restriction on the microbiome in mice</i>	41
2.1 Introduction	43
2.2 Results	46
2.2.1 A longitudinal high-resolution analysis of the ageing murine microbiome	46
2.2.2 DR age-related changes in the faecal microbiome	48
2.2.3 DR specific changes of the faecal microbiome	49
2.2.4 The ability of the microbiome to adapt to DR is high but declines with age	52
2.2.5 DR switch-resistant ASVs - Candidates for a microbiome memory of AL feeding	55
2.2.6 Identification of bacteria associated with DR-mediated longevity	56
2.2.7 Identification of bacteria species associated with a microbiome memory of AL feeding or DR-mediated longevity	57
2.2.8 A longitudinal high-resolution analysis of the ageing murine faecal metabolome	59
2.2.9 The ability of the faecal metabolome to diverge from AL is high but decreases with older age of DR onset	62
2.2.10 DR switch-resistant faecal metabolites - Candidates for a metabolomic memory of AL feeding	64
2.2.11 Shared microbiome changes upon DR and reduced IIS and TOR signalling	66
2.3 Discussion	70
2.4 Supplementary figures	77

3. <i>The effect of dietary restriction on the B-cell receptor repertoire in mice</i>	81
3.1 Introduction	83
3.2 Results	86
3.2.1 DR slows the age-associated decline of BCR repertoire diversity in the spleen	87
3.2.2 DR attenuates clonal expansions with age in the spleen	90
3.2.3 DR maintains the somatic hypermutation rate and CDR3 length distribution at old age in the spleen	92
3.2.4 Midlife onset of DR has more positive effects on the BCR repertoire of the spleen than late-life onset DR	93
3.2.5 Effects of DR and ageing on the intestinal BCR repertoire	95
3.2.6 Late-onset DR has no effect on the intestinal BCR repertoire	99
3.2.7 The ageing microbiome responds to late-onset DR	100
3.2.8 DR-related BCR metrics are associated with healthier phenotypes	101
3.3 Discussion	104
3.4 Supplementary figures	109
4. <i>Appendix: Primers and oligonucleotides</i>	117
5. <i>List of figures</i>	119
6. <i>Bibliography</i>	121

II. Acknowledgements

First, my sincere thanks to Prof. Dame Linda Partridge who welcomed me into her lab and has always trusted and encouraged me to do my best work. I am very thankful for her patience, support and input on these projects. I also want to express my gratitude to Prof. Andreas Beyer, who put his ideas, invaluable expertise and resources at my disposal. My thanks also go to Prof. Dario Valenzano, who was an excellent collaborator with incessant scientific curiosity. I want to especially thank my brilliant supervisor Dr. Sebastian Grönke, who shared with me the enthusiasm and passion about these projects, and with whom I had tireless scientific discussions about experimental designs and biological interpretation. None of the work in this thesis would have been possible without their guidance and supervision. I am very thankful for the freedom and confidence they gave me to pursue my interests, both in biological and bioinformatic topics, and for their support in seeing these projects through.

The biggest thank you to my dearest twin Lisonia Gkioni for being my lab-partner since day one; she not only performed many of the lab experiments in this thesis, but also put her giant heart and brain into these projects; none of them would have been possible without her. And to Nathalie Jauré, the more reasonable and wiser other half of my bioinformatic brain, for always seeing problems with another perspective, giving ideas that improved the projects and helping me out of the analysis holes I dug myself into. Their scientific brilliance and commitment have been a true inspiration; we keep pushing! Together with our wonderful friend Mehdi, who is the coolest person ever and was always a great source of fun and life teachings, they became my home away from home and many of my favourite parts of this thesis would not have been possible without them. They are outstandingly wonderful people, and I am forever thankful for their great friendship and incredible support during these years. You made me feel special!

Furthermore, I am sincerely grateful to all my fellow PhD Students: Maarouf from whom I learned so much about science and life, Sophie and Bruna with whom I had great fun and played amazing games, Larissa and Mara who always listened to my ramblings, Dennis and Jonathan with whom I shared many of the experiences of being a bioinfo in a wet lab, (DJ) Helena and Pingze with whom I shared great laughs, and Annika and Sina. They have all directly or indirectly contributed to this thesis. But most importantly, they are an inspiring group of excellent scientists, always supportive, happy to discuss ideas, and ready to have great social fun. Lots of thanks to our wonderful Postdocs Dr. Javier Morón, Dr. Luke Tain and Dr. Jitin Bali for always sharing their wisdom and experience; and to the many masters students from the LP and JD labs who brought lots of joy and made us feel proud. As well as Christine

Lesch, Daniela Morick, Oliver Hendrich, all technicians, and other past and present members of the Partridge Department for their help, support, enthusiasm, and for making the group such a pleasant and friendly place in which to work.

In addition, I would like to thank a number of other scholars who have also made a strong positive impact in this thesis, and my scientific work. Thanks to Dr. Joris Deelen, for his continuous invaluable feedback and advice that helped shape the projects into this final work, and for supporting me in my quest to teach and supervise. To Dr. Lisa Drews for providing tissues and performing the original experiment from which I based my thesis on. To Jenny Fröhlich, Ramona Hoppe, Ola Placzek and Jens Seidel for working with me on generating the data for this thesis and sharing their ideas and passion for science. To Carolina Leote for her advice on machine learning algorithms. And to Azahara Fuentes and Alicia Serrano from INCLIVA, for infecting me with their love for B cell receptors and sharing with me their knowledge, friendship and passion for science over the years.

Moreover, I would like to thank Patrick and Frederik from the Metabolomics facility, Xinpeng from Proteomics, and Jorge from Bioinformatics, as well as all caretakers from the Mouse House at the MPI for Biology of Ageing, for supporting my experiments and analysis.

Thank you as well to the many scientists I have worked with previously to coming to the MPI: my mentor Dr. Paco García and the Systems Genomics group at the Príncipe Felipe Research Centre; Prof. Vicente Arnau at the University of Valencia; and Dr. Javier Chaves' incredible Unit of Genomics and Genetic Diagnosis at INCLIVA, with special mention to Victoria Adam, Dr. Pilar Rentero, Dr. Kike Seda and Dr. Tani Blesa, my mentors on all things sequencing. All of them have taught me valuable lessons that have made me grow as a scientist and person.

My love and thanks to Dr. Álvaro, Cristina, Marta (x2), my dearest Montonet friends, my Cataluña, Monzó, García and Torres families, and many other people who I have unaccountably failed to mention. Thank you for always welcoming me with open arms, for your love, friendship and encouragement throughout this lengthy process. I am the luckiest girl for having all of you in my life! A heartfelt thank you to Cristina Ros, my first friend in my first internship at IATA-CSIC, thank you for believing in me even before I believed in myself. And to Rocío Penas, thank you for holding me together and helping me through the final stretch.

Finally, my deepest and sincerest thanks to my family. Mamá, Papá, Alba, I can't express how grateful I am to be your favourite middle child, for all of the adventures we have had together, for having you as the spectacular role models that you are, and for your endless love and support. Gràcies per tot, vos vuic en locura.

III. Abbreviations

α -diversity	Intra-individual variability (Richness, Shannon, Simpson etc.)
AIRR	Adaptive Immune Receptor Repertoire
AL	<i>Ad libitum</i>
AL_DR16M	Midlife onset DR at 16 months of age
AL_DR20M	Late-life onset DR at 20 months of age
AMP	Antimicrobial peptides
ANOSIM	Analysis of similarities
ASV	Amplicon Sequence Variant
AUC	Area under the curve
β -diversity	Inter-individual variability (RDI, UniFrac, Bray Curtis etc.)
BCR	B-Cell Receptor
DR	Dietary restriction
GLME	Generalised linear mixed effects models
HPC	High Performance Computing
HSC	Haematopoietic stem cells
<i>Igh</i>	Immunoglobulin Heavy Chain Complex
<i>IghC</i>	Immunoglobulin heavy chain constant domain
<i>IghD</i>	Immunoglobulin heavy chain diversity domain
<i>IghJ</i>	Immunoglobulin heavy chain joining domain
<i>IghV</i>	Immunoglobulin heavy chain variable domain
IMGT	International immunogenetics information
P20	Frequency of 20 most present BCR clones
PCA	Principal Component Analysis
PcOA	Principal Coordinates Analysis
PRC	Principal response curve
R1	Forward reads
R2	Reverse reads
RDA	Redundancy analysis
RDI	Repertoire Dissimilarity Index
SCFA	Short-chain fatty acids
SHM	Somatic Hypermutation
SLURM	Simple Linux Utility for Resource Management
UMI	Unique Molecular Identifier
WAT	White adipose tissue

IV. Aim of the thesis

IV.I Summary

The human body is densely populated by microbes, and the interplay between microbiome and host physiology is important for health. During ageing, the composition of the microbiome changes and recent research in killifish and mice suggests that the intestinal microbiome might play a causal role in the determination of organismal lifespan. Dietary restriction (DR) and reduced activity of the insulin/IGF1 (IIS) and mTOR network increase lifespan and improve health in mice. However, whether changes in the microbiome induced by these longevity interventions contribute to the positive effects on survival is currently unknown. Ageing also negatively affects the adaptive immune system, but how longevity interventions affect the ageing adaptive immune system and whether amelioration of immune function contributes to the improved health of these animals is still not well understood. In my PhD thesis, I used a systems biology approach to address: (I) How does the intestinal microbiome and metabolome change in response to longevity interventions in mice. (II) Does DR affect the adaptive immune system during ageing in mice and is this associated with the increase in longevity upon DR.

(I) In the first study, I performed a systematic longitudinal analysis of age-related changes in the faecal microbiome and metabolome of mice under DR. Furthermore, in order to identify changes in the microbiome that are common between longevity interventions, I analysed the microbiome of mice with reduced IIS and mTOR signalling. I show that DR mitigates age-related changes in microbiome community structure, including the decline in alpha diversity, increase in beta diversity, and loss of equilibrium between *Firmicutes* and *Bacteroidetes* phyla. Furthermore, by studying the faecal microbiome and metabolome of late-life DR switches that either increase or not increase lifespan, I identified an age-dependent memory of AL feeding in the microbiome associated with lifespan. Finally, I identified bacteria that were shared between DR, reduced mTOR and IIS signalling, suggesting that these bacteria may contribute to the health benefits observed in these long-lived mouse models.

(II) In the second study, I analysed how DR affects the adaptive immune system during ageing. Therefore, I performed B cell receptor sequencing on spleen and intestine of mice during ageing and in response to DR to assess changes in the systemic and intestine-specific immune repertoire, respectively. Furthermore, as mice lose their responsiveness in lifespan to DR between 16 and 20 months of age, we also measured changes in the B cell repertoire in response to both diet switches, to identify changes in the B cell receptor repertoire that correlate with the longevity response. Interestingly, neither diet nor age had a strong influence

on the B cell receptor repertoire of the intestine. In contrast, in the spleen, DR delayed the age-associated decline of within-individual spleen repertoire diversity and the increase in clonal expansions. Thus, DR-mediated longevity is characterised by the preservation of a more diverse spleen repertoire, which is less prone to clonal expansions. Importantly, I show that reduced within-individual diversity and increased clonal expansions are associated with increased pathology in these mice, suggesting that changes in B cell repertoire dynamics contribute to the health benefits of chronic DR treatment. This is further supported by the finding that mice that started DR at 16 months have spleen repertoire diversity and clonal expansion rates indistinguishable from chronic DR mice, whereas the switch to DR at 20 months was associated with milder effects, suggesting that the responsiveness of the adaptive immune system declines in mice between 16 and 20 months of age, which might contribute to the loss in lifespan extension of the late-life DR switch.

IV.II Zusammenfassung

Der menschliche Körper ist dicht mit Mikroorganismen besiedelt. Das Zusammenspiel von Mikrobiom und Wirtsphysiologie ist wichtig für die Gesundheit. Während des Alterns verändert sich die Zusammensetzung des Mikrobioms. Aktuelle Forschungen an Kili-Fischen und Mäusen deuten darauf hin, dass das Darmmikrobiom eine kausale Rolle bei der Bestimmung der Lebensspanne spielt. "Dietary Restriction" (DR) und eine verringerte Aktivität des Insulin/IGF1- (IIS) und mTOR-Netzwerks verlängern die Lebenszeit und verbessern die Gesundheit von Mäusen. Ob Veränderungen im Mikrobiom hierbei eine kausale Rolle spielen ist derzeit jedoch unbekannt. Der Alterungsprozess wirkt sich auch negativ auf das adaptive Immunsystem aus. Wie lebenszeitverlängernde Eingriffe das Immunsystem beeinflussen und ob die Verbesserung der Immunfunktion zur verbesserten Gesundheit dieser Tiere beiträgt, ist noch nicht gut verstanden. In meiner Dissertation habe ich einen systembiologischen Ansatz verwendet, um folgende Fragen zu klären: (I) Wie verändern sich das Darmmikrobiom und das Metabolom von langlebigen Mäusen mit dem Alter? (II) Beeinflusst DR das adaptive Immunsystem von Mäusen während des Alterns? Gibt es einen Zusammenhang zwischen den Veränderungen im Immunsystem und der Langlebigkeit der DR Tiere?

(I) In der ersten Studie habe ich systematisch die altersbedingten Veränderungen im fäkalen Mikrobiom und Metabolom von langlebigen DR Mäusen gemessen. Meine Ergebnisse zeigen, dass die DR Behandlung einen großen Einfluss auf die Zusammensetzung des Mikrobioms hat und altersbedingte Veränderungen in der Zusammensetzung des Mikrobioms positiv beeinflusst inklusive der Abnahme von Alpha-Diversität, Zunahme von Beta-Diversität und dem Gleichgewicht zwischen Firmicuten und Bacteroidetes. Durch die Untersuchung des fäkalen Mikrobioms nach Diätwechselln spät im Leben, die entweder das Leben der Tiere verlängern oder nicht, konnte ich Bakterien identifizieren deren Häufigkeit im Mikrobiom mit Langlebigkeit korreliert. Um dies weiter zu untersuchen, habe ich das Darmmikrobiom von Mäusen mit verringerter Aktivität im IIS- und mTOR Netzwerk analysiert. Auf diese Weise habe ich Bakterien identifiziert, die zwischen den verschiedenen Eingriffen zur Lebenszeitverlängerung geteilt sind. Meine Ergebnisse deuten darauf hin, dass diese Bakterien eine wichtige Rolle in der Langlebigkeit und verbesserten Gesundheit dieser Tiere spielen.

(II) In der zweiten Studie habe ich untersucht, wie DR das adaptive Immunsystem während des Alterns beeinflusst. Dazu habe ich das B-Zell-Rezeptor Repertoire in der Milz und im Darm von DR- und Kontrollmäusen während des Alterns sequenziert, um Veränderungen im systemischen bzw. darmspezifischen Immunrepertoire zu analysieren. Mäuse verlieren zwischen dem 16. und 20. Lebensmonat die Eigenschaft positiv auf die DR Behandlung zu

reagieren. Deshalb habe ich zusätzlich die Veränderungen im B-Zell-Repertoire nach Diätwechseln im Alter von 16 bzw. 20 Monaten gemessen, um Veränderungen im B-Zell-Rezeptor-Repertoire zu ermitteln, die mit der Langlebigkeit korrelieren. Interessanterweise hatten weder die Ernährung noch das Alter einen starken Einfluss auf das B-Zell-Rezeptor-Repertoire des Darms. Im Gegensatz dazu, hatte die DR Behandlung einen stärkeren Einfluss auf das B-Zell-Rezeptor-Repertoire der Milz und verlangsamte die altersbedingte Abnahme der B-Zell Diversität und die Zunahme der klonaler Expansion einzelner B-Zellklone. Die geringere Diversität innerhalb eines Individuums und eine verstärkte klonale Expansion der B-Zell-Rezeptoren war mit einem erhöhten Pathologiebefund in diesen Mäusen korreliert. Dies deutet darauf hin, dass Veränderungen in der Dynamik des B-Zell-Repertoires zu den positiven Effekten der DR Behandlung auf Lebenszeit und Gesundheit beitragen. Dies wird auch durch die Feststellung gestützt, dass Mäuse, die mit 16 Monaten auf DR umgestellt wurden, eine Diversität des Milzrepertoires und klonale Expansionsraten aufweisen, die sich nicht von denen chronischer DR-Mäuse unterscheiden, während die Umstellung auf DR mit 20 Monaten mit mildereren Auswirkungen verbunden war.

1. Methods

1.1 Mice

Mice were kept in the Comparative Biology facility (Mouse House) at the Max Planck Institute for Biology of Ageing. Animals were housed in groups of 5 females in individually ventilated cages (GM500 Mouse IVC Green Line, Tecniplast) under specific- pathogen-free conditions with constant temperature (21°C), 50–60% humidity and a 12-hour light–dark cycle. For environmental enrichment, mice had constant access to nesting material and chew sticks. All protocols involving animals were carried out in accordance with the recommendations and guidelines of the Federation of the European Laboratory Animal Science Association, with all protocols approved by the Landesamt für Natur, Umwelt und Verbraucherschutz, Nordrhein-Westfalen, Germany (reference no. AZ: 84-02.04.2015.A437).

1.1.1 Mouse husbandry and DR treatment

The effect of DR on the mice and their microbiome, was studied on female F1 hybrid wild type mice (C3B6F1). Four treatment groups, including AL, DR and mice switched from AL to DR at 16 (AL_DR16M) and 20 months (AL_DR20M) of age, respectively, were used for lifespan analysis and longitudinal faecal collection (n = 220 mice), and tissue collection (n = 220 mice) (Drews et al. 2021). The DR treatment was started at 3 months of age to avoid developmental effects. Food consumption of the AL group was measured weekly, and DR animals received 60% of the food amount consumed by AL-fed animals, i.e. food intake was reduced by 40%. While AL animals had constant access to food, DR animals were fed once per day in the morning. All animals were checked daily for their well-being and any deaths. Animals were fed a commercially available rodent chow (ssniff R/M-H autoclavable, ssniff, Spezialdiäten, Germany) and were provided with sterile-filtered water *ad libitum*. Chow was enriched with essential vitamins and minerals, ensuring that DR animals were adequately supplied with all required nutrients, despite their lower food intake.

Tissues were collected and snap-frozen using liquid nitrogen at 5, 16, 20, 24 and 28 months of age. Faecal samples were collected from 12 months onwards, every 2-3 months until death. Tissues and faecal samples were provided by Dr Sebastian Grönke and Dr Lisa Drews.

1.1.2 *Irs1*^{-/-} and Rapamycin-treated mice

To study the effect of reduced insulin/IGF-1 signalling and reduced TOR signalling on the microbiome, faecal samples were collected from long-lived *Irs1*^{-/-} mutant mice (Selman et al.

2008) and wild-type mice treated with Rapamycin (Juricic et al. 2022). Faecal samples were provided by Dr Maarouf Baghdadi and Dr Sebastian Grönke, respectively.

Homozygous *Irs1*^{-/-} mutant mice were generated in the C3B6F1 background. Female *Irs1*^{-/-} and wild type control mice were fed standard chow *ad libitum*. Faecal samples were collected at 6, 20 and 28 months of age.

Female wild-type C3B6F1 mice were fed Rapamycin food (14 mg of drug per kg of food encapsulated in Eudragit S100, Evonik) from 3 months of age onwards. Control animals received food with Eudragit S100 only. Rapamycin treatment was administered continuously (Rapamycin-continuous) until the age of 12 months. In addition, mice were fed from 3-6 months of age with rapamycin and were then switched back to control food (Rapamycin-memory). Faecal samples were collected at 6 and 12 months of age.

1.2 Biochemistry and molecular-biology methods

1.2.1 Microbiome metabolomics and sequencing

1.2.1.1 Metabolites extraction and DNA pellet separation

A pilot study performed by Jens Seidel tested metabolites extracted from a range of faecal weights (3 to 70 mg) on the mass spectrometer. The study identified 40 mg as the maximum weight of faecal pellets for extraction to avoid metabolite saturation, and established the protocol. Faecal samples were weighed and adjusted to a weight between 5 to 40 mg. For pellet homogenization, two 7 mm diameter stainless steel beads were added to the sample in 2 ml tubes. Samples were homogenised by bead beating in a Tissue Lyzer (Qiagen) for 30 seconds at a frequency of 25 Herz/s.

Per batch, 24 samples were processed in parallel. Metabolite extraction buffer was prepared fresh for each batch including 31.25 ml of methanol (VWR Chemicals), 12.5 ml of chloroform (VWR Chemicals), 6.25 ml of water (VWR Chemicals), 1.5 µl of each internal standard lipid (Lyso PC-C₂₆H₅₂NO₇P, PC-C₄₁H₇₃D₇NO₈P, TG-C₅₁H₈₉D₇O₆) (Sigma-Aldrich) and 12.5 µl of the mix of internal standards amino acids (13C15N Leu, 13C15N Iso, 13C15N Phe) (Cambridge Isotope Laboratories). 800 µl of metabolite extraction buffer was added per faecal sample, and mixed by vortexing. Metal beads were removed using magnetic sticks. Another 800 µl of metabolite extraction buffer was added to samples with a weight between 20 and 40 mg. Samples were incubated for 45 min shaking at 1400 rpm at 4 °C. Samples were briefly vortexed and a volume corresponding to 5 mg of sample was transferred to a new 2 ml tube as backup. Samples were centrifuged at 4 °C for 15 min at 20.000 g. 600 µl of supernatant were transferred into a new 2 ml tube, and 300 µl of chloroform (VWR Chemicals) and 300 µl of mass-spec grade water (VWR Chemicals) were added. Samples were briefly vorted and subsequently incubated at 4 °C for 15 min shaking at 1400 rpm. Samples were then centrifuged at 4 °C for 15 minutes at 10.000 g. 500 µl of the upper phase, corresponding to polar metabolites, and 250 µl of the lower phase, corresponding to non-polar metabolites, respectively, were collected. Non-polar metabolites were stored at -20 °C, and polar metabolites were dried in the speed vac for 5 h. Finally, the dried polar metabolites were also stored at -20 °C.

1.2.1.2 Metabolomics

Metabolomics measurements were done by the mass-spectrometry facility of the Max Planck Institute for Biology of Ageing (Cologne, Germany). Per treatment group, faecal samples of 10 female mice were used. Based on their survival time, the 5 longest lived animals, and the 5

animals with a lifespan closest to the median lifespan were chosen for the analysis, to test whether the faecal metabolome of long-lived animals differed from that of normal lived animals within the treatment groups. In total 438 samples were measured.

To create a reference standard, metabolites extracted from 5 AL, 5 DR, 5 AL_DR16M and 5 AL_DR20M 26-month-old mice were pooled. Non-polar metabolites were pooled, mixed and split again in 20 tubes. Polar metabolites were resuspended in 500 µl of mass-spec grade water, pooled, mixed, split in 20 tubes and dried in the speed vac for 5 h. In addition, negative controls consisting of metabolite extraction buffer, and reference food metabolites extracted from rodent chow (ssniff R/M-H autoclavable, ssniff, Spezialdiäten, Germany) were also measured.

Finally, polar and non-polar metabolites from all time points of 10 mice from AL, chronic and midlife/late-onset DR groups (5 longest lived and 5 centred at the age-of-death distribution; total of 438 samples), as well as 38 pooled reference standards, 23 blanks and 4 food pellets were run on the mass spectrometer by the Metabolomics facility at the MPI-AGE. Untargeted metabolomics assays were performed in order to obtain polar neutral (BZ-polar, amino acids), and non-polar (lipids) metabolites.

1.2.1.3 DNA extraction

DNA extractions were performed in batches of randomly assigned 81 samples. 2 spoonfuls (43 mm) of Zirconium beads (Carl Roth) were added per dried faecal pellet. DNA extraction buffer was prepared by mixing 27 ml of 20% SDS and 540 mg of lysozyme (Sigma-Aldrich). Subsequently, the buffer was incubated at 38 °C for 20 minutes and shaking at 100 rpm in order to correctly dissolve the lysozyme. 300 µl of DNA extraction buffer was added to each sample. Samples were homogenised by bead-beating twice for 3 minutes at 30 Hz using a Tissue Lyzer (Qiagen). Afterwards, samples were centrifuged at 15 °C for 6 min at 4.000 g. 80 µl of supernatant was then transferred to a 96 well plate (Biozym). Another 80 µl of supernatant was transferred to a backup plate. Plates were stored at -20 °C.

To extract DNA, 2 µl RNase A solution (Qiagen) was added to each sample and plates were incubated at 37 °C for 30 minutes. 10 µl of Proteinase K (ThermoFisher Scientific) and 10 µl 20% SDS were added. After mixing, plates were incubated at 56 °C for 1 h. 40 µl IRS solution (Qiagen) was added and plates were mixed and incubated at 4 °C for 5 min. Plates were centrifuged for 5 min at 2000 g. 100 µl of the supernatant was transferred into a new 96 well plate. DNA was purified using CleanNGS beads (CleanNA) at 1x concentration. 100 µl beads were added to the sample and were thoroughly mixed. Samples were incubated at RT for 5 min to allow binding of DNA to the beads. Plates were then put on a magnetic rack

(ThermoFisher Scientific) and incubated for 5 min to bind the beads to the magnet. Supernatant was removed and samples were washed twice with 200 µl of freshly prepared 80% ethanol. After the last wash, additional ethanol was removed by pipetting using a P10 pipette. Samples were dried for 5 min at RT. DNA was eluted in 20 µl nuclease-free water for 5 min at RT. DNA was stored at -20 °C until library preparation.

1.2.1.4 16S rRNA library preparation

Purified DNA was diluted in water to 5 ng/µl. The genomic region of the 16S rRNA was amplified in two successive rounds of PCR. In the first PCR round the V4 region of the 16S gene was amplified using 515F-806R V4 primers (Appendix 4.1). The PCR reaction mix contained 10 µl of DNA, 12 µl of 2x Kapa Hifi HotStart polymerase (Roche) and 3 µl 10 µM primer mix of 515F-806R V4 primers (Appendix 4.1). PCR reaction conditions were: 98 °C for 3 min, followed by 21 cycles of: 98 °C for 30 s, 61 °C for 30 s and 72 °C for 30 s. A final extension at 72 °C for 5 min was added. Also, several controls were included to control for: DNA extraction buffer, food microbiome DNA, and PCR reactions. To generate them, libraries were prepared from the controls from previous steps of the DNA extraction protocol, and also from the PCR reaction mixes.

PCR products were purified using 1x CleanPCR beads and 80% ethanol in order to remove contaminants including remaining primers, salts and dNTPs. PCR products were eluted in 30 µl nuclease-free water. To add sample barcodes, a second PCR was performed. Therefore, 5 µl of purified PCR products were mixed with 2.5 µl of i5-i7 Illumina barcodes and 12.5 µl of 2x Kapa Hifi HotStart Polymerase. The reaction volume was brought to a total of 25 µl using nuclease-free water, and the resulting mix was incubated at: 98 °C for 3 min, followed by 7 cycles of: 98 °C for 30 s, 61 °C for 30 s and 72 °C for 30 s, finishing with a last extension at 72 °C for 5 min. PCR-2 products were then purified using 1x CleanPCR beads in order to remove contaminants, and eluted in 30 µl with water. Total DNA concentration of each sample was quantified using PicoGreen assay (ThermoFisher Scientific) and adjusted to 1 ng/µl by adding water. Size distribution of DNA fragments was measured on a random subset of samples from each plate on a TapeStation 4200 (Agilent, D1000 tape) including all negative controls. 2 µl from each library were pooled, re-purified using 0.8x CleanPCR beads to remove smaller unspecific amplifications.

Finally, faecal V4-16S rRNA libraries consisting of: longitudinal faecal collections of 220 mice from AL, chronic and DR switch groups (total of 2118 samples); 50 cross-sectional-diet cecal collections (5 biological replicates per condition: 5 months AL and DR; 16 months AL; 20 months AL, DR and AL_DR16M; and 24 months AL, DR, AL_DR16M and AL_DR20M); 60

cross-sectional *Irs1^{-/-}* mice (10 biological replicates of wild type and *Irs1^{-/-}* at 6, 20 and 28 months); and 50 cross-sectional Rapa mice (10 biological replicates per condition: 6 months control and Rapamycin; and 12 months control, Rapamycin-Memory and Rapamycin-Continuous). As well as 170 blanks and 8 control food pellets, were sequenced in 3 successive runs using 250x2 paired-end sequencing on an Illumina HiSeq 2500 at Admera Health, US.

1.2.1.5 Shotgun metagenomics library preparation

Purified DNA from 24-month-old AL, DR, AL_DR16M and AL_DR20M mice (3 per diet group), was diluted in water to 8 ng/μl. Libraries were prepared following the Illumina DNA Library Prep workflow. First, a tagmentation reaction was performed on the faecal DNA. In this reaction, Illumina patented transposons fragmentate the genomic DNA into ~350 nt long fragments and add Illumina adapters to the terminals. Therefore, 30 μl of DNA was mixed with 10 μl of Bead-Linked Transposons and 10 μl of Tagmentation Buffer. After 15 min incubation at 55 °C, the tagmentation reaction was stopped by adding 10 μl of Tagment Stop Buffer and incubation on ice for 5 min. Next, the mix was kept at 37 °C for 15 min, and then placed on a magnetic stand for ~3 min. After discarding the supernatant, the adapter-tagged DNA bound to the beads was cleaned twice using Tagment Wash Buffer (Illumina).

Supernatant was removed and a PCR master-mix composed of 20 μl Enhanced PCR polymerase and 20 μl of nuclease water was added. In each individual sample, a unique combination of Nextera CD i5-i7 barcodes (10 μl total volume) was added. This resulting mix was incubated at 68 °C for 3 min and 98 °C for another 3 min to denature DNA. Subsequently, amplification was done using 5 cycles at 98 °C for 45 s, 62 °C for 30 s, and 68 °C for 2 min, followed by a last extension step at 68 °C for 1 min.

To purify the amplified products, samples were first centrifuged at 280 g for 1 min. 45 μl of the supernatant was transferred to a new plate and diluted with 40 μl nuclease-free water. 45 μl of Sample Purification Beads (Illumina) were added, and the solution was incubated at RT for 5 min. After 5 more minutes in the magnetic stand, 125 μl of the supernatant was transferred to a new plate and 15 more μl of Sample Purification Beads were added. Solutions were mixed and incubated at RT for 5 min. Two rounds of bead clean-up with 80% ethanol were performed. Ethanol was removed and beads were air-dried for 5 min. To elute the DNA library, beads were resuspended in 32 μl of Resuspension Buffer. Total concentration of each sample was quantified using Qubit and TapeStation 4200 (Agilent, D1000 tape), which also showed the distribution of DNA fragment size. 2 μl of each sample, diluted at 2 ng/μl were pooled. As negative control, an extra library preparation with no DNA was performed and sequenced.

Finally, faecal shotgun metagenomics libraries of 3 biological replicates of 24-month-old AL, DR, AL_DR16M and AL_DR20M, and negative controls, were sequenced at 250x2 paired-end sequencing on an Illumina HiSeq 2500 at Admera Health, USA.

1.2.2 B-cell receptor repertoire sequencing

1.2.2.1 RNA extraction from spleen and ileum

Spleen and ileum samples were homogenised in 1 mL TRIzol (Life Technologies) using a FastPrep-24 (MP Biomedicals) and the following programme: 6 times bead-beating at 4 m/s for 30 sec. Homogenised samples were incubated at RT for 5 min. 200 µl of chloroform (0.2 ml of chloroform per 1 ml of TRIzol) was added and mixed by vortexing. Samples were incubated at RT for 10 min and subsequently centrifuged at 4 °C and 12000 g for 15 min. The aqueous upper phase was collected and transferred to a new RNase free tube. 500 µl of isopropanol, 50 µl of 3.0 M NaOAc and 1.5 µl of glycogen (ThermoFisher Scientific) were added and tubes were shaken by hand. Samples were incubated at -80 °C for 30 to 45 min to precipitate RNA and then centrifuged at 4 °C and 12.000 g for 10 min. The RNA pellet was washed twice with 1 ml of ice-cold 70% ethanol, air-dried for 5-10 min and then resuspended in 30 µl RNase free water (ddH₂O DMPC). As negative control, an extra RNA extraction without sample RNA was performed.

1.2.2.2 DNase Treatment

To remove potential DNA contamination from the RNA sample, 3 µl of 10x TURBO DNase Buffer and 1 µl of DNase (ThermoFisher Scientific) was added to 30 µl RNA. Samples were incubated at 37 °C for 30 min. Then another 1 µl of DNase was added and samples were incubated for another 30 min. 3 µl of DNase Inactivation Buffer were added. Samples were incubated at room temperature for 5 min and were mixed occasionally. Finally, samples were centrifuged at 10000 g for 1.5 min, and the supernatant including the DNA-free RNA was transferred to a new tube.

1.2.2.3 RNA quantification with Qubit (Invitrogen) and TapeStation

To quantify RNA content, the Qubit® RNA BR Assay kit (ThermoFisher Scientific) was used. Therefore, a master mix containing 199 µl of Qubit® RNA BR buffer and 1µl of Qubit® RNA BR reagent was prepared. 199 µl of the master mix and 1 µl of RNA were added to qubit tubes. For the standard, 190 µl of master mix and 10 µl of Qubit broad range standard was added. The content of each qubit tube was quantified independently in a Qubit 4 Fluorometer (ThermoFisher Scientific).

To evaluate RNA quality, a random subset of 30 samples was run on a TapeStation 4200. Therefore, 1 μ l of RNA was mixed with 5 μ l of RNA Sample Buffer and denatured at 72 °C for 3 min. Samples were incubated on ice for 2 min and then run using a D5000 Screen Tape. All samples had a RIN value above 7 as recommended for BCR-Seq (Turchaninova et al. 2016).

1.2.2.4 Reverse transcription and template switch

Reverse transcription of RNA was performed using SMARTScribe Reverse Transcriptase (Clontech), according to Turchaninova et al. (Turchaninova et al. 2016). 600 ng of RNA were mixed with 2 μ l 10 μ M isotype-specific primer mix including: IgM, IgD, IgG, IgA and IgE (Appendix 4.2). Samples were incubated for 2 min at 70 °C to denature RNA, and 3 min at 42 °C to anneal isotype-specific primers. The mixture was then combined with 12 μ l of reverse-transcription master-mix: 4 μ l 5x First-strand buffer (Clontech) + 2 μ l 20 mM DTT + 2 μ l 10 μ M 5'-Template switch adaptor (Appendix 4.3) + 2 μ l 10 mM dNTP solution + 2 μ l 10x SMARTScribe Reverse Transcriptase (Clontech). The reaction was incubated at 42 °C for 1 h and then mixed with 1 μ l of uracil DNA glycosylase (New England Biolabs), and incubated for 40 min at 37 °C to digest the template-switch adapter. Finally, the reaction product was purified using MinElute PCR Purification columns (Qiagen) and eluted in a volume of 10 μ l.

1.2.2.5 Library preparation for BCR-Seq

To generate libraries for B cell receptor sequencing (BCR-Seq), three successive rounds of PCR were performed. To decide on the amount of cDNA input and sequencing depth per tissue, a pilot study was performed, identifying 1 μ l of Spleen or 5 μ l of Ileum cDNA, and a target of 5 million reads for Spleen and 3 million reads for Ileum, to obtain a minimum coverage of 5 reads per unique molecular identifier (UMI). In the first reaction, double stranded cDNA was made generated using the following reaction mix: 1 μ l of Spleen or 5 μ l of Ileum cDNA + 12.5 μ l of 2x Kapa HiFi HotStart polymerase (Roche) + 1 μ l 10 μ M 5'- template switch primer (Appendix 4.4) + 1 μ l 10 μ M 3'-nested immunoglobulin isotype primer mix (Appendix 4.4) + nuclease-free water to 25 μ l. The reaction was incubated at 95 °C for 1.5 min, followed by 18 cycles of 95 °C for 10 s, 60 °C for 20 s and 72 °C for 40 s, followed by a last extension at 72 °C for 4 min. PCR products were purified using 0.8x Agencourt AMPure XP beads (Beckman Coulter) and eluted with 30 μ l water. The second PCR adds internal sample barcodes and Illumina sequencing adapters, and further amplifies the library. Therefore, 1 μ l of purified PCR product was mixed with: 2 μ l 10 μ M primer mix (5' and 3' primers with sample barcodes) (Appendix 4.5), 12.5 μ l of 2x Kapa HiFi HotStart polymerase (Roche) and 9.5 μ l nuclease-free water. Reaction conditions were: 1 x 95 °C for 1 min 30 s; 13 x: 95 °C for 10 s, 60 °C for 20 s and 72 °C for 40 s, followed by a last extension at 72 °C for 4 min. PCR products were purified

using 0.8x Agencourt AMPure XP beads (Beckman Coulter) in order to remove contaminants as well as nonspecific amplifications with nucleotide length below ~400 nt. Samples were eluted in 20 µl water. Size distribution of amplified DNA fragments was measured using a TapeStation 4200 (Agilent, D1000 tape). Samples tagged with different internal barcodes were then pooled in equal concentrations in groups of 10 samples, in a total of 10 libraries. As negative control, an extra library preparation with no DNA was performed and sequenced.

Finally, spleen and ileum BCR repertoire libraries of a total of 50 mice (5 mice per biological condition: 5-month AL and DR; 16 months AL; 20 months AL, DR and ALDR16M; and 24 months AL, DR, ALDR16M and ALDR20M mice) were sent to the sequencing core facility of the Max Planck Institute for Molecular Genetics (Berlin, Germany). There, ligation of Illumina adaptors (including i5 and i7 indices), library pooling and asymmetric 400+100-nt paired-end sequencing on an Illumina NovaSeq 6000 were performed.

1.3 Computational and biostatistical methods

Data processing and analysis were performed on the MPI-AGE High Performance Computing (HPC) cluster, using the Simple Linux Utility for Resource Management (SLURM) for parallel distribution of jobs. All Python (v.3.7.3) scripts were run on a stable Conda virtual environment and R (v.4.0.2) scripts on a singularity container. Tracking of scripts and versions was implemented on git and backed up on github repositories (<https://github.com/carolinamonzo>).

1.3.1 Morbidity Index

Repository: https://github.com/carolinamonzo/CM_BCRseq

After mouse dissections, gross pathological findings were recorded. As a summary metric of the health state of the mice, a morbidity index was designed and calculated for this thesis, based on (Ikeno et al. 2009; Treuting et al. 2008; Bokov et al. 2011a). The morbidity index was based on the combination of tumour and non-tumour pathologies. For each mouse, a score of 0 to 2 was assigned to describe tumoral state: 0 indicated no tumours detected, 1 indicated only 1 organ affected by tumours, and 2 indicated 2 or more organs affected by tumours; representing metastatic cancer. Non-tumour pathologies were analysed as presence/absence (0/1) of pathologies per organ. The morbidity index was calculated as:

$$\text{Morbidity_index} = \text{neoplasia_degree} + \sum(\text{non-neoplastic_pathology}_{\text{organ}})$$

The algorithm classified the presence of a non-neoplastic pathology equally as bad as having one organ affected by tumours, while the weight of metastasis in the model was doubled. A high morbidity index indicated a high degree of sickness at death, while a lower index represented health.

1.3.2 Microbiome 16S rRNA-Sequencing

Repositories:

https://github.com/carolinamonzo/CM_16S_longitudinal

https://github.com/carolinamonzo/CM_16S_cross-sectional

https://github.com/carolinamonzo/CM_16S_IRS

https://github.com/carolinamonzo/CM_16S_Rapa

1.3.2.1 Microbiome 16S rRNA-Sequencing data preprocessing

Unless otherwise specified, data processing was performed using dada2 R-package (v.1.18) (Callahan et al. 2016). The formatted reference Silva database was obtained from the dada2

repository (<https://zenodo.org/record/4587955>). The pipeline was fully wrapped and automatized, running with different numbers of runs, samples and reads, for re-use in different projects.

1.3.2.1.1 Demultiplexing and data cleaning

After sequencing, samples were demultiplexed using the bcl2fastq Illumina tool. By demultiplexing, raw image files generated by the Illumina sequencer were sorted into sequenced reads, separated into files corresponding to independent samples. Next, reads were split according to their respective sequencing lanes using AWK programming language, as they might have different sequencing error profiles to correct. Reads where no primer was identified were discarded, and cutadapt (v.3.4) (M. Martin 2011) was used to remove amplification primers.

1.3.2.1.2 Filtering, consensus read-building and error correction

For each individual run and lane, forward (R1) and reverse (R2) read files were processed together. The dada2 R-package (v.1.18) (Callahan et al. 2016) was used for data processing. Reads were filtered by a minimum quality threshold of 25 Phred. Next, the dada2 “learnErrors” function was used, which calculates the parametric error model from the data through a machine learning algorithm estimating error rates, and inferring sample composition until they converge into a consistent solution. Next, the function “dada” was applied in order to use the estimated error models for error correction and sample inference. Paired R1 and R2 reads were merged and chimeric merges were removed. We used procrustes analysis (vegan R-package v.2.4-2) (Paliy and Shankar 2016; Peres-Neto and Jackson 2001) to confirm that the calculated count tables had comparable information. Finally, tables from all sequencing lanes were merged into a single count table.

Samples that were sequenced twice were only merged when the smaller duplicate, i.e the sample with less reads, had at least 30% of the number of reads than the larger duplicate. Otherwise, only the samples with the higher read counts were considered for downstream analyses.

1.3.2.1.3 Quality control and bacteria annotation

A minimum of 1500 reads was established as the lower cut-off to remove experimental noise, based on read distribution in water controls and blanks. Consistently, samples with less than 1500 reads were removed from the longitudinal dataset. Amplicon Sequence Variants (ASVs) were defined as high resolution clusters of sequencing reads differing by single-nucleotide differences over the sequenced V4 region of the 16S rRNA gene. ASVs present in less than

3 samples or with less than 5 reads in total were removed from the analysis. In the cross-sectional datasets, the filtering criteria was less conservative as fewer samples were studied; samples with less than 1500 reads and ASVs present in less than 2 samples or with fewer than 4 reads were removed.

After normalising using z-score, the taxonomy of the cleaned and normalised count tables was annotated using dada2 with the Silva database (v.123), using a Native Bayesian classifier of the Ribosomal Database Project (Q. Wang et al. 2007). Number of reads after each processing step of the dada2 pipeline were recorded for quality control and processing comparisons. No significant differences between lanes or sequencing runs with regards to the number of reads lost during the processing of the dada2 pipeline were found. Statistical analysis of procrustes (vegan R-package v.2.4-2) spatial correlation of sequencing runs and lanes was used to confirm the adequate merging of data (Paliy and Shankar 2016; Peres-Neto and Jackson 2001). FastQC analysis (quality control of raw fastq files) was run before and after read quality filtering to ensure adequate data. Coefficients of variation and Pearson correlation between biological replicates, as well as Principal Coordinates analysis (PCoA) (scipy Python-library v.1.6.2, seaborn Python-library v.0.10.1) were used to confirm correct grouping.

1.3.2.2 Analysis of microbiome 16S rRNA-Sequencing data

The annotated table and metadata information of the samples were stored together in a phyloseq (v.1.34) (McMurdie and Holmes 2013) object for downstream analysis. A maximum likelihood phylogenetic tree of sequence relationships was built using neighbour joining according to the calculated distance between sequences. Linear models were calculated to identify bacteria increasing or decreasing through age.

1.3.2.2.1 *Intra-individual bacteria diversity (alpha)*

The Phyloseq function “estimate_richness” was used to calculate alpha diversity metrics (within-individual variability). Where “Observed” corresponds to Richness, or overall number of different bacteria in the samples; “Shannon” to a diversity metric taking into account not only number of species but also their distribution in the population; and “Simpson” to a metric of population evenness, where more dominant bacteria have a higher impact in the calculation.

Alpha diversity through age was visualised using Lowess-adjusted line plots. One-way ANOVA and Student’s t-tests were used to compare between diets within-time points. Linear regression was used to study changes with age (scipy Python-library v.1.6.2) and generalised linear mixed effects (GLME) models to compare alpha diversity through age between diets

(correcting for mouse contribution by including it as a covariate in the model:

$$\alpha \sim \text{month} * \text{diet} + (1 | \text{Mouse}); \text{lme4 R-package v.1.1-23}.$$

1.3.2.2.2 Inter-individual bacteria diversity (beta)

Beta diversity (between-individual variability), evaluates the distance between pairs of samples. Here, we calculated 3 metrics. First, the phyloseq function “distance” was used to calculate unweighted UniFrac (Lozupone et al. 2007), which only considers the presence or absence of taxa, and divides the number of shared bacteria species between 2 samples by the total number of bacteria. Second, weighted UniFrac was calculated, taking into account the relative abundance of each type of bacteria in the distance metric (Lozupone et al. 2007). Third, Bray-Curtis dissimilarity (Bray, Roger Bray, and Curtis 1957) was calculated by taking the sum of the minimum relative abundance of common species between 2 samples divided by the total number of bacteria between both samples.

Beta diversity through age was visualised using Lowess-adjusted line plots. For evaluation of individual time points, PCoA was plotted (scipy Python-library v.1.6.2, seaborn Python-library v.0.10.1). Analysis of similarities (ANOSIM) was calculated to evaluate the significance of biological replicates clustering, and permutational ANOVA (PERMANOVA) to compare between biological groups within each time point (vegan R-package v.2.4-2). Linear regression was used to study changes with age (scipy Python-library v.1.6.2), and GLME models to compare patterns through age between diets (correcting for mouse contribution by including it as a covariate in the model:

$$\beta \sim \text{month} * \text{diet} + (1 | \text{Mouse}); \text{lme4 R-package v.1.1-23}.$$

To evaluate the impact of repeated measurements on beta diversity in the longitudinal study, compositional tensor factorization was used to deconvolute microbiome dynamics (gemelli Python-library v.1.0). The tensor was built as a 3-dimensional object, where the axes are mouse, bacteria and time (Martino et al. 2021). The tensors corresponding to each beta diversity distance metric were visualised using PCoA (seaborn Python-library v.0.10.1), and ANOSIM was used to validate the impact of repeated-measurements from each mouse (vegan R-package v.2.4-2).

1.3.2.2.3 Random forest-based classifier of AL and DR bacteria throughout age

The repeated-measurements per mouse in the longitudinal study required a multivariate analysis taking into account both linear and non-linear relationships between bacteria. For this analysis, bacteria present in less than 5% of the samples were excluded. To identify bacterial signatures specific for DR and AL treatment with age, we used a random forest-based approach. Random Forest (Ho, n.d.) is a machine learning algorithm that works by generating

N random datasets with replacement, i.e. 1 sample being in 1 random dataset does not exclude it from being also in another dataset. A decision tree is independently trained for each dataset, and a new set of random datasets is generated. Next, the process is repeated. This means that there is bootstrap aggregating “bagging” of the variables (M classifiers are trained independently), and “bootstrapping” with replacement of the samples (in each iteration, a classifier depending on the previous step results is generated). The forest was built as: $diet \sim asv_table * months + (1|months) + (1|Mouse)$, with the aim of predicting “diet” (either AL or DR) using the *asv_table* information, and its interaction with the “months” of age at faecal collection. With added covariates “months”, as we expect a common signature between mice of the same age, and “Mouse” since we have repetitive measurements per individual. The Random Forest classifier, computed using “`sklearn.ensemble.RandomForestClassifier`” function from scikit-learn Python-library (v.1.0.2), was trained on 70% of all mice (83 mice, 702 samples), and tested on the remaining 30% of mice. Further, as quality control, out-of-bag estimates of error rate (probability that any given prediction is not correct within the test data), accuracy (true positives), Receiver Operating Characteristic curves (relationship between false positive rate and true positive rate), and 10-Fold Cross validation score (it calculates a Random Forest Classifier model 10 times, where in each case 90% of the samples are train data, and the 10% test data is different in each classifier trained) were calculated. Once the Forests were trained and passed quality controls, “`permutation_importance`” function from eli5 Python-library (v.0.11) was used to calculate the importance of each bacteria to explain the separation between AL and DR. Importance was calculated by taking out the value of the bacteria, substituting it by a random value, training the model again and using it to evaluate if there is still relevance in the classification from the out-of-bag calculation. Finally, the trained Forest on AL and DR samples was run on AL_DR16M and AL_DR20M to obtain the accuracy of classification into DR (on the ages after the diet switch had occurred). The Random Forest classifier was further validated using 16S rRNA sequencing data from [chapter 3](#) and data from AL and DR mice from an independent project provided by Lisonia Gkioni.

1.3.2.2.4 Elastic net regression to predict a microbiome-based ageing clock

To evaluate the age-specific microbiome, log₂ transformed and z-scored centred bacterial abundance table from the longitudinal study was used. An Elastic Net (Zou and Hastie 2005) is a machine learning method that combines the penalties of Ridge regression and Lasso regression. Where Ridge regression shrinks the regression coefficients so variables with minor contribution to predict the outcome have their coefficients close to zero, Lasso regression assigns exact zero to minor contributors. The Elastic Net was trained with 70% of AL mice, using “months” as the dependent variable, using the “`sklearn.linear_model.ElasticNet`”

function from scikit-learn Python-library (v.1.0.2). First, Ridge and Lasso penalties (alpha and L1_ratio) were calculated using an iterative model fitting with Cross validation to find the best penalty fit on the training dataset by running the function "sklearn.linear_model.ElasticNetCV". Next, the Elastic Net model was built on AL samples (*months ~ asv_table*), and tested on the remaining 30% of AL mice. As quality controls, accuracy percentage (true positives), Mean Absolute Error (sum of absolute variance from the model compared to random), and 5-Fold Cross validation score (calculating the Elastic Net regressor 5 times, where in each case 80% of samples are train data, and the 20% test data is different in each Elastic Net trained) were calculated. Inspection of the AL-Aging Clock generated using the Elastic Net revealed that the age of young samples was overestimated, and the age of old samples was under-estimated. Therefore, an Ordinary Least Squares regression was fit on top of the predictions from the Elastic Net, thus including a linear correction on the age prediction from the Elastic Net (scikit-learn Python-library v.1.0.2). Finally, the Elastic Net picked 107 bacteria as relevant for the AL ageing clock (coefficients of importance different than 0), and eliminated the other 2484 bacteria. Once the AL-Ageing Clock passed accuracy quality controls, it was used to predict age in all samples from DR, AL_DR16M and AL_DR20M mice.

1.3.2.2.5 Generalised Linear Mixed Effects Models for bacteria comparison in the longitudinal analysis

Diet specific bacteria identified by the Random Forest Classifier were further compared through age and between diets using GLME models (lme4 R-package v.1.1-23): $ASV \sim months*diet + (1|Mouse)$. Bacteria that differed through age between AL and DR were overlapped with those different between DR and AL_DR16M or AL_DR20M to identify switch-resistant bacteria. DR-specific bacteria were defined as those where their abundance levels were not recapitulated by either AL_DR16M nor AL_DR20M. Bacteria that changed upon AL_DR16M but not upon AL_DR20M, were considered of interest for a possible association with the differences in longevity between AL_DR16M and AL_DR20M. Bacteria of interest were visualised as Kronas plots and networks (Ondov, Bergman, and Phillippy 2015) in order to account for relative abundance of bacteria and overlaps of Phylum, Family etc.

1.3.2.2.6 Principal response curves in the longitudinal study

To further study time-dependent diet effects on the faecal microbiome, Principal Response Curves (PRCs) were calculated on the longitudinal 16S-Seq data (vegan R-package v.2.4-2) (Paliy and Shankar 2016). PRCs are a special case of Redundancy Analysis. They take into account interaction between bacteria and calculate how much of the variation in one set of variables can be explained by the variation in another set of variables. PRC were calculated

including AL as controls, therefore the abundance of each bacteria was modelled as $(AL_ASV_mean_abundance + effect_of_diet_at_the_time + error) \sim (diet*month + (1|month))$. The weights of the response variables represent the resemblance of the bacteria abundance to that of controls, and dose-time coefficients represent the effect size of diet at a time t , relative to AL at the same time t . Thus, also the estimated diet effect between time points can be compared. To obtain significance values of the effect of diet in each bacteria and identify the period of time where differences are significant, 500 Monte Carlo permutations were run and p-values for each pairwise diet comparison were obtained for each time point (vegan R-package v.2.4-2) (Vendrig, Hemerik, and ter Braak 2017).

1.3.2.2.7 Differential abundance of bacteria

Differences in microbiome abundance between diets at each time point were evaluated using DESeq2 (R-package v.4.2) (Love, Huber, and Anders 2014) with count data as input. The mvabund R-package (v.4.2.1) (Y. Wang et al. 2012) was used to evaluate bacterial distributions and the adequacy of using a statistical method based on a negative binomial distribution for differential abundance analysis. Bacteria of interest identified by DESeq2 were visualised using logFC heatmaps (seaborn Python-library v.0.10.1), and Venn diagrams to indicate overlaps between treatments.

1.3.2.2.8 Repeated Measures Correlation of sets of bacteria of interest in the longitudinal analysis

Repeated measures correlation is a 3-dimensional correlation unit that takes into account time, mouse and bacteria. We calculated repeated measures correlation on bacteria of interest from the longitudinal dataset using the time points after the diet switch, and the rmcrr R-package (v.0.4.6) (Bakdash and Marusich 2017). The output of repeated correlations are co-inertia tables of bacteria of interest, including positive and negative co-inertia values. Bacteria networks of co-inertia were visualised using Cytoscape (v.3.9.1) (P. Shannon et al. 2003).

1.3.2.2.9 Cox regression of bacteria of interest in the longitudinal study

Association of bacteria of interest with longevity was calculated using univariate Cox regressions. For each ASV of interest, DR, AL_DR16M and AL_DR20M mice were split into two groups: one where the relative ASV abundance was above the mean, and a second group with abundance below the mean. Kaplan-meier curves and Cox proportional hazards were calculated using the lifelines python library (v.0.27.1). Longevity associated bacteria were defined as those where significant lifespan differences were identified according to bacteria abundance.

1.3.3 Whole microbiome shotgun metagenomic sequencing

Repository: https://github.com/carolinamonzo/CM_ShotgunMetagenomics

1.3.3.1 Microbiome shotgun metagenomics data preprocessing

Samples were demultiplexed to separate reads according to samples using the bcl2fastq Illumina tool. Both sequencing lanes were concatenated to have only one forward (R1) and one reverse (R2) file per sample using bash scripting, as libraries were equally split between the two lanes for sequencing. Trimomatic (v.0.39) (Bolger, Lohse, and Usadel 2014) tool was used to remove Nextera adaptors, and to quality-trim reads using a minimum Phred score of 25 as threshold. A reference fasta file (Bolger, Lohse, and Usadel 2014) with all known Nextera adaptor sequences was used to recognize primer sequences and remove them from the sequencing reads. Only reads with at least 36 nt were used to avoid reads that only consist of primers or adaptors. Kraken2 (v.2.1.2) (Wood, Lu, and Langmead 2019), a taxonomic classification system based on exact k-mer matches, was used for taxonomy assignment using the “Mouse Gastrointestinal Bacterial Catalogue” database (Beresford-Jones et al. 2022). To estimate species abundance, Bracken (v.2.5) (Lu et al. 2017) was used, and tables of bacterial relative abundances were generated. Finally, z-score was applied to normalise the dataset.

1.3.3.1.1 Quality control and spatial correlation with 16S-Seq data

Quality control of reads before and after quality trimming was performed using FastQC and MultiQC (v.1.11) to facilitate sample comparison (Ewels et al. 2016). Number of reads was compared between samples to identify possible mistakes in the PCR reactions, and the percentage of classified reads per sample was evaluated. The relationship of biological replicates was evaluated using Pearson correlation (scikit-learn Python-library v.1.0.2). Mantel test was used to test for correlation in β -diversity between 16S rRNA sequencing and shotgun metagenomics samples (skbio Python-library v.0.5.6). PCA visualisation (factoextra R-package v.1.0.7.999; seaborn Python-library v.0.10.1), and procrustes analysis (vegan R-package v.2.4-2) were used to evaluate the spatial correlation in sample distribution between the 2 datasets (Paliy and Shankar 2016; Peres-Neto and Jackson 2001).

1.3.3.2 Downstream analysis of microbiome shotgun metagenomics data

The mvabund R-package (v.4.2.1) (Y. Wang et al. 2012) was used to analyse the distribution of bacterial species in samples. Having a bacterial distribution fitting a negative binomial curve, differences in abundances of microbiome species between diets were evaluated using

DESeq2 (v.4.2) (Love, Huber, and Anders 2014; Durazzi et al. 2021). ANOSIM was calculated to corroborate clustering according to diet, mouse and age (vegan R-package v.2.4-2). Repeated measures correlation taking into account time, mouse and bacteria, was calculated for DR-specific and microbiome memory of AL feeding bacteria using the rmcrr R-package (v.0.4.6) (Bakdash and Marusich 2017). Bacteria networks of co-inertia were visualised using Cytoscape (v.3.9.1) (P. Shannon et al. 2003).

1.3.4 Faecal metabolomics

Repository: https://github.com/carolinamonzo/CM_Metabolomics

1.3.4.1 Filtering and normalisation of faecal metabolomics data

Of the 438 samples used for the metabolomics analysis, 3 samples were removed because of low metabolite content i.e. the total area under the curve (AUC) of these 3 samples was 10% below the median AUC. To decrease noise in the data set, metabolites in which the average of all samples was not two times higher than the blank average, were excluded. Metabolite measurements were normalised to faecal pellet weight. The dilution factor 0.75 was multiplied in samples where we used 800 µl of metabolite extraction buffer, and 0.375 when 1600 µl were used. Since there was a slight batch effect according to sample-run-order, a similar approach to the “internal reference standard” normalisation described in (Plubell et al. 2017) was applied to the metabolomics datasets. This normalisation calculates the geometric average of each overlapping window of 2 pooled standards, and averages all pooled standards to calculate correction factors per metabolite, for each set of samples within each window. Samples were then multiplied by the corresponding correction factors. Finally, z-score values were calculated from the log₂-AUC of each metabolite per sample. Data were visualised using PCA (factoextra R-package v.1.0.7.999; seaborn Python-library v.0.10.1).

1.3.4.2 Analysis of faecal metabolomics data

Two data sets were independently analysed including (1) untargeted polar and (2) untargeted non-polar metabolites. Linear models were calculated to identify metabolites increasing or decreasing through age for each independent diet group.

1.3.4.2.1 Differential abundance analysis of faecal metabolomics data

Changes in metabolite abundances throughout age and between diets were evaluated for each metabolite using GLME models (lme4 R-package v.1.1-23):

metabolite ~ *diet*months* + (1|*Mouse*) + (1|*Num_Thawed*). Mouse identity and number of thawing times were included as covariates in order to control for these effects in the analysis.

Bonferroni multiple testing correction was applied. ANOSIM (skbio Python-library v.0.5.6) on Bray-curtis distances between samples (skbio Python-library v.0.5.6) was used to validate clustering according to age and diet. Temporal metabolite trends were evaluated using PRCs (vegan R-package v.2.4-2). Furthermore, the mvabund R-package (v.4.2.1) (Y. Wang et al. 2012) was used to evaluate metabolite distribution per sample, and test whether the negative-binomial approach was the adequate method for differential abundance analysis. Metabolite abundance differences between diets at each individual time point were evaluated using DESeq2 (v.4.2) (Love, Huber, and Anders 2014). Data were visualised using log2FC heatmaps (seaborn Python-library v.0.10.1), and Venn diagrams to indicate overlaps between treatment groups or ages.

1.3.5 BCR-Sequencing

Repository: https://github.com/carolinamonzo/CM_BCRseq

1.3.5.1 BCR-Sequencing data preprocessing

Unless otherwise specified, data preprocessing was performed using the pRESTO (v.0.7) (Heiden et al. 2014) and Change-O (v.1.2) (Gupta et al. 2015) tools from the Immcantation framework. Reference mouse *Igh* sequences were obtained from the International ImMunoGeneTics information (IMGT) database (Giudicelli, Chaume, and Lefranc 2005).

1.3.5.1.1 Demultiplexing of internal barcodes

Ten forward and 10 reverse FastQ files were generated by Illumina sequencing, each of them containing 10 internally-barcoded samples. To separate sequencing reads into those corresponding to individual mice of origin, demultiplexing was performed using internal barcodes included during the PCR-2 (Appendix 4.5). Sequencing reads with an average Phred score below 25 were excluded from the analysis. Internal barcodes are unique combinations of 8 nucleotides per sample. Therefore, to avoid read assignment to incorrect mice, minimal mismatch tolerance (--maxerror 0.1) was allowed. Internal barcode sequences and the 5' invariant part of the template-switch adapter were masked in the reads. Barcode information was stored in the identifier information of each read of the FastQ files, in the section "PRIMER". Demultiplexing of sample reads using the annotated barcode was then performed in order to obtain a set of R1 and R2 paired FastQ files for each individual mouse sample. The information about the FastQ file of origin (R1 or R2) was then added to the read headers of each sample FastQ files.

1.3.5.1.2 UMI extraction, consensus-read building and pair merging

In order to generate consensus reads representative of each original RNA molecule, reads identified with the forward M1S primer (Appendix 4.5), corresponding to the 5' sequence of the template-switch adapter, underwent a second round of masking using the 3' invariant part of the template-switch adapter sequence (CTTGGGG, stored in "presto_TSA.fa"). Next, the 16 nucleotides corresponding to the read's unique molecular identifier (UMI), were extracted and recorded in each read's header. As the match sequence for this second round of masking is shorter and more error-prone than the primer sequences used in the first round, an increased mismatch tolerance (--maxerror 0.5) was permitted, increasing the number of reads with successfully-extracted UMIs.

To span the whole 700 nt of the *IghV-IghD-IghJ* region of interest, sequencing was performed in an un-stranded manner. Therefore, reads from both 5' and 3' directions were stored in both the R1 and R2 original FastQ files. After internal-barcodes demultiplexing, 5' reads were originally stored in both <R1_S#_R1> and <R2_S#_R1> files. To correct this and have all 5'-forward reads in one file (files ending in <S#_R1.fastq>) and all 3'-reverse reads in a second file (files ending in <S#_R2.fastq>), the files were concatenated using base shell scripting. Sequence identifier duplicates were removed using seqkit (v.2.2) (Shen et al. 2016), as these duplicates correspond to PCR primer-dimers.

Next, in order to generate a single consensus sequence for each UMI-cluster annotation, 5' and 3' reads were synchronised (i.e. sorted according to read identifier to have paired reads in the same order), discarding reads that did not have a mate (due to differential processing of the 5' and 3' files), and copying the UMI annotations to the 3' reads. Followed by consensus-reads generation as a result of grouping and collapsing reads based on UMI sequences. Reads with a mismatch rate from the consensus of more than 10% were discarded from the dataset (--maxerror 0.1). No gap-correction was used in order to avoid bias in collapse of reads with different lengths. This same consensus-read-generation step was also performed on the 3' reads. The resulting FastQ file contained a single consensus sequence for each UMI-cluster annotation, labelled with total number of reads contributing to that consensus sequence, and primers contributing to the consensus.

Files were synchronised and annotations unified between mate-reads i.e. mate-reads where one read of the pair failed a quality control were discarded. Consensus-read-pairs were assembled de novo into a contiguous sequence using pRESTO (v.0.7) (Heiden et al. 2014). Where this was not possible, consensus reads were aligned with BLASTN (Camacho et al. 2009; Altschul et al. 1990) to a reference of *IghV* sequences (imgt_mouse_ig_v.fasta) to

generate a merged sequence. When BLASTN was used, N characters were included to separate pairs that aligned in a non-overlapping manner on the same VH segment. Finally, the information about the number of reads contributing to the 5' and 3' consensus sequence were copied to the new merged sequence (specified by --1f and --2f). Sequence pairs for which both alignment approaches failed were discarded.

1.3.5.1.3 Annotation of Igh isotypes

Antibody isotypes were annotated according to the isotype-specific sequence present in the 1st PCR 3' primer. Assembled reads were aligned to the primer sequences (stored in "presto_PCR1_ISOTYPES.fasta") and isotype identifiers were recorded in each read header. Due to the nature of asymmetric sequencing, each original RNA sequence was sequenced at least twice (once 400+100 and a second time in reverse 100+400 nt) in order to be assembled into a full-length ~650 nt read. Therefore, no singletons were removed.

1.3.5.1.4 V(D)J annotation and discovery of novel IghV alleles

To annotate each read with its germline *IghV-IghD-IghJ* alleles and identify relevant sequence structures such as the CDR3 hypervariable sequence. IMGT reference sequences were built into a database using modified helper scripts from the Immcantation portal (Gupta et al. 2017). The resulting BLAST-formatted database was queried using IgBLAST (Ye et al. 2013). Following annotation of *IghV*, *IghD* and *IghJ* alleles, the IgBLAST results were formatted into a standardised data-table in adaptive immune receptor repertoire (AIRR) format (Vander Heiden et al. 2018).

IgBLAST classified sequences as productive (full *IghV-IghD-IghJ* rearrangement) or unproductive (rearrangement lacking an *IghJ* allele). Unproductive sequences were filtered out. Sequences not correctly mapped to immunoglobulin heavy chains (the pattern "IGHV" was not found in column "v_call" using regular expressions), were removed.

IghV-IghD-IghJ allele assignment was done by matching sequences against reference alleles from the IMGT reference database (Giudicelli, Chaume, and Lefranc 2005). However, current databases are incomplete due to the high diversity of the BCR repertoire. The R-package TIgGER (v.1) (Gadala-Maria et al. 2015) was used to identify mouse-specific *IghV* genotypes and alleles that would improve the *IghV* gene annotations. For each *IghV* gene allele, the function "findNovelAlleles" evaluates sequences assigned to each allele, and calculates the mutation frequency at each position as a function of sequence-wide mutation counts. High mutation frequency in specific nucleotide positions, even when the sequence-wide mutation count was low, distinguished polymorphisms from somatic hypermutations. To avoid calling

novel alleles from clonally-related sequences, newly identified alleles are classified as such only when found in sequences with different *IghJ* genes and CDR3 lengths. Function “inferGenotypeBayesian” improved *IghV* gene calls by analysing the posterior probabilities of possible allele distributions, considering four different simulated alleles per *IghV* gene (corresponding to a known gene that would have undergone duplication and further mutations). Best allele fit was identified through comparison of the posterior probabilities of the four possible models, and calculation of a Bayes factor, which reflects the confidence of the genotyping call for each model.

Subject-specific genotyping and novel allele information was included into AIRR databases and Fasta files, reducing the number of ambiguous and erroneous gene calls. Log files containing information of novel alleles and genotyping statistics were generated, and all novel allele calls were manually examined.

1.3.5.1.5 Clonotype and germline inference

Accurate identification of clonal relationships is crucial for repertoire analysis. An appropriate distance threshold for clonotype assignment is required to classify sequences as clonally-related (belong to the same clone) or not clonally related (belong to independent clones). Distance thresholds were calculated using either hierarchical clustering when distance distributions were bimodal, or spectral clustering when unimodal. Hierarchical clustering was performed using R-package SHazaM (v.1.1) (Gupta et al. 2017). Sequences were classified into groups sharing the same *IghV* and *IghJ* gene assignments and CDR3 lengths. Nearest neighbour distances between sequences in each group were calculated using Hamming distances as the underlying somatic hypermutation (SHM) model in the “distToNearest” function. The threshold was calculated as the value that separates the two modes of the smoothed distances distribution. Distance threshold for samples with unclear distributions was calculated using R-package SCOPer (v.1.1) (Nouri and Kleinstein 2018). This method is based on spectral clustering. It uses an adaptive unsupervised threshold to adapt the required level of similarity among sequences in the same group (same *IghV* and *IghJ* gene assignments and CDR3 length). All calculated thresholds and distance distribution histograms were plotted and manually checked.

Clonotype inference, i.e. definition of sequences clonally-related, was performed using Change-O (v.1.2). Sequences were grouped according to shared *IghV* and *IghJ* genes, as well as CDR3 length. Pairwise Hamming distances (--model ham) were calculated between CDR3 sequences in each group. Previously inferred distance thresholds were included in parameter --dist for each sample. Each clonotype was annotated with its unique ID.

Full-length germline sequences were assembled using alignment information (-d) and reference IgBLAST database (-r). Argument --clone was used to assign the same germline to all sequences of the same clone. To facilitate downstream analysis, information of sample_id and biogroup (age and diet) were added to the AIRR databases. AIRR databases from each tissue were merged for downstream analysis.

1.3.5.1.6 Quality control of BCR-Sequencing datasets

Quality control of reads was performed using FastQC (Andrews, 2010) on merged raw sequencing fastq files. Number of reads was compared between samples to identify possible failed sequences. Validation of novel allele calls and selected distance thresholds was performed manually. Biological replicates relationship was evaluated using Pearson correlation (scipy Python-library v.1.6.2). Rarefaction curves were assessed to compare depth of sequencing between samples (vegan R-package v.2.4-2).

1.3.5.2 Analysis of BCR repertoires

1.3.5.2.1 Clonal diversity: Hill Diversity

Clonal diversity of BCR repertoires were analysed using Hill Diversity (Hill 1973). Therefore, Hill Diversity was quantified using the “alphaDiversity” function from the R-package Alakazam (v.1.1) (Gupta et al. 2017). To overcome sequencing depth variations between samples, input sequences were uniformly resampled and clone size distribution and diversity were calculated (Chao et al. 2014). Diversity was calculated over a range of diversity orders (q): q = 0 represents Richness, q = 1 Shannon index, and q = 2 Simpson index. These metrics are not only relevant individually, but also in combination, as they represent relationships of richness, divergence and evenness of the clonal populations, respectively.

Richness indicates the total number of different clones in the dataset. Shannon index, also known as entropy, is the weighted geometric mean of the proportional abundances of different clones (C. E. Shannon 1948). The more even the clonal population structure is, the larger is the Shannon index. Simpson index is the weighted arithmetic mean of the proportional abundances of different clones. In this case, the index measures the probability that two BCRs taken at random from the dataset belong to the same clone (Simpson 1949). Thus, the more even the population is, the larger is the Simpson index.

1.3.5.2.2 Repertoire Dissimilarity Index

To quantify the average variation between BCR repertoires when comparing samples and diet groups, the repertoire dissimilarity index (RDI) was calculated using the RDI (v.1) R-package

(Bolen et al. 2017). RDI is a non-parametric method used to quantify differences in *IghV*, *IghD* and *IghJ* gene usage and compare between BCR repertoires. To overcome sequencing depth variations between samples, it uses bootstrapped sub-sampling and data simulation.

1.3.5.2.3 Clonal abundance and expansions

Clonal abundance of BCR repertoires was evaluated using the “estimateAbundance” function from the R-package Alakazam (v.1.1) (Gupta et al. 2015). This function uses resampling strategies to correct for variations in sequencing depth and inference of complete clonal abundance distributions (Chao et al. 2015). Clone size was calculated as the number of unique sequences assigned to a clonal ID. To obtain relative frequencies of clones, clone size was divided by the total number of unique sequences. Clonal frequencies were ranked in descending order. 200 iterations of bootstrap were used to obtain confidence intervals. To evaluate the degree of clonal expansion, the sum of frequencies of the 20 most frequent clones were compared (P20).

1.3.5.2.4 Somatic hypermutation and mutational status

SHM frequencies were calculated using the R-package Shazam (v.1.1) (Gupta et al. 2015). The “observedMutations” function was used to calculate total mutation count and mutation frequency of non-synonymous (amino acid-changing) and synonymous mutations. Mutational status of *IghV-IghD-IghJ* segments was classified as SHM⁺ (mutated, post antigen exposure), for those segments with > 1% mutations, and SHM⁻ (not-mutated, pre antigen exposure) when the number of mutations in the segment was < 1% according to (C. Wang et al. 2014).

1.3.5.2.5 Relative abundance of BCR isotypes

The number of RNA molecules (merged BCR assemblies according to UMI), per BCR isotype were extracted from the AIRR database. Relative abundances of isotypes per sample were calculated as the number of molecules corresponding to each isotype, divided by the total amount of sequenced molecules.

1.3.5.2.6 Analysis of naïve and class switched BCRs

To study differences in naïve and class switched BCRs, clones were classified into 3 groups: IgM⁻IgD⁻, clones where all isotypes have switched and are therefore post-antigenic; IgM⁺IgD⁺SHM⁻, clones where SHM has not yet added variability to the V(D)J segment are naïve; and IgM⁺IgD⁺SHM⁺, clones that underwent SHM after being exposed to antigens. Frequency of clones corresponding to each group were calculated.

1.3.5.2.7 IghV and IghJ gene usage

IghV and *IghJ* gene usage frequencies per sample and isotype were calculated using the “countGenes” function of the R-package Alakazam (v.1.1) (Gupta et al. 2015). *IghV* and *IghJ* gene usage were compared between diet groups and throughout age and visualised using heatmaps, clustering by means of euclidean distance of genes or allele frequency profiles (seaborn Python-library v.0.10.1).

1.3.5.2.8 CDR3 length analysis

Length of the CDR3 hypervariable region was extracted from the AIRR database for each RNA molecule. Centre and deviation of CDR3-length, gaussian distributions, as well as variability between biological replicates, were calculated to evaluate differences throughout age and between diet groups. To compare variability between CDR3 length distributions, CDR3 length distributions of samples were fit into Kolmogorov Smirnov curves. The number of significant differences between biological replicates was compared between biological groups (scipy Python-library v.1.6.2).

1.3.5.2.9 Statistical analysis of the BCR dataset

Linear regression was used to test for age-related changes. Two-way ANOVA was used to test for significant differences between AL and DR through age. Linear regression and two-way ANOVA were calculated using the statsmodels (v.0.12) and scipy (v.1.6.2) Python-libraries (Seabold and Perktold 2010; Virtanen et al. 2020). Kruskal-Wallis with Mann-Whitney U-test for pairwise comparisons were calculated to evaluate differences between diet groups per time point using the scipy Python-library. For CDR3 length distribution variability, linear regression, 2-way ANOVA and Fisher’s tests were used to compare the proportion of significantly different biological replicates by age and diet. The relationship between each BCR metric of both spleen and ileum, and the morbidity index ([algorithm](#)), was calculated using linear regression and spearman correlation (scipy Python-library v.1.6.2). Plots were generated using Seaborn (v.0.10.1).

2. The effect of dietary restriction on the microbiome in mice

Author contributions:

Conception of the study predominantly by Carolina Monzó, Sebastian Grönke, Dario Valenzano and Linda Partridge.

Provision of tissues by Lisa Drews, Lisonia Gkioni, Sebastian Grönke and Maarouf Baghdadi.

Execution of experiments: Carolina Monzó, Lisonia Gkioni and Jens Seidel. Carolina Monzó, Lisonia Gkioni, Jens Seidel, Jenny Fröhlich, Aleksandra Placzec and Ramona Hoppe performed longitudinal microbiome experiments. Carolina Monzó performed shotgun metagenomics and cross-sectional microbiome experiments of *Irs1*^{-/-} and Rapamycin-treated mice.

Bioinformatic analysis by Carolina Monzó. Advised by Andreas Beyer.

Statistical evaluation by Carolina Monzó. Advised by Andreas Beyer.

Graphical representation by Carolina Monzó.

Writing of the manuscript predominantly by Carolina Monzó, with substantial contribution by Lisonia Gkioni, Sebastian Grönke and Linda Partridge.

Late-onset dietary restriction largely reverses the adverse age-associated changes in faecal microbiome and metabolome: a longitudinal study

Authors:

Carolina Monzó^{1,2}, Lisonia Gkioni¹, Jens Seidel¹, Jenny Fröhlich¹, Aleksandra Placzek¹, Ramona Hoppe¹, Andreas Beyer², Dario Riccardo Valenzano¹, Sebastian Grönke¹, Linda Partridge^{1,3}

Affiliations:

1. Max Planck Institute for Biology of Ageing, Cologne, Germany
2. CECAD Research Centre, Cologne, Germany
3. Institute of Healthy Ageing, University College of London, United Kingdom

2.1 Introduction

The human body is populated by trillions of microbes that play an important role in many physiological functions. Especially the microbial communities in the digestive tract have been associated with organismal health (Bana and Cabreiro 2019; Ghosh, Shanahan, and O'Toole 2022). Importantly, with age the composition of the gut microbiome changes. While the composition of the microbiome is relatively stable during mid-life, during old age, the microbiome becomes less diverse and more different between individuals (Maynard and Weinkove 2018; Nagpal et al. 2018). Moreover, perturbations of microbiome homeostasis have been associated with frailty, immune diseases, colon cancer and other morbidities (Sekirov et al. 2010; Zapata and Quagliarello 2015). In addition, correlation studies have shown that both microbiome composition and degree of dissimilarity predict survival in old humans (Galkin et al. 2020; Wilmanski et al. 2021a). Furthermore, faecal transfer experiments in killifish and mice indicate a causal role of the microbiota in the determination of longevity (Bradshaw et al. 2022; Bárcena et al. 2019). Thus, changes in microbiota composition might contribute to interventions that target the ageing process.

Reduced activity of nutrient sensing pathways by dietary, genetic or pharmacological interventions improves health and extends longevity in mice and potentially humans (Green et al. 2021; Tyshkovskiy et al. 2019; Fontana, Partridge, and Longo 2010). The evolutionarily conserved insulin/IGF1 (IIS) and mTOR pathways are the two most important signalling networks that have been implicated in extension of lifespan. Treating mice with the drug

rapamycin, an inhibitor of mTORC1, extends lifespan. Furthermore, mice that are lacking the *Irs1* gene, a key component of the insulin/IGF1 pathway, directly downstream of the insulin/IGF receptor, are long-lived and healthier at old age (Juricic et al. 2022; Richard A. Miller et al. 2014; Selman et al. 2008; Baghdadi, 2022). Positive effects on health and longevity can also be achieved by directly manipulating food uptake. Dietary restriction (DR), which refers to reducing food intake without malnutrition, is a robust way to extend lifespan in mice and improve health in humans (Fontana and Partridge 2015; Green, Lamming, and Fontana 2022). The specific mechanisms mediating the beneficial effects of DR are only partially understood. Recent work from our lab showed that in mice, DR is only effective in extending lifespan when introduced relative early in life, but not at old age (24 months) (Hahn et al., 2019). Mice that were switched from *ad libitum* (AL) feeding to DR at the age of 24 months, did not benefit in their survival from the DR treatment and many genes, especially in the white adipose tissue (WAT), did not change in expression in response to the DR switch, indicating a memory of prior AL feeding in the fat tissue of these animals (Hahn et al., 2019). More recent work from our lab showed that mice lose their ability to respond with lifespan extension to DR between the age of 16 and 20 months (Drews et al. 2021). While the underlying molecular mechanisms are currently unclear, comparing molecular responses between the early and late switch might reveal factors involved in DR mediated longevity. DR has been shown to directly affect the composition of the gut microbiome (Kok et al. 2018; Fabbiano et al. 2018; C. Zhang et al. 2013; Bartley et al. 2017; Duszka et al. 2018). This includes the attenuation of age-related changes in relative abundance of bacteria, maintenance of low dissimilarity through age, metabolic improvements and increased abundance of *Bacteroidetes* (C. Zhang et al. 2013; Bartley et al. 2017; Duszka et al. 2018; Fabbiano et al. 2018; Kok et al. 2018). In addition, it has been shown that the microbiome of mice that were switched from AL to DR at 20 months of age, showed a shift towards a “younger state” (Zeng et al. 2019). However, as this study did not include an earlier switch nor did it measure the lifespan of these animals, a direct correlation of bacteria associated with longevity was not possible.

The microbiome influences ageing and metabolism indirectly, through production of metabolites during digestive processes (Bana and Cabreiro 2019; Krautkramer, Fan, and Bäckhed 2021). DR triggers distinct structural and functional changes in the intestinal microbiome, and thereby affects microbiome-produced metabolites that can affect the health of the host (David et al. 2014; Maynard and Weinkove 2018; Kok et al. 2018; von Schwartzberg et al. 2021). For example, DR-induced production of short-chain fatty acids (SCFA) via carbon fermentation have been correlated with increased health (Dalile et al. 2019; Frampton et al. 2020; Morrison and Preston 2016). However, only few studies have evaluated how ageing or DR affect the microbiome-produced metabolome. Age-associated reduction in

acetate SCFA in AL mice, and increased bile acids in old AL mice compared to DR were found using a targeted metabolomics (van der Lugt et al. 2018). However, the microbiome-produced metabolome of AL, DR, or mice under late-onset DR, and the different metabolite profiles associated with DR-mediated longevity are currently unexplored.

To address how ageing and DR affect the faecal microbiome, and to identify bacteria and metabolites associated with longevity, we extracted DNA and metabolites from a longitudinal collection of faecal samples from a lifespan cohort of AL and DR mice. In addition, we collected faecal samples from animals that were switched from AL to DR at 16 and 20 months of age. We performed 16S rRNA sequencing and metabolomics analysis on these samples. Our results show that the DR microbiome not only maintains “young-like” bacterial community structure with age, but also induces an independent ageing profile that is distinct compared to AL. We also show that the ability of the microbiome and the faecal metabolome to adapt after switching diets to DR is high, but progressively decreases as the age of DR onset increases. This finding suggests that there is an age-dependent microbiome and faecal metabolomic memory of AL feeding impeding full adaptation to DR-like patterns. Finally, we identify bacteria associated with longevity, not only during DR, but also in mice with reduced IIS and mTOR signalling.

2.2 Results

2.2.1 A longitudinal high-resolution analysis of the ageing murine microbiome

Age-dependent perturbations of microbiome homeostasis are correlated with impaired health (Zapata and Quagliarello 2015; Langille et al. 2014; Bana and Cabreiro 2019). One of the contributing factors to the health and longevity benefits linked to DR, could be the preservation of microbiome homeostasis with age. To investigate the effects of ageing and DR on the microbiome we studied female wild type C3B6F1 hybrid mice fed AL or DR (Fig 2.1). DR mice received 40% less food than AL fed animals (Drews et al. 2021). DNA was extracted from faecal samples collected longitudinally from 12 months of age, every 2 months until death (AL n = 70, DR n = 50, AL_DR16M n = 50, AL_DR20M = 50; Fig 2.1). The V4 region of the 16S rRNA gene was sequenced in 2118 faecal samples. Amplicon sequence variants (ASVs), were defined as high resolution clusters of sequencing reads that differ by single-nucleotide differences over the sequenced V4 region of the 16S rRNA gene (Callahan, McMurdie, and Holmes 2017). Bacteria taxonomy on ASVs was assigned using the Silva reference database (Quast et al. 2013).

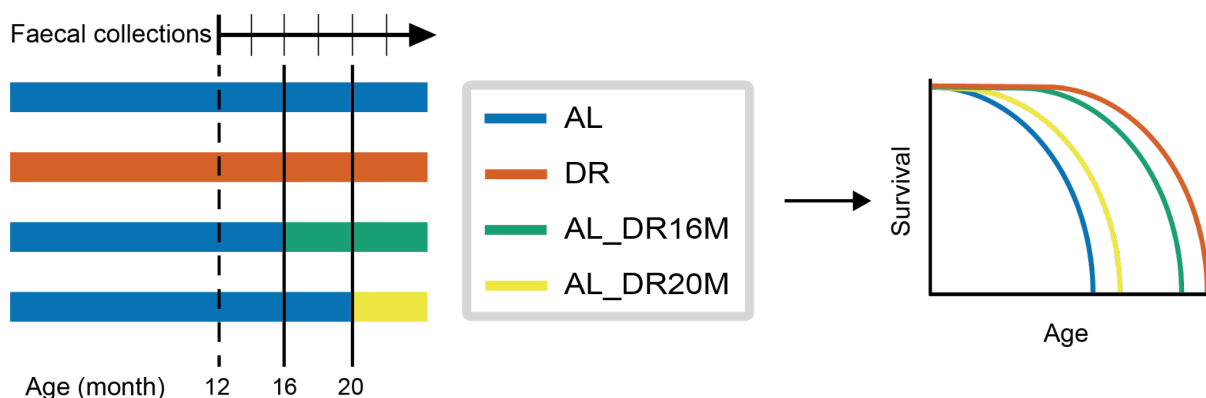


Figure 2.1: Scheme of the experimental design and lifespan of studied diet groups, adapted from (Drews et al. 2021). Black dotted lines correspond to age of start of bi-monthly faecal collections and solid lines to age of DR onset. n = 70 AL mice and n = 50 mice for DR, AL_DR16M and AL_DR20M treatments.

To evaluate age-dependent changes in the microbiome, we calculated Shannon entropy, i.e. within-individual variability (alpha diversity) represented by the number of different ASVs and the distribution of relative abundance of ASVs in the microbiome population (C. E. Shannon 1948). In line with previous studies in mice and humans (Nagpal et al. 2018; Maynard and Weinkove 2018), alpha diversity significantly declined with age in AL mice (Fig 2.2A).

To further understand the different microbiome characteristics that may be associated with differences in lifespan between AL mice (Drews et al. 2021) (Fig 2.1), we examined intra-individual dissimilarity (beta diversity). Beta diversity quantifies bacterial community distances between mice, and has been previously shown to have an opposite trajectory to alpha diversity (Nagpal et al. 2018). With increasing age individuals become more distinct from one another as a result of proliferation of different bacteria in different individuals. We calculated beta diversity using the Bray Curtis dissimilarity index, whereby the compositional dissimilarity between two samples is represented by the number of common ASVs divided by the sum of specific ASVs of each compared sample (Bray, Roger Bray, and Curtis 1957). Beta diversity of AL mice increased with age (Fig 2.2B), consistent with previous research. (Wilmanski et al. 2021b; Nagpal et al. 2018). Thus, while at young age, the microbiomes of mice were more similar to each other, at old age microbiome populations became more different between individuals.

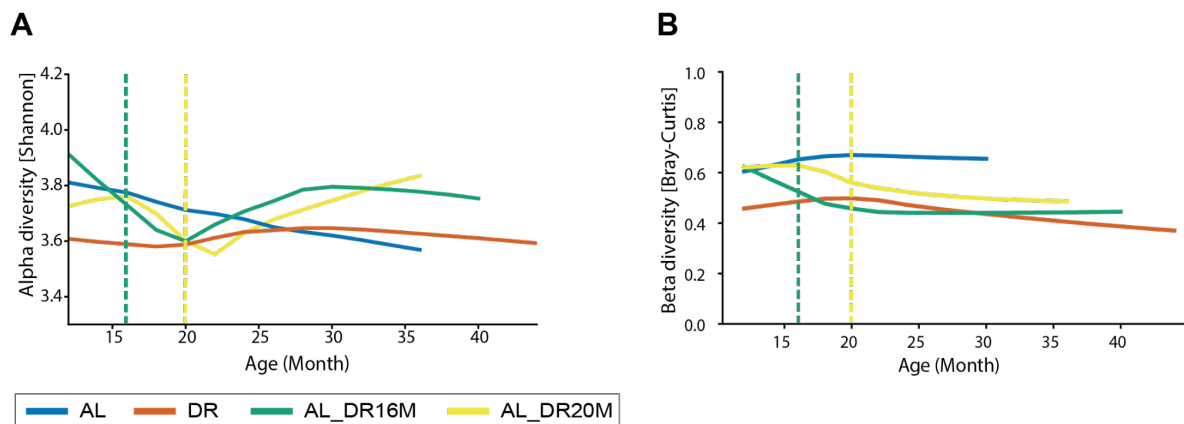


Figure 2.2: A) Lowess-corrected Shannon diversity of the microbiome. Significant differences through age (linear regression): AL p-value = 2.2×10^{-4} . Significant longitudinal differences through age between diets (GLME): DR vs AL adjusted p-value = 0.0016; AL_DR16M vs AL adjusted p-value = 0.003; AL_DR20M vs AL adjusted p-value = 0.004; AL_DR20M vs DR adjusted p-value = 0.0001. Significant difference between slope of changes during 6 months post-switch (GLME): AL_DR16M vs AL_DR20M p-value = 0.002. **B)** Lowess-corrected Bray-Curtis diversity of the microbiome. Significant differences through age (linear regression): AL p-value = 5.2×10^{-146} . Significant clustering of samples (ANOSIM): diet p-value = 0.01; age p-value = 0.002, mouse p-value = 0.001. Significant differences through age between diets (2-way ANOVA): DR vs AL adjusted p-value = 2.0×10^{-16} ; AL_DR16M vs DR adjusted p-value = 4.1×10^{-15} ; AL_DR16M vs AL adjusted p-value = 4.5×10^{-6} ; AL_DR20M vs DR adjusted p-value = 2.9×10^{-15} ; AL_DR20M vs AL adjusted p-value = 0.0045. Significant difference between slope of changes during 8 months post-switch (linear regression): AL_DR16M vs AL_DR20M p-value = 0.013. Not significant p-values in Supplementary File 1.

To study how bacterial abundance changes with age and to identify ASVs most affected by ageing, linear regressions were run on the longitudinal bacteria abundances of AL mice. In general, bacterial abundances decreased with age, consistent with previous findings (Badal et al. 2020; van der Lugt et al. 2018; Flemer et al. 2017). Abundance of 156 ASVs decreased with age, and only 77 ASVs showed increased abundance at older age (Fig 2.3). *Bacteroides* and *Firmicutes* were the phyla most affected by ageing, consistent with previous findings (Wilmanski et al. 2021b; Badal et al. 2020; Elderman et al. 2017; Flemer et al. 2017; van der Lugt et al. 2018).

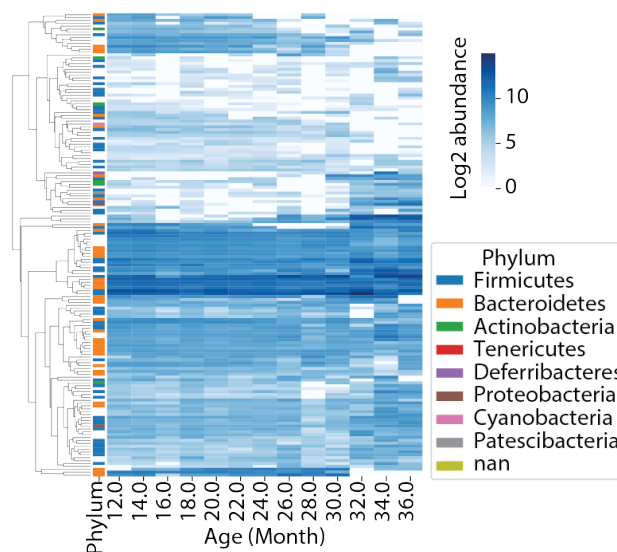


Figure 2.3: Heatmap depicting ageing microbiome trends of AL mice.

2.2.2 DR age-related changes in the faecal microbiome

To evaluate whether DR ameliorates the observed age-associated decrease in alpha diversity and increase in beta diversity, we studied longitudinal 16S rRNA sequencing of DR-fed mice. First, to test for any batch effects affecting the microbiome composition, the beta diversity distance matrix was evaluated using analysis of similarities (ANOSIM). ANOSIM compares distances between samples of the same group of interest, versus distances from a random subset of samples. Significant grouping of samples was found according to diet, age and mouse (Fig 2.5C). Next, including individual mice as covariates in the model, AL and DR were longitudinally compared using generalised linear mixed effects (GLME) models. As previously reported (C. Zhang et al. 2013; Kok et al. 2018; Duszka et al. 2018), both alpha and beta diversity of DR mice were significantly different compared to AL (Fig 2.2A-B). More specifically, DR mice displayed significantly lower alpha diversity earlier in life (12 to 22 months of age)

(Sup File 1; Fig 2.2A). However, as a result of the alpha diversity remaining stable during ageing, DR was characterised by higher diversity compared to AL at old age (Sup File 1; Fig 2.2A). Similarly, beta diversity of DR mice did not significantly change with age, but was significantly lower than AL across all studied timepoints (Fig 2.2B). In summary, while alpha diversity decreased and beta diversity increased with age in AL mice, this was not the case in DR animals. Thus, the microbiome community structure of DR mice seems to be more stable during ageing.

To study ageing trends in bacterial abundance of DR mice and identify ASVs most affected by age, linear regressions were run on the longitudinal bacteria abundances of DR mice. Contrary to the observed downregulation of ageing bacteria in AL mice, DR mice were characterised by an overall upregulation of bacterial abundances (234 ASVs increasing with age), while only few bacteria were downregulated with age (84 ASVs; Fig 2.4). Nevertheless, there was no significant difference between the number of common upregulated (25; 8.7%) and downregulated (30; 13.9%) bacteria between AL and DR (chi squared p-value = 0.56).

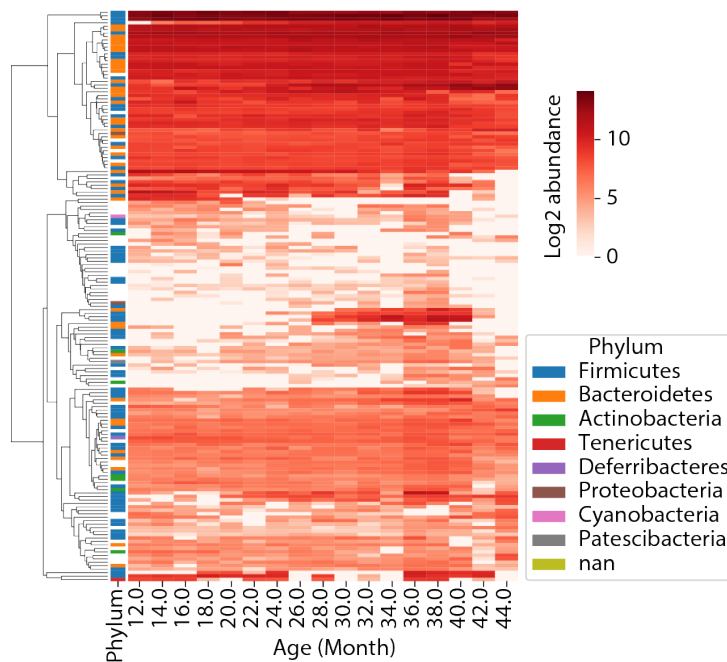


Figure 2.4: Heatmap depicting ageing bacterial trends of DR mice.

2.2.3 DR specific changes of the faecal microbiome

To study whether the DR microbiome represents a “younger” AL-like microbiome or if it has an independent profile, two machine learning models were built; one model to classify samples as either AL or DR, and a second model to predict biological age of AL mice. First, to identify

which ASVs are most relevant in drawing a distinction between AL and DR, a Random Forest classifier was modelled using 70% of AL and DR mice. The model classified the remaining 30% of mice as fed AL or DR with an accuracy of 98.17%, and an out of bag estimate of error rate of 1.57% (Fig 2.5A). Out of 2591 studied ASVs, 571 (19.3%) were identified as being relevant to distinguish between AL and DR, i.e. bacterial markers of DR. Second, to study the characteristics of the ageing microbiome, an age predictor of AL samples was modelled using an Elastic Net. To avoid predicting biological age confounded by diet-specific bacteria, 70% of AL mice only, were used to build the ageing model. Testing of the remaining 30% of AL mice on the model reported high accuracy (95%) and low mean absolute error (0.163) (Fig 2.5B). Tenfold cross-validation of the Elastic Net AL-age-predictor, showed that the best model to predict biological age was based on 107 (4.1%) ASVs. However, when DR samples were run in the AL-age-predictor, the age-assignment was random (Fig 2.5B). Therefore, the DR microbiome does not seem to represent a “younger-like” state of AL microbiome; it encompasses a rather distinct microbiome in itself.

Next, to evaluate the impact of repeated measurements of the microbiome throughout age, AL and DR diets, compositional tensor factorization was used to deconvolute microbiome dynamics (Martino et al. 2021). The tensors corresponding to each Bray-curtis beta diversity were visualised using principal coordinates analysis (PCoA), revealing that the first coordinate, explaining 77.3% of the variation, separated the samples according to diet, while the second coordinate, explaining 22.6% of the variation separated the samples according to age (Fig 2.5C). These results were consistent with our observations that the Random Forest classifier found a higher percentage of bacteria differentiating between AL and DR, than the Elastic net AL-age-predictor in predicting age (Fig 2.5A-B). Thus, these results suggest that DR has a stronger impact on the microbiome than age.

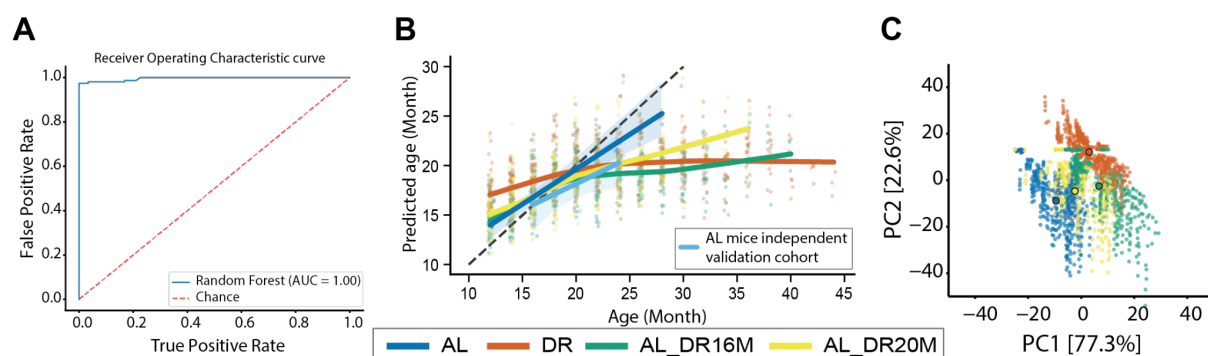


Figure 2.5: A) Random Forest classifier receiver operating characteristic curve. **B)** Elastic net AL-age-predictor, predicted age (y-axis) versus chronological age (x-axis). **C)** PCoA of compositional tensor factorization of Bray-Curtis beta diversity.

In order to validate the machine learning models to predict dietary regime and age, we performed 16S rRNA sequencing on mice from an independent (cross-sectional) ageing cohort: 20 AL mice and 15 DR (aged 5, 16, 20 and 24 months; [Chapter 3](#)). 5 months old AL and DR animals were included to address the effect of DR on the microbiome at young age. The Random Forest model correctly classified 33 (94.2%) samples as AL or DR mice. Only 2 5-month-old DR mice were erroneously classified as AL (out of five DR 5-month-old; 40%). Further, when evaluated using the previously built AL-age-predictor, the age of AL mice between 16 and 24 months of age, was also accurately predicted ([Fig 2.5B](#)). These findings indicate that at 5 months of age, 2 months after starting DR, the DR microbiome is still not as different from AL as in older animals.

To identify the bacterial taxa that are differentially abundant between AL and DR longitudinally, we used GLME. 213 ASVs were identified as longitudinally different between AL and DR. The 213 ASVs identified by GLME were also found as important to differentiate between AL and DR in the Random Forest classifier ([Fig 2.6](#)). Similar to previous reports in ageing studies performed on AL and DR mice; while most bacteria with significantly higher abundance in AL mice pertained to the phylum *Firmicutes* (~95%), DR mice had differentially higher abundances of *Firmicutes* (~58%) and of *Bacteroidetes* (~38%) (Ke et al. 2021; J. Xu et al. 2016; C. Zhang et al. 2013; Kok et al. 2018; Duszka et al. 2018).

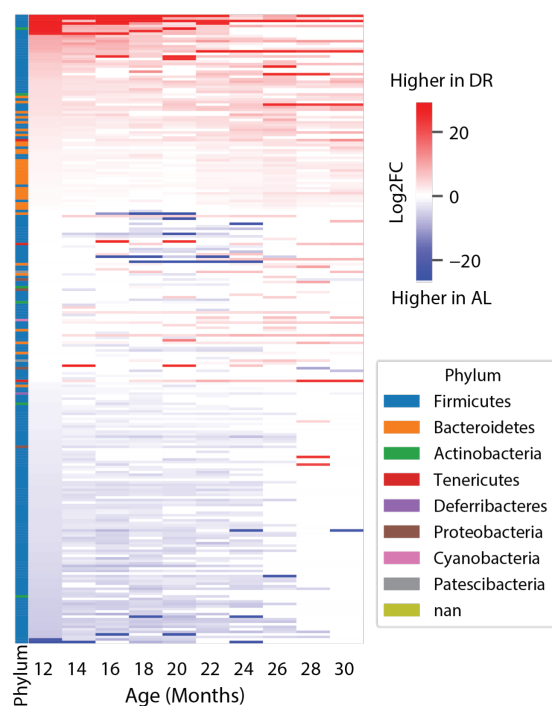


Figure 2.6: Heatmap of 213 longitudinally differently abundant bacteria between AL and DR. Log₂FC of bacteria abundance was calculated using DESeq2 for each individual time point. Differential abundance adjusted p-values for each time point in Supplementary file 1.

2.2.4 The ability of the microbiome to adapt to a DR-like pattern is high but declines with age

Initiating DR at 16 months of age (AL_DR16M) is sufficient to extend lifespan in mice almost to the same degree as chronic lifelong DR. In contrast, onset of DR at 20 months of age (AL_DR20M) does not significantly extend lifespan (Drews et al. 2021). In order to address whether this age-dependent response in lifespan to DR is also reflected in changes of the microbiome, we performed 16S rRNA sequencing on longitudinally collected faecal samples from AL_DR16M and AL_DR20M mice past their respective switch.

First, to evaluate differences between diets in the distribution of relative abundance of ASVs in the microbiome population, alpha diversity was studied. In both AL_DR16M and AL_DR20M mice, there was a two-phase response to the switch to DR diet. After onset of DR, there was an acute decrease in alpha diversity, followed by increased alpha diversity in the long-term (Fig 2.2A). To evaluate the short-term effect of the diet-switches (i.e. how fast the microbiome population structure from each group of mice adapted to DR-like alpha diversity), windows were defined as the faecal collections spanning the last time point before diet switch (baseline), and 6 months after start of DR diet (age 14 months to 22 were evaluated for AL_DR16M, and 18 to 26 for AL_DR20M). After overlapping the windows corresponding to AL_DR16M and AL_DR20M, and comparing their slopes using linear regression, we found significantly different slopes (speeds) of alpha diversity response to introduction of DR diet between AL_DR16M and AL_DR20M. Interestingly, the speed of alpha diversity decrease was higher in AL_DR16M mice (Fig 2.2A), suggesting that with younger age, changing diets had a stronger acute effect on the microbiome population structure. Furthermore, evaluation of the long-term effects of AL_DR16M and AL_DR20M on the alpha diversity, in a longitudinal manner, revealed similar responses to the diet switch. AL_DR16M mice became significantly higher than AL, but were not significantly different from DR (Fig 2.2A). On the other hand, alpha diversity of AL_DR20M mice significantly increased compared to AL, but did not significantly recapitulate the DR-like structure (Fig 2.2A). Therefore, with younger age, changing diets had a stronger acute effect on the microbiome population structure, and AL_DR16M mice recapitulated the DR-like microbiome community structure in the long-term.

Next, to investigate the differences in microbiome community dynamics between samples, we quantified distances between bacterial communities of these mice. After onset of DR, there was also a two-phase effect on beta diversity. Short-term effects generated a steeper slope of beta diversity change (higher speed) in AL_DR16M when compared to AL_DR20M in the 6 months window after starting of DR (Fig 2.2B). The steeper slopes of alpha and beta diversity after starting the DR diet in AL_DR16M mice highlight the acute response of the young microbiome to the new diet. Furthermore, evaluation of the long-term effects on Bray Curtis beta diversity, revealed that AL_DR20M mice did not fully recapitulate the DR intra-individual variability (Fig 2.2B). However, they significantly reduced their intra-individual variability compared to AL (Fig 2.2B), rather remaining in between AL and DR. Taken together, switching to DR diet at both 16 and 20 months of age reverts the age-related decline in alpha and increase in beta diversity, but to a larger extent when DR is started at 16 months of age.

We next asked whether the acute changes in the microbiome structure of late-life DR switch animals occurred via changes in the relative abundance of pre-existing bacteria, or through gain or loss of bacteria. Therefore, we calculated two more beta diversity metrics that use a phylogenetic tree of relationship among taxa as central information: unweighted UniFrac, which only considers the presence or absence of taxa, and weighted UniFrac, which accounts for the relative abundance of taxa and their phylogenetic distance (Lozupone et al. 2013). In both DR switch groups the same pattern emerged on the first time point measured after starting DR, i.e. 18 and 22 for AL_DR16M and AL_DR20M, respectively. There was significant grouping by diet in unweighted UniFrac (Fig 2.7A), but not in weighted UniFrac (Fig 2.7B). This suggests that the microbiome of both AL_DR16M and AL_DR20M responds to the diet switch through an acute remodelling of the microbiome structure, where the effects of gain/loss of taxa (unweighted UniFrac) occur later than the changes in relative abundance of taxa (Weighted UniFrac). Thus, changes in the abundance of pre-existing bacteria primarily govern the acute response of the microbiome to DR initiation.

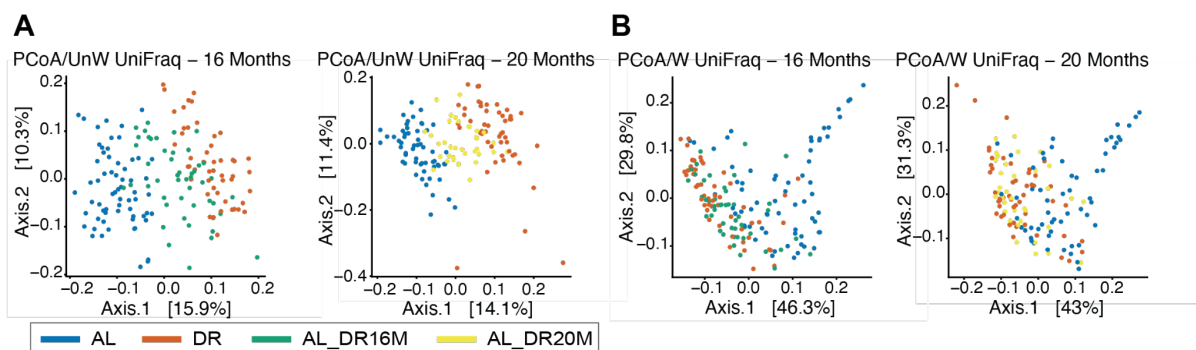


Figure 2.7: Principal coordinate analysis of **A)** Unweighted UniFrac after the start of DR. Significant

clustering of samples (ANOSIM): diet (AL_DR16M vs DR vs AL p-value = 0.001; AL_DR20M vs DR vs AL p-value = 0.001). **B**) Weighted UniFrac after the start of DR.

In order to test whether the microbiome populations after onset of DR at 16 or 20 months of age recapture the DR-like microbiome (Fig 2.5A), we evaluated AL_DR16M and AL_DR20M microbiomes in two ways. First, the faecal samples from AL_DR16M and AL_DR20M were classified using the Random Forest classifier to predict diet treatment (Fig 2.5A). Before switching to DR, faecal samples from AL_DR16M and AL_DR20M were correctly classified as AL (accuracy of 100%) (Fig 2.8A). However, after the start of DR, while the AL_DR16M was classified as DR with an accuracy above 90% in all time points, the AL_DR20M was classified as DR with lower accuracy, reaching as low as 65% (Fig 2.8A). Second, we used principal response curves (PRC) (Fuentes et al. 2014; Vendrig, Hemerik, and ter Braak 2017) to evaluate the longitudinal temporal trends of ASVs after DR onset. PRCs use redundancy analysis (RDA) allowing for temporal trends and interaction between explanatory variables in the control group to be corrected for, facilitating the estimation of the effects from the diet groups. Immediately after the start of DR in both AL_DR16M and AL_DR20M, there was a significant divergence from AL microbiome (Sup File 1; Fig 2.8B). However, while the AL_DR16M group fully recapitulated the microbiome pattern of DR mice, the microbiome of AL_DR20M only partially adapted to the DR-like state (Fig 2.8C). Interestingly, the microbiome of the most long-lived AL mouse (sole survivor from 34 months of age until death at 38 months), also converged to a DR-like microbiome, and was indistinguishable from that of DR mice in the last time points (Sup File 1; Fig 2.8C). In summary, the ability of the microbiome to adapt to DR-like patterns after diet switch is high, but progressively decreases the later DR is initiated.

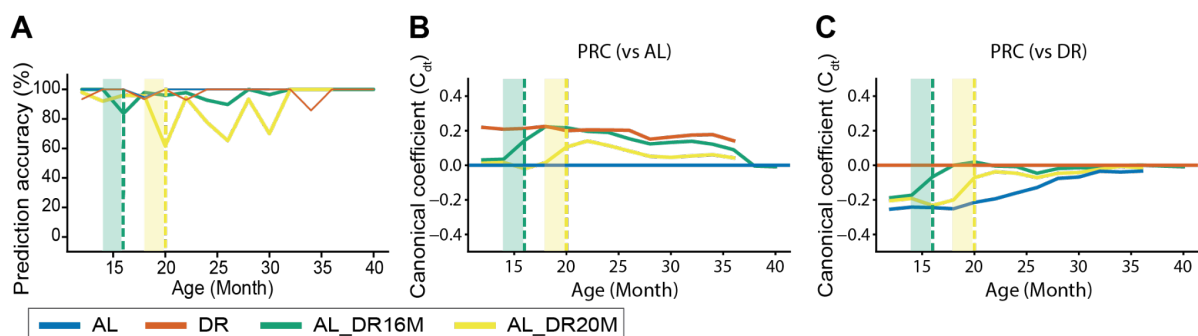


Figure 2.8: A) Prediction accuracy of Random Forest classifier as AL (before dotted line) and DR (after dotted line). **B)** Principal response curve of microbiome compared to AL. **C)** Principal response curve of microbiome compared to DR. Green and yellow shaded areas correspond to time between

faecal collections before and after onset of DR. Adjusted p-values for Monte Carlo permutations between diets of PRC in Supplementary File 1.

2.2.5 DR switch-resistant ASVs - Candidates for a microbiome memory of AL feeding

To identify bacteria that correlate with the response in longevity, “DR-specific” bacteria, ASVs identified as significantly different from DR in AL, AL_DR16M and AL_DR20M mice using both PRCs and GLME models were analysed. Of the 213 ASVs that were longitudinally different between AL and DR (Fig 2.5), 70 (33%) were longitudinally different between AL_DR16M and DR (Fig 2.9A), and 67 (31%) were different between AL_DR20M and DR (Fig 2.9B), indicating there are “switch resistant” bacteria that do not recapitulate the levels of DR after diet switch. The amount of “switch-resistant” bacteria was not significantly different between AL_DR16M and AL_DR20M (chi squared p-value = 0.3). Interestingly, of the bacteria differentially abundant between the switched groups and DR, only 32 (15%) were different between AL_DR16M vs DR, and also between AL vs DR (Fig 2.9A). And 44 (21%) were different between AL_DR20M vs DR, and also between AL vs DR (Fig 2.9B). These findings were similar to the results obtained from the random forest classifier and PRCs, where we observed that the ability of the microbiome to recapitulate the DR-like pattern was slightly higher in AL_DR16M than in AL_DR20M (Fig 2.8A-C). Notably, there were 14 “DR-specific” ASVs that did not adapt to DR-like abundances after changing diets at either 16 or 20 months of age (Fig 2.9A-C; Sup Fig 2.1A). To further understand their interactions as a community, a co-inertia network of the 14 “DR-specific” bacteria was generated by calculating repeated measures correlation between bacteria, to include the longitudinal aspect of the dataset in the model (Fig 2.9C). The most connected bacteria, all highly abundant in DR mice, were *Christensenellaceae*, *Lachnospiraceae*, and *Ruminococcaceae*, producers of short-chain fatty acids (SCFA). These “DR-specific” bacteria are candidates for a microbiome memory of AL feeding. Bacteria under a microbiome memory of AL feeding, could be associated with the decreased health span and slightly reduced maximum lifespan reported in AL_DR16M and AL_DR20M when compared to DR (Drews et al. 2021).

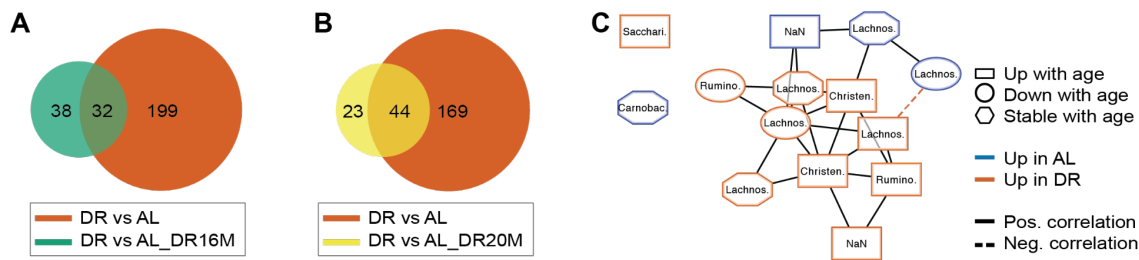


Figure 2.9: Venn diagrams depicting the overlap of longitudinally differentially abundant bacteria genus comparing DR to **A)** AL_DR16M and **B)** AL_DR20M. **C)** Repeated measures co-inertia network of ASVs of microbiome memory of AL feeding; DR-specific bacteria. Adjusted p-values for longitudinally different bacteria between DR vs AL, DR vs AL_DR16M, and DR vs AL_DR20M in Supplementary File 1.

2.2.6 Identification of bacteria associated with DR-mediated longevity

Having identified bacteria involved in a microbiome memory of AL feeding, we sought to identify bacteria that could be associated with the improved longevity reported in AL_DR16M when compared to AL_DR20M mice (Drews et al. 2021) (Fig 2.1). ASVs possibly associated with DR-mediated longevity, were defined as those that recapitulated DR relative abundances in AL_DR16M mice, but not in AL_DR20M (Fig 2.9A-B). 30 DR-mediated longevity ASVs were identified (Fig 2.10A; Sup Fig 2.1B). Including the longitudinal aspect of the dataset in the model, we calculated repeated measures correlation between possible DR-mediated longevity bacteria, and evaluated the co-inertia relationships as a network (Fig 2.10A). The network differentiated two groups of ASVs negatively correlated with each other: one where abundance was high in AL mice, and another where abundance was high in DR mice (Fig 2.10A; Sup Fig 2.1B). The latter was also characterised by being more densely connected, suggesting tighter community structure interaction through age in the ASVs highly abundant in DR mice. Furthermore, the ASVs more abundant in AL were mostly *Firmicutes* such as *Lachnospiraceae*. While ASVs adapted to DR abundances in AL_DR16M mice, that had higher abundance through age in DR mice compared to AL, encompassed not only *Firmicutes*, but 30% of them were *Bacteroidetes*, including *Rikenellaceae*, *Muribaculaceae* and *Lactobacillaceae* genera (Sup Fig 2.1B). Therefore, these bacteria may also be a contributing factor to both, the improved health and longevity reported in mice fed DR starting at 16 months of age (Drews et al. 2021).

To further study the association of AL_DR16M bacteria that adapted to DR-like abundances, with the DR-mediated longevity, we studied the relationship between faecal samples of DR,

AL_DR16M and AL_DR20M at 24 months (after both AL_DR16M and AL_DR20M have reached similar bacterial profiles as DR; Fig 2.8C), and age at death. We iteratively studied each of the 30 ASVs by separating mice into two groups based on their ASV abundance (i.e. above or below the mean of abundance), and we assessed the prognostic value of these ASV biomarkers by calculating univariate Cox regressions. Given that the 30 bacteria in study had significantly different abundance between AL and DR, (2.9A-B; Sup Fig 2.1B), AL samples were not evaluated in this model. Two out of 30 ASVs evaluated were significantly associated with longevity in our mouse cohort at adjusted p-value < 0.05 (ASV17 *Muribaculaceae* and ASV224 *Clostridiales*) (Fig 2.10B-C). Therefore, these results not only indicate there are multiple microbiome bacteria associated with ageing patterns, but also identify possible biomarkers of DR-mediated longevity in mice.

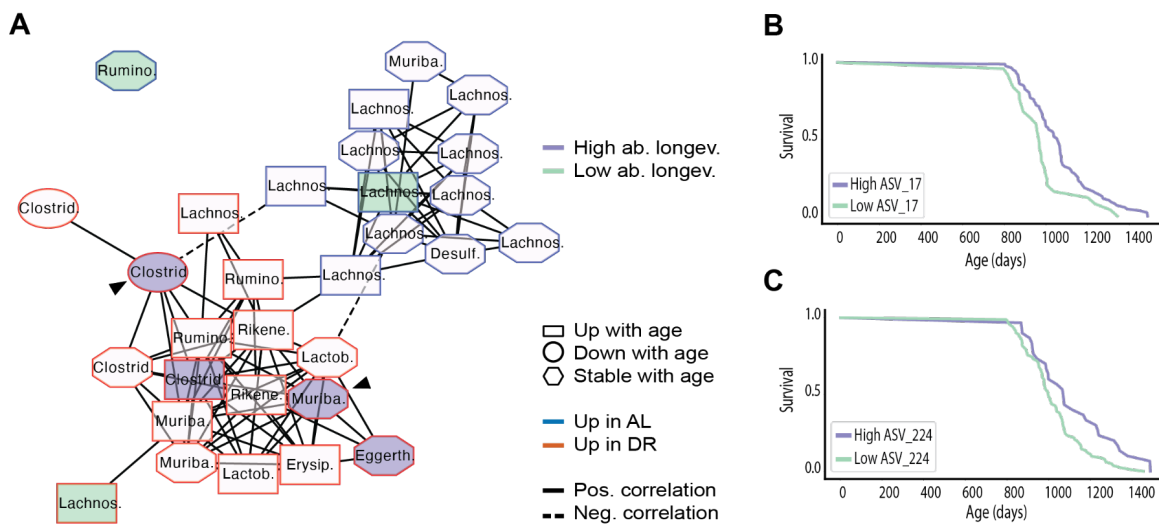


Figure 2.10: A) Repeated measures co-inertia network of the 30 ASVs adapting to DR-like abundances in AL_DR16M but not in AL_DR20M. Black arrowheads point to ASVs significantly associated with longevity by Cox univariate regression. **B)** Kaplan-Meier curve demonstrating the association between overall survival and abundance of Muribaculaceae (Cox regression adjusted p-value = 0.01) and **C)** Clostridiales (Cox regression adjusted p-value = 0.006). Adjusted p-values for longitudinally different bacteria between DR vs AL, DR vs AL_DR16M, and DR vs AL_DR20M in Supplementary File 1.

2.2.7 Identification of bacteria species associated with a microbiome memory of AL feeding or DR-mediated longevity

16S rRNA sequencing only allows to identify bacteria on the genus level, while information about bacteria species and strains cannot be retrieved. In order to better characterise DR associated microbiome changes also on the species level, we performed shotgun metagenomics using 24-month-old mice of each diet group (AL, DR, AL_DR16M and AL_DR20M). The 24 months time point represents the time after both AL_DR16M and AL_DR20M have reached similar microbiome composition as DR (Fig 2.8C). Superimposition of the 16S rRNA sequencing and shotgun metagenomics datasets confirmed that they represented the same variance between samples (procrustes with 999 permutations, p-value = 0.001), and ANOSIM corroborated significant clustering according to diets in the shotgun metagenomics dataset (p-value = 0.007).

Here, we reported “DR-specific” bacteria genera associated with a microbiome memory of AL feeding (Fig 2.9C). To investigate the bacteria species under a microbiome memory of AL feeding, species significantly different from DR by means of DESeq2 were analysed. Of the 288 bacteria species significantly different between DR and AL (Fig 2.11A-B), 21 (7.3%) were significantly different between AL_DR16M and DR (Fig 2.11A), and 24 (8.3%) were different between AL_DR20M and DR (Fig 2.11B). The proportion of these “switch-resistant” species was different between AL_DR16M and AL_DR20M (chi squared p-value = 0.005). 7 (2.4%) bacteria different between AL_DR16M and DR were different between DR and AL (Fig 2.11A), while in the case of AL_DR20M mice, there were 13 (4.5%) species (Fig 2.11B). Furthermore, there were 2 “DR-specific” bacteria species that did not adapt to DR-like abundances after late-onset DR regimen: *Lachnospiraceae sp000403845* and *Anaeroplasmataceae UMGS268* had significantly higher abundance in DR compared to all other treatment groups (Sup Fig 2.2A). Taken together, high abundance of *Lachnospiraceae sp000403845* and *Anaeroplasmataceae UMGS268* specific of chronic DR mice may contribute to the improved health and lifespan of these mice compared to AL_DR16M and AL_DR20M mice (Drews et al. 2021).

Next, we sought to identify bacteria species associated with DR-mediated longevity. Eleven DR-mediated longevity species were identified (Fig 2.11A-B; Sup Fig 2.2B). Four *Lachnospiraceae* (*TF01-11-MCGC-nov-622*, *14-2-MCGC-nov-380*, *UBA7182-MCGC-nov-266* and *Eubacterium-J-MCGC-nov-279*) and *Erysipelatoclostridiaceae CHKCI006-MCGC-nov-506*, had significantly higher abundance in AL and AL_DR20M compared to DR and AL_DR16M mice (Sup Fig 2.2B). While *Prevotellamassilia sp002933955* and five *Clostridia*

(*Oscillospirae P3106-MCGC-nov-344*, *UBA3700-MCGC-nov-147*, *UBA3700-MCGC-nov-146*, *CAG-552-MCGC-nov-154*, and *Borkfalkiaceae-MCGC-nov-237*) were significantly enriched in DR and AL_DR16M (Sup Fig 2.2B). The abundance and interaction of these 11 bacteria species might be associated with DR-mediated longevity, and the improved longevity of AL_DR16 mice compared to AL_DR20M and AL.

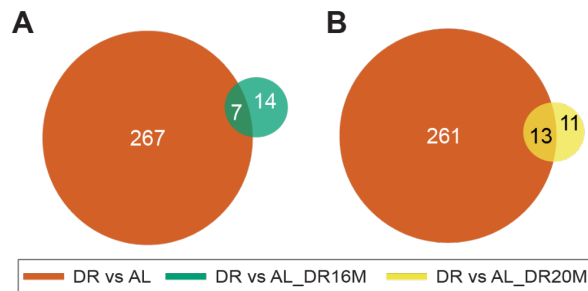


Figure 2.11: Venn diagrams depicting the overlap of differentially abundant bacteria species at 24 months of age comparing DR to **A)** AL_DR16M and **B)** AL_DR20M. Adjusted p-values for differential abundance analysis in Supplementary File 1.

2.2.8 A longitudinal high-resolution analysis of the ageing murine faecal metabolome

The microbiome influences ageing and metabolism indirectly, through production of metabolites during digestive processes (Bana and Cabreiro 2019; Krautkramer, Fan, and Bäckhed 2021). To investigate the faecal metabolomic response to the observed age- and DR-related changes in the microbiome composition, we explored faecal metabolites extracted from the same faecal pellet used for microbiome analysis. Additionally, to study different metabolome characteristics that may be associated with differences in lifespan within treatment groups, 438 samples were run on a mass spectrometer, corresponding to all studied time points of a subset of mice with age at death in the median (centre-lived) or maximum lifespan (long-lived) of their diet group (n = 10 for AL, DR, AL_DR16M and AL_DR20M; Fig 2.12). To cover as many metabolites as possible, we generated two datasets: untargeted polar (4295 detected), and untargeted non-polar (2161 detected) metabolites, that enable unbiased profiling of the faecal metabolome, representing polar (amino acids, nucleic acids, small organic acids etc.) and non-polar (lipids), respectively. However, it is challenging to connect metabolites from untargeted data generation to specific pathways, as most are unknown and remain unannotated.

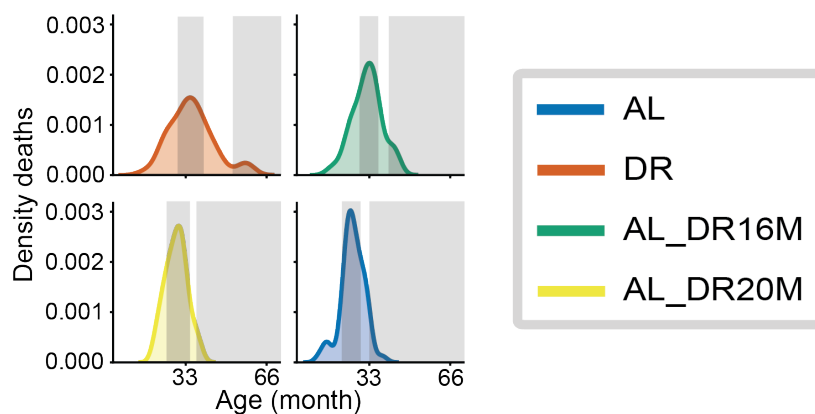


Figure 2.12: Density distribution of mice deaths. Grey areas represent median and maximum lifespan. n = 5 mice per grey area.

To study ageing trends in metabolites abundance and identify those metabolites most affected by age, linear regressions were run on the longitudinal metabolites of AL mice. 450 (10.5%) untargeted polar metabolites increased with age, and 235 decreased (5.5%; Fig 2.13A). Untargeted non-polar metabolites distinguished 375 (17.3%) metabolites increasing with age, and 77 decreasing (3.6%; Fig 2.13B). There was no significant difference between upregulation or downregulation of metabolites with age in polar metabolites (chi squared p-value = 0.3), but there was a significant age-associated upregulation in non-polar metabolites (chi squared p-value = 0.005). Next, to assess whether DR mice had similar metabolite ageing patterns as AL mice, linear regressions were run on the longitudinal metabolites of DR mice. There was no significant difference in age-related up- or downregulation of polar metabolites in DR mice (chi squared p-value = 0.07); 1077 (25%) polar metabolites increased with age, and 604 decreased (14%; Fig 2.13C). However, there was a significant upregulation of non-polar metabolites with age (chi squared p-value = 10^{-5}); 1060 (49%) untargeted non-polar metabolites increased with age, and 298 decreased (13.8%; Fig 2.13D). Nevertheless, there was a significantly higher amount of common upregulated polar and non-polar metabolites between AL and DR (12.9% and 3.2%, respectively) than common downregulated (1.3% and 1.2%, respectively) (chi squared p-value < 10^{-5} for both polar and non-polar metabolites). Therefore, similar to the results from AL mice, DR mice underwent a general upregulation of faecal metabolites with age.

To evaluate differences in ageing trends of long- and centre-lived mice, linear regressions were calculated and proportion of affected metabolites were compared. Long-lived mice had more metabolites affected by age than centre-lived animals (chi squared p-value < 10^{-5} for both polar and non-polar metabolites; Sup Fig 2.3A). Interestingly, a group of metabolites

affected by age only appeared due to the high abundance during the latest timepoints, affecting specially the non-polar metabolites (Fig 2.13A-D; Sup Fig 2.3B). This could be a result of the bias of selection in the mice, as we studied centre-lived and long-lived mice of each treatment (Fig 2.12). Thus, ageing trends of metabolites from centre-lived and long-lived mice were evaluated. There was a general upregulation of polar and non-polar faecal metabolites with age in both AL and DR mice (chi squared p-value < 10^{-5} in all cases; Sup Fig 2.3A-C). Furthermore, there was an upregulation of metabolites during the latest timepoints only in the long-lived mice (chi squared p-value < 10^{-5} ; Sup Fig 2.3B-C), suggesting the faecal metabolome of centre-lived and long-lived mice right before death was different.

To evaluate whether different longitudinal faecal metabolome characteristics are associated with differences in lifespan within treatment groups, longitudinal metabolite abundances of mice with median or maximum lifespan were compared (Sup Fig 2.3B-C). Thirteen (0.3%) unannotated polar metabolites differentiated median-lived and long-lived AL_DR16M mice, and 9 (0.2%) unannotated polar metabolites AL_DR20M mice (Sup File 1). Furthermore, differences in non-polar metabolite abundances between median-lived and long-lived mice were only evident by 56 (2.6%) unannotated metabolites in DR, and 14 (0.6%) in AL_DR16M mice (Sup File 1). However, AL mice had no significant metabolites differentiating longevity. These few different metabolites identified by means of longitudinal analysis of metabolites between the ages of 12 months and the age of death of centre-lived mice within each treatment group (22 months for AL and 34 for DR) (Sup Fig 2.3B-C), indicate there are only few differences between centre-lived and long-lived mice during their early lives. The observed metabolic signal suggested longevity within late-onset DR groups was affected by amino acids, while the longest-lived treatments (DR and AL_DR16M) had a longevity signal involving lipids.

To evaluate the differences between DR and AL ageing metabolites, longitudinal age-dependent trajectories of faecal metabolites were evaluated. GLME models to study longitudinal changes of metabolites were calculated, and differential abundance analysis of metabolites in each time point was performed (Fig 2.13E-F). Compared to AL, there was high upregulation of DR metabolites in both metabolite fractions (Fig 2.13E-F). However, DR mice had higher abundances of spermidine and putrescine, while ageing effects in AL mice involved upregulation of bile acids and glycine deoxycholic acid, thus suggesting different ageing patterns depending on diet.

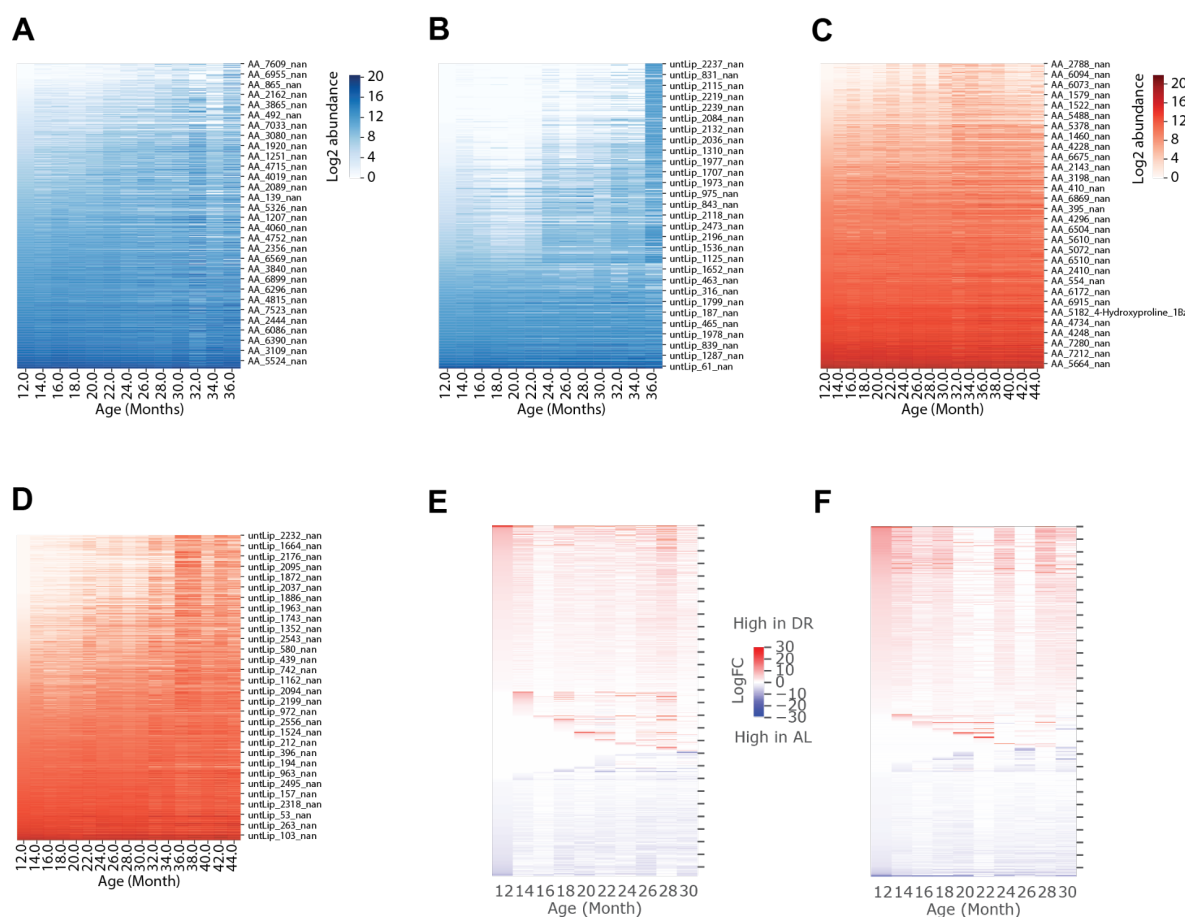


Figure 2.13: Heatmaps depicting ageing metabolites trends of AL mice in **A)** untargeted polar, and **B)** untargeted non-polar. Heatmaps of ageing trends of DR mice in **C)** untargeted polar, and **D)** untargeted non-polar metabolites. Heatmaps of longitudinally differentially abundant metabolites between AL and DR for **E)** untargeted polar, and **F)** untargeted non-polar. P-values of linear regressions through age, GLME to compare longitudinal changes between AL and DR, and per time point differential abundance analysis of metabolites in Supplementary File 1.

2.2.9 The ability of the faecal metabolome to diverge from AL is high but decreases with older age of DR onset

To study the effects of late-onset DR on the faecal metabolome composition and structure, we studied the faecal metabolome of AL_DR16M and AL_DR20M mice in comparison to AL and DR controls. First, ANOSIM on the distance matrix quantifying dissimilarity between samples for each metabolomics dataset (Bray-Curtis), revealed significant clustering according to mouse, age and diet (Fig 2.14A-B). Further, for both polar and non-polar metabolites, DR and AL were the most distant clusters of samples, while the AL_DR16M and AL_DR20M samples grouped closer to DR and AL, respectively (Fig 2.14A-B). To study the faecal metabolome

response to DR onset in a longitudinal manner, PRCs were calculated and temporal trends evaluated (Fig 2.14C-D). For both polar and non-polar metabolites, PRCs of DR mice were significantly different from AL (Fig 2.14C-D). However, there was a significant divergence from AL faecal metabolites in both polar and non-polar fractions immediately after the start of DR in both AL_DR16M and AL_DR20M (Fig 2.14C-D). In AL_DR16M mice, this divergence from AL lasted for ~10 months in both polar and non-polar metabolites (Fig 2.14C-D), and ~6 months in AL_DR20M mice; after this time, the metabolome profiles reverted back to those of AL mice (Fig 2.14C-D). Given that our data set contained centre-lived and long-lived mice of each treatment (Fig 2.12), we next evaluated whether the observed convergence into AL-like faecal metabolome of AL_DR16M and AL_DR20M mice at ~26 months might be explained by a bias between the two longevity cohorts, i.e. because all centre-lived AL mice were dead before 26 months. PRCs for centre-lived and long-lived mice were calculated independently. While there was no convergence in the centre-lived mice, a similar pattern of convergence was observed in the long-lived mice (Sup Fig 2.4A-B). Thus, long-lived AL_DR16M and AL_DR20M mice had more similar faecal metabolome profiles to long-lived AL than to DR. Surprisingly, this pattern did not occur in the microbiome (Sup Fig 2.4C). Not only was there a faecal metabolomic memory of the previous AL feeding, but also the response to late-onset DR was not different from the metabolome of AL mice with maximum lifespan.

To further assess the different metabolic responses to age of DR onset, PRCs including DR mice as reference baseline were calculated (Fig 2.14E-F; Sup Fig 2.4A-B). Corroborating the observations from sample comparisons to AL mice, AL_DR16M and AL_DR20M mice adapted to DR-like levels for similar periods of time in the untargeted polar and non-polar datasets (~8 and ~4 months respectively) (Fig 2.14E-F; Sup Fig 2.4A-B). Thus, switching to DR at 16 months had a longer lasting impact on the faecal metabolome than starting DR at a later time point. However, at 26 months of age they had converged into AL-like profiles, until switching back into DR-like faecal metabolomes at ~34 months of age, when the only the 3 longest-lived AL_DR16M and AL_DR20M mice, and the longest-lived AL mouse remained alive (Fig 2.14E-F; Sup Fig 2.4A-B). These results suggest that the longest-lived mice between diet groups have the most similar faecal metabolomic profiles at the end of their lives.

Taken together, although the longitudinal faecal metabolomic profiles diverged from AL for a longer period when 16-month-old mice were switched to DR, the faecal metabolome of DR mice was not fully recapitulated in the long-term by onset to DR at 16 or 20 months. There was a faecal metabolomic memory of AL feeding impeding full adaptation to DR-like patterns, and metabolites diverging differently from AL between AL_DR16M and AL_DR20M mice could also be associated with differences in the lifespan of these mice

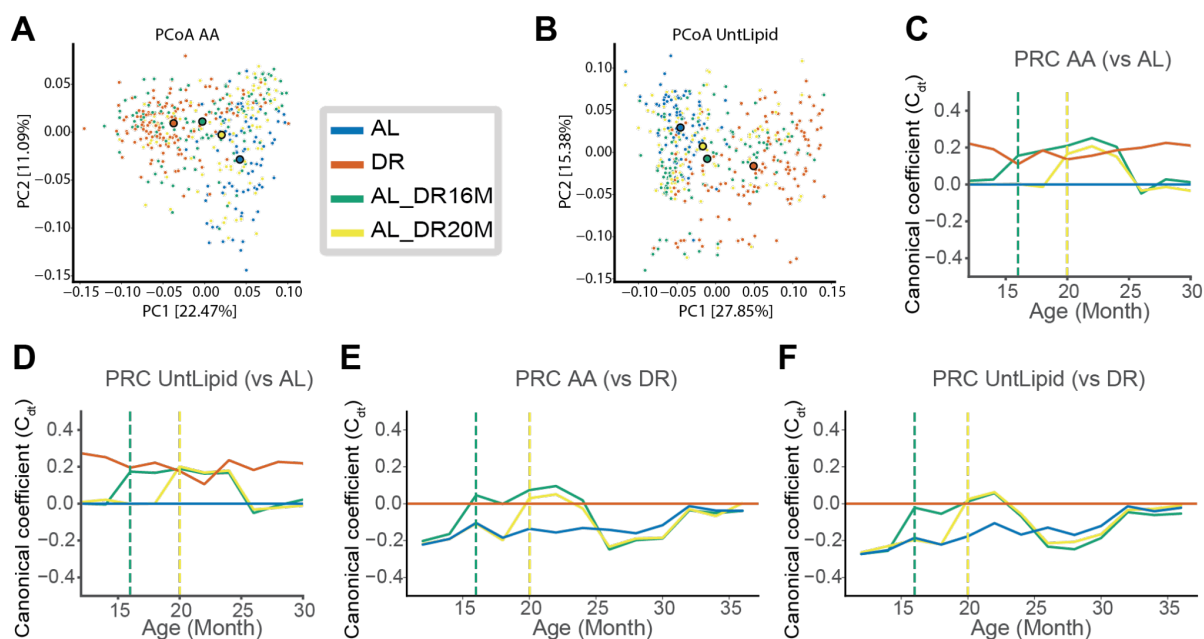


Figure 2.14: **A)** PCoA of Bray-Curtis distances between samples for polar untargeted metabolites. Significant clustering of samples (ANOSIM): mouse p-value = 0.001; age p-value = 0.001; diet p-value = 0.001. **B)** PCoA of Bray-Curtis distances between samples for non-polar untargeted faecal metabolites. Significant clustering of samples (ANOSIM): mouse p-value = 0.001; age p-value = 0.001; diet p-value = 0.001. **C)** PRCs of faecal metabolomes compared to AL for polar untargeted metabolites. **D)** PRCs of faecal metabolomes compared to AL for non-polar untargeted faecal metabolites. **E)** PRCs of faecal metabolomes compared to DR for polar untargeted metabolites. **F)** PRCs of faecal metabolomes compared to DR for non-polar untargeted faecal metabolites. Minimum of 3 reference mice for PRC calculations. Adjusted p-values for per-time point Monte Carlo permutations between diets of PRCs in Supplementary File 1.

2.2.10 DR switch-resistant faecal metabolites - Candidates for a metabolomic memory of AL feeding

To investigate the faecal metabolites under a microbiome memory of AL feeding on AL_DR16M and AL_DR20M, GLME models were used to longitudinally compare metabolites between diets. First, untargeted polar metabolomics found 1551 metabolites longitudinally different between AL and DR (Sup File 1; Fig 2.15A). Of those, 289 (25.1%) were different between AL_DR16M and DR, and 993 (86.3%) were different between AL_DR20M and DR (Sup File 1; Fig 2.15A). Second, untargeted non-polar metabolomics found 919 metabolites longitudinally different between AL and DR (Sup File 1; Fig 2.15B). Of those, 402 (43.9%) were different between AL_DR16M and DR, and 671 (73.1%) were different between

AL_DR20M and DR (Sup File 1; Fig 2.15B). There was a significantly lower proportion of polar and non-polar metabolites affected by DR onset at 16 months than onset at 20 months (chi squared p-value < 10⁻⁵). Therefore, there were microbial metabolites under a memory of AL feeding that was stronger the longer mice were originally fed AL i.e. higher memory in AL_DR20M than in AL_DR16M mice. The untargeted polar metabolomics dataset encompassed the strongest difference in AL memory between AL_DR16M and AL_DR20M, while the untargeted non-polar metabolites (lipids) were the most switch-resistant of the studied metabolite fractions.

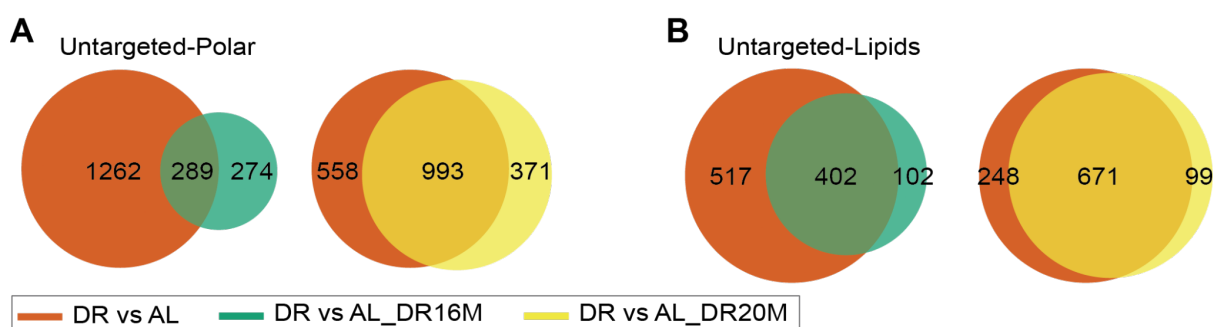


Figure 2.15: Venn diagrams depicting the overlap of longitudinally differentially abundant metabolites comparing DR to AL_DR16M and AL_DR20M. **A)** Untargeted polar metabolites. **B)** Untargeted non-polar metabolites. Adjusted p-values of longitudinal GLME analysis of metabolites between diets in Supplementary File 1.

To unravel the “DR-specific” functional profiles, and those associated with DR-mediated longevity, the 100 annotated polar metabolites were evaluated using GLME models. We identified 16 switch-resistant metabolites in AL_DR20M mice (Fig 2.16A-B), encompassing the 7 switch-resistant metabolites found in AL_DR16M mice (Fig 2.16A and Sup Fig 2.5A): S-adenosyl methionine, histamine, tryptamine, N2-acetylornithine, adenine, alpha-aminobutyric-acid and glycine-deoxycholic-acid. Network analysis of the co-inertia interactions of these metabolites revealed a highly connected network where metabolites abundantly found in DR were negatively correlated to those abundantly present in AL mice (Fig 2.16A). These “DR-specific” faecal metabolites representing a microbiome memory of AL feeding, could be associated with the reduced health and lifespan of mice starting DR late in life (Drews et al. 2021).

To identify faecal metabolites that could be associated with the improved longevity reported in AL_DR16M when compared to AL_DR20M (Drews et al. 2021; Fig 2.1), metabolites that recapitulated DR-like relative abundances in AL_DR16M mice, but were switch-resistant in AL_DR20M mice were extracted (Fig 2.16B). Nine polar metabolites recapitulating DR levels

in AL_DR16M were identified (Fig 2.16B and Sup Fig 2.5B): gamma-glutamyl-L-putrescine, tryptophane, alanine-glycine, arginine, N-acetylspermidine, tyrosine, lysine, histidine and aspartic acid. Thus, these 9 metabolites possibly associated with DR-mediated longevity, may be involved in the improved survival response of AL_DR16M mice.

Taken together, although there is a strong faecal metabolomic memory of AL feeding impeding full adaptation to the DR-like metabolome, there was an acute response to onset of DR in both AL_DR16M and AL_DR20M mice. Nevertheless, similar to the pattern observed in the microbiome sequencing data, the metabolomic memory of AL feeding was evidently stronger in AL_DR20M than in AL_DR16M. Therefore, the faecal metabolome is also a factor that may be involved in the differences in longevity between mice switched to DR diet at 16 and 20 months of age.

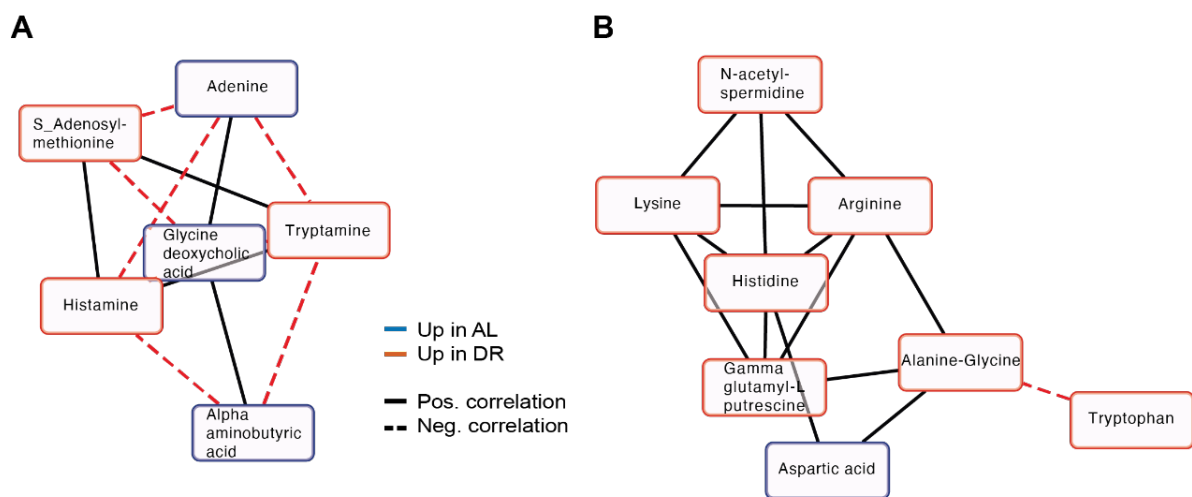


Figure 2.16: **A)** Repeated measures co-inertia network of the 7 annotated polar metabolites classified as faecal metabolome memory; DR specific metabolites. **B)** Repeated measures co-inertia network of the 9 annotated polar metabolites adapting to DR-like abundances in AL_DR16M but not in AL_DR20M. Edges represent repeated measures correlation cutoff adjusted p-value < 0.05.

2.2.11 Shared microbiome changes upon DR and reduced IIS and TOR signalling

The gut microbiome influences health and longevity (Bana and Cabreiro 2019; Ghosh, Shanahan, and O’Toole 2022). To gain further insights into this relationship, we performed 16S rRNA sequencing on faecal pellets of mice with reduced IIS and reduced TOR signalling, two nutrient pathways involved in the regulation of lifespan. To study reduced IIS, we used mice that carry a null mutation in the insulin receptor substrate 1 (*Irs1^{-/-}*) gene, which are long

lived and healthier at old age (Selman et al. 2008). Reduced TOR signalling was studied using mice fed with the TORC1 inhibitor Rapamycin. These mice are long-lived when fed continuously with Rapamycin (Fok et al. 2014). Interestingly, transient Rapamycin treatment during mid-life was also sufficient to extend lifespan in mice (Bitto et al. 2016). Furthermore, short Rapamycin treatment during early life has a long-lasting effect on gut health (Juricic et al., 2022), suggesting a memory effect of Rapamycin treatment on health and lifespan. In order to address how reduced IIS and TOR signalling affect the murine microbiome, we performed 16S rRNA sequencing on faecal samples of: *Irs1^{-/-}* and wild type control females at 6, 20 and 24-months of age (Baghdadi, 2022); mice treated continuously with Rapamycin from 3 months of age (Rapamycin-continuous), mice treated with Rapamycin only between 3 and 6 months of age (Rapamycin-memory) and control wild type at 6 and 12-months of age (Juricic et al. 2022). Analysis of α - and β -diversity revealed no significant global differences in inter- or intra-individual variability between *Irs1^{-/-}* mutant or Rapamycin treated mice compared to their respective controls at young or old age (Fig 2.17A-D). Thus, these longevity interventions only caused minor changes in the overall composition of the faecal microbiome. Consistently, Fisher's test did not find significant alterations in the microbiome composition of *Irs1^{-/-}* mice and only 0.6 % (3/464) of ASVs showed significant changes in abundance (Fig 2.18A). However, both the Rapamycin-continuous and the Rapamycin-memory treatment induced significant changes in microbiome composition with 2.16 % (10/464) of ASVs in Rapamycin-continuous, and 2.58 % (12/464) of ASVs in Rapamycin-memory mice showing significant changes in abundance compared to their respective controls (Fig 2.18A). Although the overall number of differentially regulated ASVs was low, we next addressed whether reduced TOR and IIS signalling affect similar ASVs, which might indicate a role for these bacteria in longevity. Furthermore, we also include ASVs regulated in response to DR in this analysis. As we only included 10 biological replicates in the analysis of *Irs1^{-/-}* and Rapamycin treated animals, we used a random subset of 10 AL and 10 DR mice at 12 and 20 months of age for this comparison (Fig 2.18A). Overall, there was a significantly higher amount of bacteria genera differentially regulated in response to DR than in *Irs1^{-/-}*, Rapamycin-continuous or Rapamycin-memory treated animals (Fig 2.18A), suggesting that diet has a bigger influence on the microbiome than the genetic and pharmacological longevity interventions, consistent with recent findings (Maynard and Weinkove 2018). Interestingly, we identified 5 bacteria genera that showed differential abundance in both the Rapamycin-continuous and Rapamycin-memory faecal microbiomes, suggesting a memory in the faecal microbiome of previous Rapamycin treatment (Fig 2.18A-C). Importantly, all 5 bacteria were lowly abundant in WT control mice, and their relative abundance changed dramatically under anti-ageing interventions ($\log_2FC > 7x$; Fig 2.18B-C). Three of these ASVs also showed differential abundance upon DR treatment and include the butyrate producing bacteria: *Lachnospiraceae*

UCG-001, *Ruminiclostridium 5*, and *Lachnoclostridium* (Fig 2.18B). *Lachnospiraceae* UCG-001 and *Ruminiclostridium 5* are anti-inflammatory bacteria that have been associated with modulation of circadian rhythm (Abbring et al. 2021; Thompson et al. 2021; Kim et al. 2021). *Lachnospiraceae* UCG-001 was highly enriched ($\log_2FC > 20x$) in the faecal microbiome of both Rapamycin-continuous and Rapamycin-memory animals and slightly enriched in DR animals (Fig 2.18B). In contrast, *Ruminiclostridium 5* was highly enriched in the faecal microbiome of Rapamycin-continuous animals, less enriched in Rapamycin-memory animals and depleted in DR animals (Fig 2.18C). Thus, only abundance of *Lachnospiraceae* UCG-001 was positively correlated with lifespan extension in both DR and Rapamycin treated animals. High abundance of *Lachnoclostridium* has been associated with poor health in mice with adenoma, obesity, inflammation and old age (Liang et al. 2020; Y. Zhang et al. 2020). Consistent with the improved health of Rapamycin animals, abundance of *Lachnoclostridium* was strongly depleted in the faecal microbiome of Rapamycin-continuous and Rapamycin-memory animals and slightly depleted in DR animals (Fig 2.18D). Interestingly, the other two bacteria shared between the faecal microbiomes of the Rapamycin-continuous and Rapamycin-memory groups, were also identified as differentially abundant genera in *Irs1*^{-/-} and DR animals (Fig 2.18A and 2.18C).

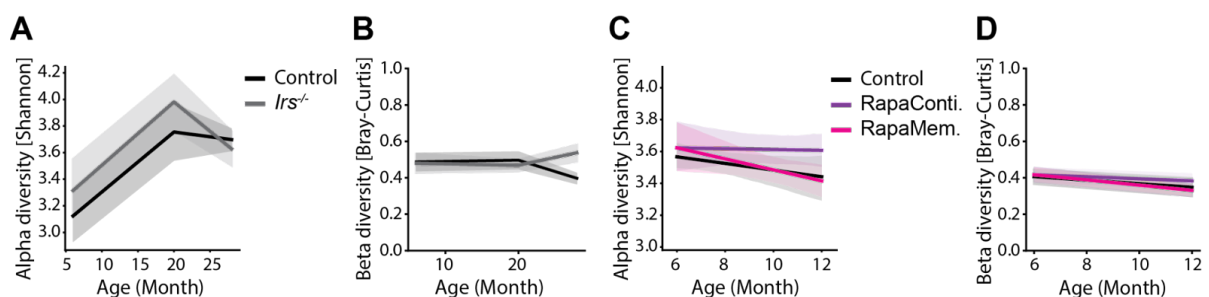


Figure 2.17: A) Shannon and B) Bray-Curtis diversity of the faecal microbiome of *Irs1*^{-/-} mutant mice. C) Shannon and D) Bray-Curtis diversity of the faecal microbiome of Rapamycin treated mice. P-values of linear regression through age, 2-way ANOVA to compare conditions through time, and Mann-Whitney between conditions in each time point, in Supplementary File 1.

These 2 bacteria genera include *Lachnospiraceae* NK4A136, which has been associated with butyrate production (Stadlbauer et al. 2020), and *Muribaculaceae*, which has been associated with extended lifespan in previous studies (Smith et al. 2019; Shenghua et al. 2020). *Muribaculaceae*, was also identified in the current work as significantly associated with DR-mediated longevity by means of Cox regression (Fig 2.10B). However, while *Lachnospiraceae*

NK4A136 was highly enriched in the faecal microbiome of all tested longevity interventions, *Muribaculaceae* was enriched in *Irs1*^{-/-}, Rapamycin-memory and DR mice, but depleted in Rapamycin-continuous mice. In summary, abundances of *Lachnospiraceae NK4A136* and *Lachnospiraceae UCG-001* were positively correlated with longevity, while the abundance of *Lachnoclostridium* was negatively-correlated with longevity. *Muribaculaceae* and *Ruminiclostridium 5* showed a more complex response, and their abundances were not strictly correlated with longevity in the different treatments. Thus, the nutrient associated anti-ageing interventions investigated here share a common set of differentially regulated ASVs in their faecal microbiome, which suggests that these bacteria might contribute to improved health at old age and longevity.

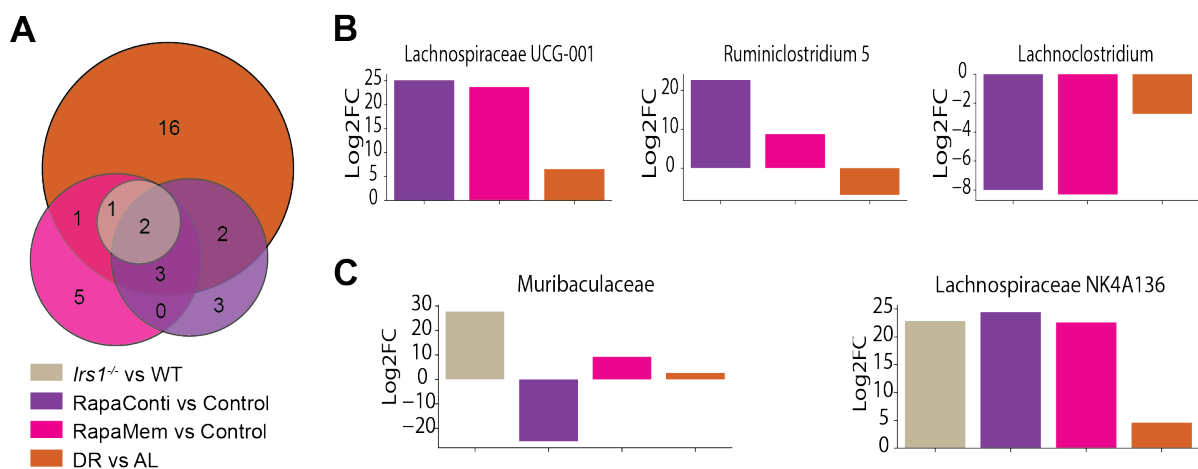


Figure 2.18: A) Venn diagram depicting the overlap of differentially regulated ASVs in the faecal microbiome of DR, *Irs1*^{-/-}, Rapamycin-continuous and Rapamycin-memory treated animals. Fisher's test for alteration of microbiome composition by: DR p-value = 1.0×10^{-5} ; Rapamycin-continuous p-value = 0.0019; Rapamycin-memory p-value = 0.0005; *Irs1*^{-/-} p-value = 0.25. Hypergeometric test to compare proportion of differentially abundant bacteria compared to DR vs AL: Rapamycin-continuous vs Control p-value = 5.9×10^{-8} ; Rapamycin-memory vs control p-value = 3.6×10^{-7} ; *Irs1*^{-/-} vs WT p-value = 1.4×10^{-4} . **B)** Bacteria genera differentially abundant between Rapamycin-treated mice compared to control-fed, and DR vs AL. **C)** Bacteria genera differentially abundant between all anti-ageing interventions compared to their respective controls. Adjusted p-values for differentially abundant bacteria between all comparisons in Supplementary file 1.

2.3 Discussion

Lifelong DR is a robust strategy that can lengthen the lifespan of different model organisms and delay age-related health decline (Green, Lamming, and Fontana 2022; Fontana and Partridge 2015). Here, we examined the longitudinal consequences of ageing and DR in the microbiome. In accordance with earlier cross-sectional studies on DR and caloric restricted mice, we demonstrate that DR mitigates age-related changes in the microbiome community structure, including: decline in alpha diversity, increase in beta diversity, and loss of equilibrium between *Firmicutes* and *Bacteroidetes* phyla (Bartley et al. 2017; Duszka et al. 2018; Fabbiano et al. 2018; Kok et al. 2018; C. Zhang et al. 2013; Badal et al. 2020). Further, we find that DR affects the microbiome more than age and that it is not a “younger-like” condition of the AL microbiome but rather a distinct microbiome in itself.

Despite the many benefits of a lifelong DR regimen, it is impractical to apply lifelong DR in humans. DR should be initiated later in life to promote adherence and translational application (Flatt and Partridge 2018). Therefore, several studies have examined various impacts of initiating DR in mice later in life (Hahn et al. 2019; Zeng et al. 2019; Weindruch et al. 1986; Dhahbi et al. 2004; Drews et al. 2021). In relation to the microbiome, a prior study of late-onset DR found that two months of DR in mice, started at month 20, rejuvenated the ageing-induced structural imbalance of the gut microbiota (Zeng et al. 2019). However, Zeng *et al.* evaluated only seven AL mice switched to DR at ages 20 to 22, and did not evaluate lifespan, only the microbiomes of young and 22–24-month-old mice. Therefore, Zeng *et al.*, could not evaluate the long-term impact of late-onset DR on the microbiome, nor identify bacteria linked to variation in longevity depending on the age of DR onset. Additionally, Drews *et al.* reported that onset of DR as late as 16 months of age is sufficient to recapitulate the lengthened longevity of mice receiving lifelong DR feeding. Conversely, beginning DR at age 20 months does not recapitulate the extended DR lifespan (Drews et al. 2021). Thus, here we investigated the microbiome consequences of starting DR at 16 and 20 months, with a large cohort of control and diet-switched groups. We report acute responses of the microbiome community structure to late-onset of DR, led by changes in relative abundance of taxa, and followed by gain/loss of taxa. Remarkably, consistent with DR lifespan recapitulation only when DR is started as late as 16 months of age (Drews et al. 2021), we found that the DR alpha diversity trajectories with age - that is, stable alpha diversity with age as opposed to the loss we observed in AL mice - could only be recapitulated when DR was initiated in 16-month-old mice. Further, we demonstrated that the microbiome has a high capacity to adjust to a DR-like pattern after switching diets, but that capacity gradually declined as the age of DR onset increased. The robustness of this result is supported by consistent results from the analysis

of ASVs using a Random Forest classifier, PRCs and the abundance of longitudinally different bacteria with age.

We identified 14 “DR-specific” ASVs that did not adapt to DR abundance after switching diets at either 16 or 20 months of age, suggesting these bacteria were regulated by a microbiome memory of AL feeding and could be associated with the better health of chronic DR mice (Drews *et al.* 2021). Evaluation of these 14 ASVs revealed a high degree of network connectivity of *Christensenellaceae*, *Lachnospiraceae*, and *Ruminococcaceae*. These three SCFA-producing bacteria were highly abundant in DR and have been previously associated with improved health (Vacca *et al.* 2020; Stadlbauer *et al.* 2020; Ishiguro, Haskey, and Campbell 2018; Waters and Ley 2019). SCFA, especially the primary products: acetate, propionate and butyrate, are produced by the microbiome through carbon fermentation. They are key regulators in metabolism, immune system and gut-brain signalling pathways (Dalile *et al.* 2019; Frampton *et al.* 2020; Morrison and Preston 2016). Of note, *Christensenellaceae* have not only been found in high abundance in caloric restricted mice and healthy humans, but also in human centenarians (Zeng *et al.* 2019; Waters and Ley 2019; Kong *et al.* 2016). Furthermore, our analysis allowed us to identify bacteria genera adapting to DR abundance when DR onset occurred at 16 months but not at 20 months of age, which may be related to the difference in lifespan and health span between AL_DR16M and AL_DR20M mice (Drews *et al.* 2021). The majority of these bacteria genera were: *Lachnospiraceae*, *Rikenellaceae*, *Muribaculaceae*, *Clostridiales*, *Ruminococcaceae*, and *Lactobacillaceae*. These bacteria ferment fibres to produce SCFA, and have been previously associated with protection from liver disease, cardiovascular disease, hypertension, gut inflammation, and longevity (Sung *et al.* 2019; Dziarski *et al.* 2016; Shenghua *et al.* 2020; Smith *et al.* 2019). A significant finding was the identification of two ASVs from the *Muribaculaceae* and *Clostridiales* genera as potential biomarkers of DR-mediated longevity in mice. Notably, *Muribaculaceae* has been previously associated with extended lifespan in mice treated with pharmacological anti-ageing interventions (Smith *et al.* 2019; Shenghua *et al.* 2020).

In addition, we generated a shotgun metagenomics dataset and identified bacteria species of interest. Two “DR-specific” bacteria species were found: *Lachnospiraceae* sp000403845 and *Anaeroplasmataceae* UMGS268, highly abundant in DR. The *Lachnospiraceae* genera, also identified in this study as “DR-specific” by 16S rRNA sequencing, has been previously correlated with both improved and worsened health (Vacca *et al.* 2020; Stadlbauer *et al.* 2020; Ishiguro, Haskey, and Campbell 2018). While high *Anaeroplasmataceae* genera was reported in high abundance in young-sedentary and old-active mice compared to old-sedentary mice, as well as in low abundance in humans with hypercholesterolemia (Anhê *et al.* 2022; Granado-

Serrano et al. 2019). Furthermore, 11 bacteria species differentiating the adaptation to DR abundance between AL_DR16M and AL_DR20M mice were identified. There was high abundances of *Lachnospiraceae* and *Erysipetaloclostridiaceae* in AL and AL_DR20M mice; and high abundance of *Clostridia* and *Prevotellamassilia* in DR and AL_DR16M mice. *Lachnospiraceae* and *Clostridia* have controversial roles, as high abundance of these bacteria have been reported in both health and disease in humans and mice (Vacca et al. 2020; Stoeva et al. 2021; Uzal et al. 2018). However, little is known about *Erysipetaloclostridiaceae*, they are SCFA producing bacteria enriched in ducks fed total dietary fibre (Hao et al. 2022). Interestingly, *Prevotellamassilia* found in high abundance in the longer-lived treatments, is an anti-inflammatory bacterium that undergoes an age-dependent decline in both humans and primates (Sang et al. 2022). As microbiome-produced SCFA play a major role regulating metabolism and inflammation in mice and humans (Morrison and Preston 2016; Dziarski et al. 2016; Sung et al. 2019; Smith et al. 2019), and a previous study reported an uncoupling of health span from lifespan by means of improvement in metabolic health (glucose/insulin tolerance, respiratory exchange ratio, body weight etc.) irrespective of the age of DR onset (Drews et al. 2021). To elucidate the relationship between microbiome and prolonged longevity in AL_DR16M mice, future studies should investigate the response of the innate and adaptive immune system to DR onset at 16 and 20 months of age.

To investigate the metabolomic response dependent on longevity-associated microbiome composition, previous studies have performed targeted metabolomics and compared mice to naked mole rats, and wild type mice to genetic models of progeria as model organisms of longevity (Viltard et al. 2019; Bárcena et al. 2019). Here, we generated a unique untargeted faecal metabolomics dataset, wherein polar and non-polar metabolites were extracted together with the DNA used for microbiome analysis. We evaluated the effects of ageing in a longitudinal manner, comparing the polar and non-polar faecal metabolomes of centre-lived and long-lived mice within each treatment group. Surprisingly the faecal metabolome of centre- and long-lived AL mice was not significantly different during their early lives, but developed a different pattern during the latest stages of life in the long-lived mice. However, AL mice have the smallest variance in lifespan of the studied groups (Drews et al. 2021), and therefore it is possible their faecal metabolomes may not have a long enough time to strongly diverge. A previous study using targeted metabolomics in colonic luminal content of 6 to 8 AL and DR mice at 6 and 28 months of age, reported a reduced abundance of bile acids in old DR mice compared to AL (Kok et al. 2018). Here, we analysed the longitudinal effects of ageing and DR in the faecal metabolome. We show that there is a general upregulation of metabolites with age in both polar and non-polar metabolites of AL and DR mice, and different ageing patterns depending on diet. Compared to AL, there was higher upregulation of DR

metabolites in both metabolite fractions. The metabolic pathways that were enriched under AL and DR were different; similar to the reports by Kok *et al.*, while AL induced higher upregulation of bile acids and glycine deoxycholic acid, DR was associated with stronger upregulation of spermidine and putrescine metabolites.

Several studies have evaluated different effects of initiating DR in mice later in life (Hahn et al. 2019; Zeng et al. 2019; Weindruch et al. 1986; Dhahbi et al. 2004; Drews et al. 2021), but to date, none evaluated the effect of late-onset DR on the faecal metabolome. Here, we performed polar and non-polar untargeted metabolomics in faecal samples from mice starting DR at 16 and 20 months of age. We revealed that switching to DR late in life generated a metabolic divergence from AL that only lasted temporarily. Nonetheless, this divergence lasted longer when mice were switched to DR at 16 months of age compared to the 20-month DR switch. Thus, differences in the specific metabolites responding to DR onset at 16 and 20 months, may be contributing factors to the lifespan differences observed in these mice (Drews et al. 2021). Furthermore, although there was a significantly higher amount of switch-resistant faecal metabolites when DR was introduced later in life, the untargeted polar metabolomics dataset encompassed the strongest difference in metabolome memory between AL_DR16M and AL_DR20M.

As reported in the microbiome, we identified “DR-specific” changes in abundance of 7 faecal metabolites. Interestingly, a previous study on longevity using mice and naked mole rats, associated glycine-deoxycholic-acid and adenosylmethionine with longevity (Viltard et al. 2019). Tryptamine, has also been reported to be involved in mice health in a study of inflammatory bowel syndrome (Bhattarai et al. 2020). And glycine-deoxycholic-acid, and bile acid metabolism have also been associated with longevity in yeast, progeroid mice and naked mole rats (Goldberg et al. 2010; Bárcena et al. 2018; Viltard et al. 2019). Similarly, we identified metabolites adapting to DR abundance only after diet switch at 16 months of age. The high abundance of N-acetylspermidine, known to induce autophagy (Morselli et al. 2011; Pietrocola et al. 2015), and found in DR and AL_DR16M mice, is one example of metabolite associated to longevity here and in previous studies in mice and naked mole rats (Viltard et al. 2019; Eisenberg et al. 2016). Furthermore, abundant literature has not only shown that spermidine supplementation promotes health and longevity in mice (Eisenberg et al. 2016; Madeo et al. 2018), but also that it is increased in mice under caloric restriction (Madeo et al. 2019). Hence, the autophagic flux could be one of the factors contributing to lifespan differences between AL_DR16M and AL_DR20M. In addition, we observed that the most “switch-resistant” metabolites belong to the lipid fraction, by comparing the relative abundance of metabolites adapting to DR after diet-switch late in life. A previous study on colon gene expression of 28-month-old AL and DR mice, highlighted the high expression of lipid metabolism genes upon

DR (Kok et al. 2018). And another study on mice fed AL, DR, and switched to DR starting at 24 months of age, reported that the lipidome and transcriptome of the WAT are also affected by a nutritional memory effect of AL feeding (Hahn et al. 2019). As the DR microbiome causally contributes to metabolic reprogramming in WAT (C. Zhang et al. 2013; Fabbiano et al. 2018), these results seem to implicate the WAT as one of the contributing factors to the differences in lifespan resulting from DR initiation at different timepoints. To evaluate this hypothesis and further elucidate the mechanisms of the optimal period for lifespan extension, future studies should evaluate the molecular response of the WAT to onset of DR at 16 and 20 months.

In this study we analysed the changes in the faecal microbiome of long-lived mice with reduced IIS and mTOR signalling. We show that overall, the composition of the faecal microbiome is only mildly affected in these mice. In contrast, DR had a stronger impact on the faecal microbiome, consistent with previous findings that suggest that dietary interventions affect the microbiome more than genetic or pharmacological interventions (Maynard and Weinkove 2018). Interestingly, we were able to identify changes in bacterial abundance shared between the three longevity interventions, which might indicate that these bacteria contribute to the improved health and longevity of animals with reduced nutrient signalling. Finally, we identified changes in bacterial abundances that persisted in mice even if the Rapamycin treatment ceased 6 months ago, suggesting a microbiome memory of prior Rapamycin feeding.

Reduced IIS and mTOR signalling extends lifespan in animals as diverse as flies and mice. In *Drosophila*, the microbiome affects host physiology by regulating both the IIS and the mTOR network (Shin et al. 2011; Grönke et al. 2010), suggesting a cross talk between the microbiome and organismal IIS/mTOR signalling. In this context it might be surprising, that the faecal microbiome composition of long-lived *Irs1^{-/-}* mice was not significantly altered. Noteworthy, in contrast to DR and Rapamycin mice, that were maintained in separate cages to their respective controls, *Irs1^{-/-}* mutant mice were housed together in the same cages as the control animals. Mice are coprophagic (Bogatyrev, Rolando, and Ismagilov 2020), and therefore the microbiome was probably continuously transferred between *Irs1^{-/-}* and WT mice, which might explain why we observed the smallest changes in microbiome composition in the *Irs1^{-/-}* mice. Nevertheless, we observed 3 bacteria genera that were previously associated with health and longevity (Stadlbauer et al. 2020; Smith et al. 2019; Shenghua et al. 2020), as significantly different in abundance between *Irs1^{-/-}* and WT mice (Fig 2.18A). Thus, it is possible that these bacteria contribute to the improved health of *Irs1^{-/-}* mice at older age.

We found that continuous Rapamycin treatment had a significant effect on the composition of the faecal microbiome in line with a previous report (Bitto et al. 2016). The most prominent

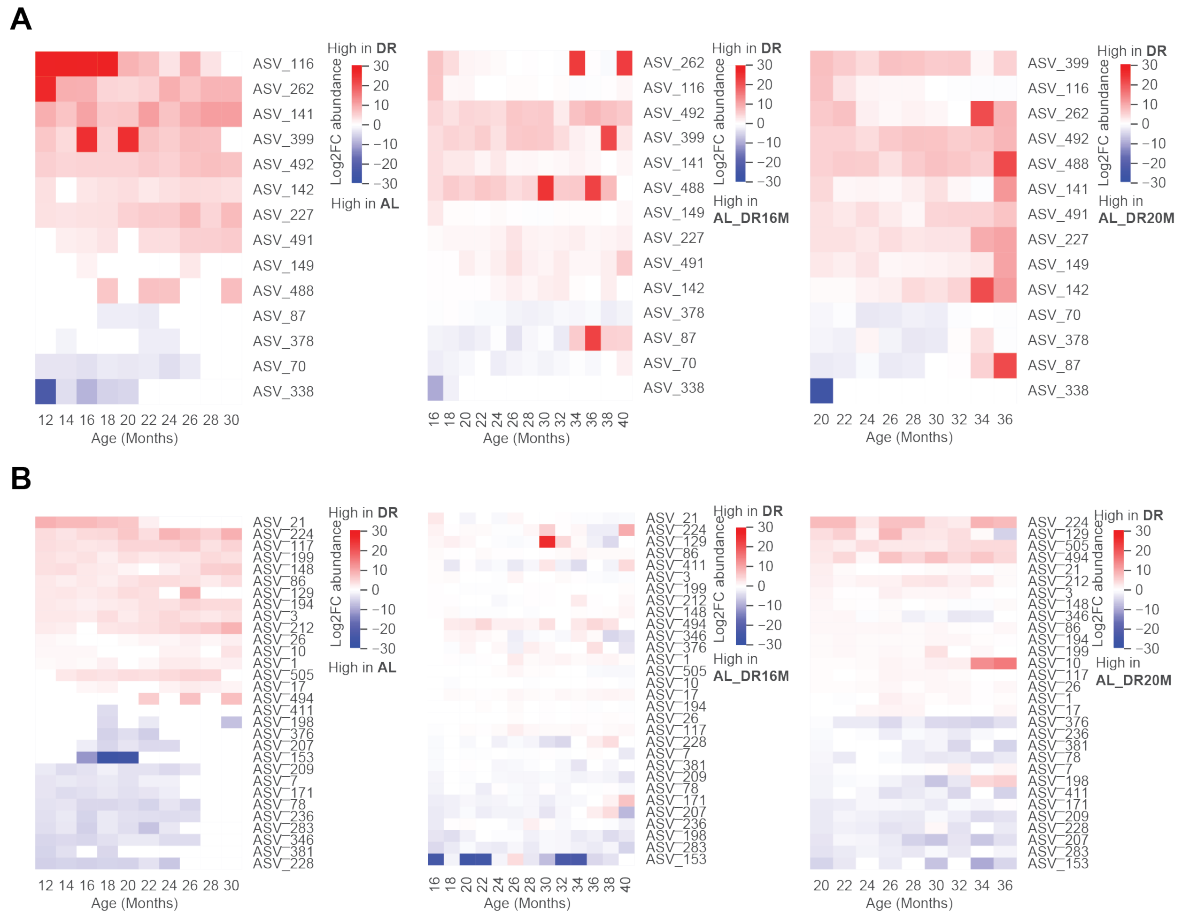
change in the study by Bitto et al, was a striking increase in the abundance of *Candidatus arthromitus* in mice under late-onset Rapamycin treatment (Bitto et al. 2016). Consistent with this finding, levels of *Candidatus arthromitus* were also increased in mice that were continuously fed with Rapamycin in our study, indicating that this is a robust response which is not dependent on specific housing conditions or differences in mouse strains. However, the abundance of *Candidatus arthromitus* was not significantly changed in DR or *Irs1*^{-/-} mice, suggesting that this change is specific to Rapamycin feeding. Furthermore, abundance of *Candidatus arthromitus* was also not changed in Rapamycin-memory animals that were fed with Rapamycin for a brief period early in life and were then kept on control food for 6 months. Early life Rapamycin treatment has been shown to have a lasting beneficial effect on gut health in mice (Juricic et al. 2022). Thus, the finding that *Candidatus arthromitus* is not differentially abundant in Rapamycin-memory mice suggests that it is not causal for the improved gut health of these mice. However, we detected increased abundance of *Lachnospiraceae UCG-001*, *Ruminiclostridium 5* and *Lachnospiraceae NK4A136*; and decreased abundance of *Lachnoclostridium*, both in continuously treated and in Rapamycin-memory mice, suggesting that these Rapamycin-induced changes in the microbiome are stable for at least 6 months after drug withdrawal (Fig 2.18A-B). Mice with Paneth cell alteration and consequently reduced secretion of antimicrobial peptides (AMP) into the small intestine, have been shown to have low abundance of *Lachnospiraceae UCG-001* and *Ruminiclostridium 5* (Chen et al. 2017). Chronic Rapamycin treatment has been shown to directly affect Paneth cell function (Y. Zhou et al. 2015) and Rapamycin-memory animals showed a change in Paneth cell architecture (Juricic et al. 2022), which might indicate changes in AMP secretion. Thus, the observed persistent changes in the faecal microbiome might be caused by long-lasting changes in Paneth cell physiology. DR also affects mTOR signalling in Paneth cells (Yilmaz et al. 2012) and affects lifespan, consistent with the high abundance of *Lachnospiraceae UCG-001* in the faecal microbiome of DR and AL_DR16M animals but not in AL_DR20M or AL mice (Fig 2.10A and 2.18B). In summary, we identified bacterial changes that are persistent for 6 months after Rapamycin withdrawal, indicating a Rapamycin induced memory of the faecal microbiome.

We identified two bacteria genera, *Lachnospiraceae NK4A136* and *Muribaculaceae*, that showed a significant change in abundance in all three longevity interventions. While late-onset DR did not affect the abundance of *Lachnospiraceae NK4A136*, *Muribaculaceae* was increased in DR and AL_DR16M mice but not in AL or AL_DR20M, and was associated with DR-mediated longevity (Fig 2.10A-B). Further, *Lachnospiraceae NK4A136* and *Muribaculaceae* have both been previously associated with health in mice (Smith et al. 2019; Shenghua et al. 2020; Stadlbauer et al. 2020), and *Muribaculaceae* has been linked to lifespan extension (Shenghua et al. 2020; Smith et al. 2019). *Lachnospiraceae NK4A136* showed

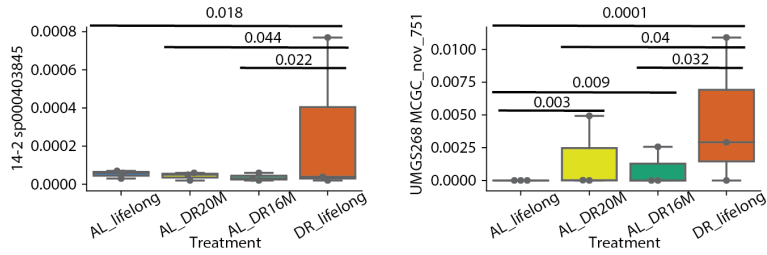
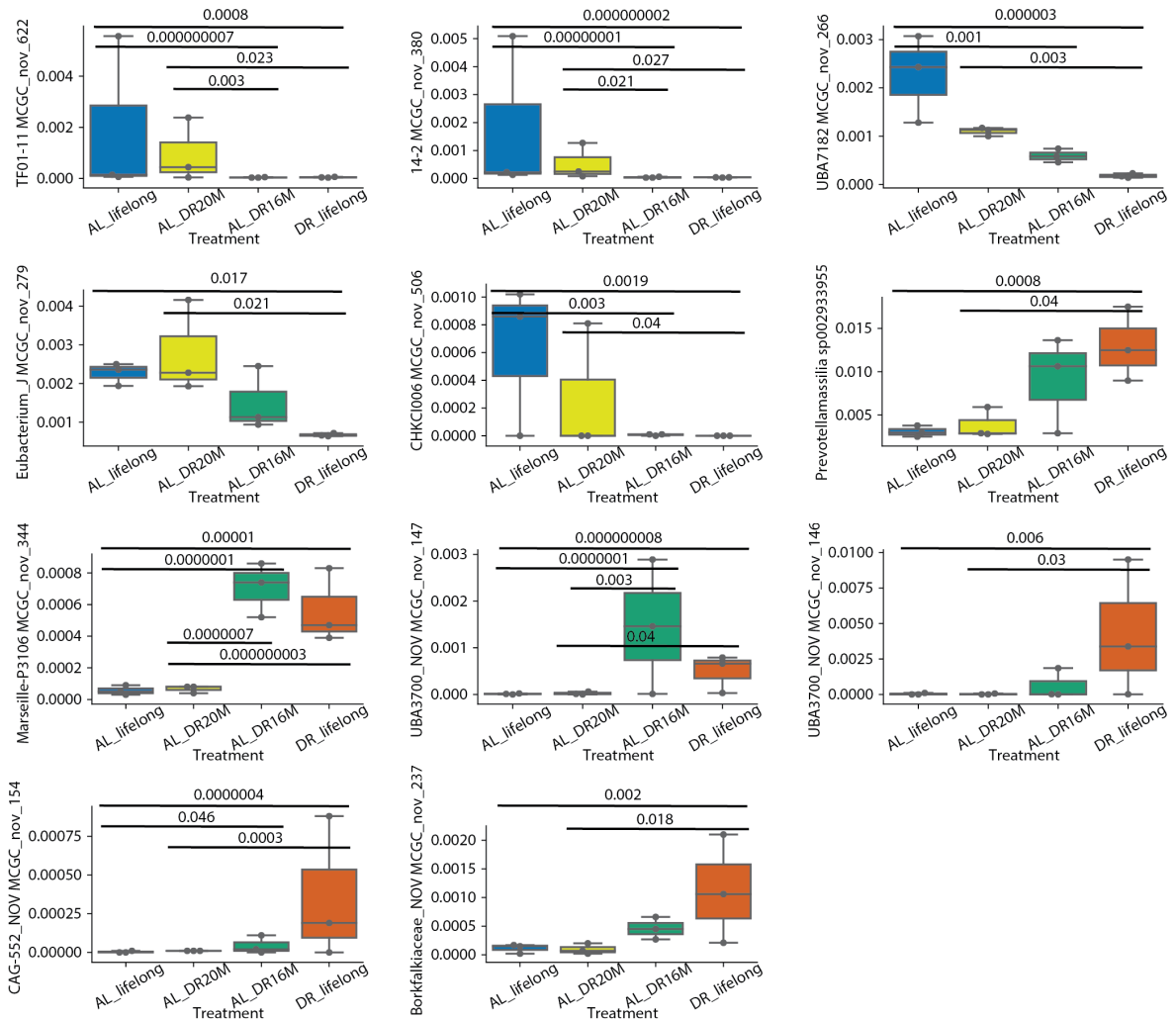
increased abundance upon reduced IIS, mTOR signalling and in response to DR, making it a good microbial biomarker for longevity. In contrast, *Muribaculaceae* levels were only strongly increased in *Irs1*^{-/-} mutants and slightly in DR and Rapamycin-memory animals, but depleted in long-lived animals treated chronically with Rapamycin. Thus, if *Muribaculaceae* levels are contributing to health and lifespan improvements, then this effect is context specific. In summary, the comparison of the microbiomes of mice under different anti-ageing interventions revealed that these interventions share commonality in their microbiome responses. Future studies involving microbial transfers of these bacteria will be required to prove a causal role for them in health and longevity.

Taken together, this study demonstrates that ageing is associated with pronounced changes in the population structure of the faecal microbiome and metabolome. DR not only delays the age-associated changes in microbial community structure, but also induces specific ageing patterns, most evidenced by the high abundance of *Bacteroidetes* in old age. Our results provide direct evidence that there is an age-dependent microbiome and faecal metabolomic memory of AL feeding associated with lifespan. Next to identifying a group of bacterial and metabolomic biomarkers that may be contributing factors to DR-mediated longevity, we also find common bacterial biomarkers of longevity between pharmacological (Rapamycin), genetic (*Irs1*^{-/-}) and dietary (DR) anti-ageing interventions. Future investigation on the causal implication of these bacterial biomarkers in longevity and DR can greatly expand our understanding of the mechanisms of attenuating ageing and pave the way to anti-ageing interventions that recapitulate the full benefits of DR.

2.4 Supplementary figures



Supplementary Figure 2.1: Heatmaps of Log2 fold change abundances of ASVs, comparing DR vs AL, DR vs AL_DR16M, and DR vs AL_DR20M. **A)** Subset of DR-specific bacteria. **B)** Subset of bacteria associated with DR-mediated longevity. Adjusted p-values of differential abundances in Supplementary File 1.

A**B**

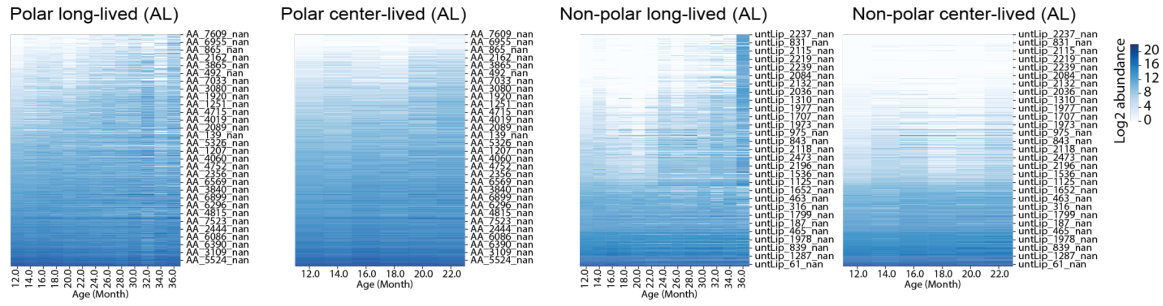
Supplementary Figure 2.2: Adjusted p-values and relative abundance for **A)** DR-specific bacteria species and **B)** DR-mediated longevity associated bacteria species. Adjusted p-values for differential abundance between all comparisons in Supplementary file 1

A

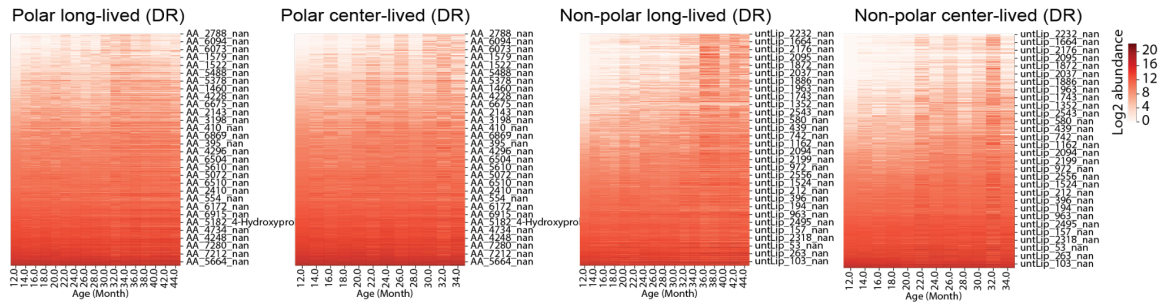
(AL) Polar	Long-lived	Center-lived	(DR) Polar	Long-lived	Center-lived
Down with age AL	307 (7.15 %)	56 (1.3 %)	Down with age DR	582 (13.5 %)	302 (7 %)
Up with age AL	411 (9.36 %)	350 (8.1 %)	Up with age DR	903 (21 %)	496 (11.5 %)

(AL) Non-polar	Long-lived	Center-lived	(DR) Non-polar	Long-lived	Center-lived
Down with age AL	93 (4.3 %)	33 (1.5 %)	Down with age DR	308 (14.2 %)	74 (3.4 %)
Up with age AL	301 (13.9 %)	90 (4.1 %)	Up with age DR	956 (44.2 %)	736 (34 %)

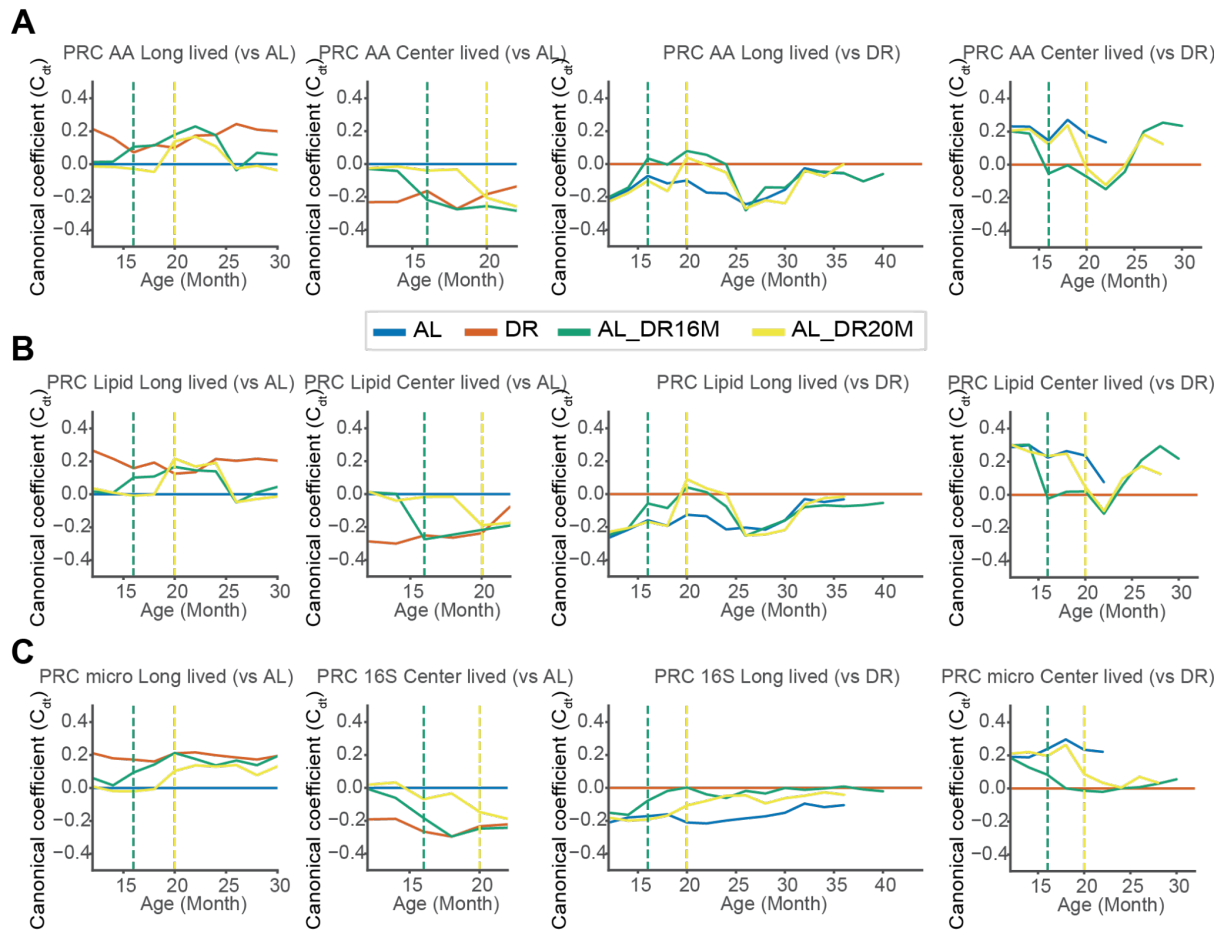
B



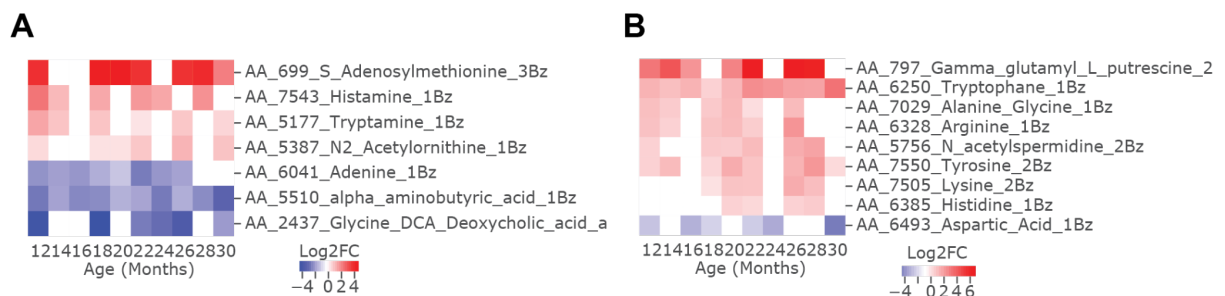
C



Supplementary Figure 2.3: A) Tables of number of faecal metabolites significantly affected by ageing trends. **B)** Heatmap of abundance of faecal metabolomes of long-lived and centre-lived AL mice through age. **C)** Heatmap of abundance of faecal metabolomes of long-lived and centre-lived DR mice through age.



Supplementary Figure 2.4: **A)** PRCs of polar faecal metabolites of long-lived and centre-lived mice compared to AL and DR. **B)** PRCs of non-polar faecal metabolites of long-lived and centre-lived mice compared to AL and DR. **C)** PRCs of microbiomes of long-lived and centre-lived mice compared to AL and DR. Minimum of 3 reference mice for PRC calculations. Adjusted p-values for per-time point Monte Carlo permutations between diets of PRCs in Supplementary File 1.



Supplementary Figure 2.5: Log2FC between DR and AL abundances of **A)** 7 annotated faecal polar metabolites classified as "memory"; DR specific metabolites. **B)** 9 annotated faecal polar metabolites adapting to DR in AL_DR16M but not in AL_DR20M.

3. The effect of dietary restriction on the B-cell receptor repertoire in mice

Author contributions:

Conception of the study predominantly by Carolina Monzó, Lisonia Gkioni, Sebastian Grönke, Dario Valenzano and Linda Partridge.

Provision of tissues by Lisa Drews and Sebastian Grönke.

Execution of experiments proportionally by Carolina Monzó and Lisonia Gkioni.

Bioinformatic analysis by Carolina Monzó. Advised by Andreas Beyer.

Statistical evaluation by Carolina Monzó. Advised by Andreas Beyer.

Graphical representation by Carolina Monzó.

Writing of the manuscript predominantly by Carolina Monzó and Lisonia Gkioni, with substantial contribution by Dario Valenzano, Sebastian Grönke and Linda Partridge.

Dietary restriction mitigates the age-associated decline in the mouse B cell receptor repertoire diversity

Authors:

Carolina Monzó^{1,2*}, Lisonia Gkioni^{1*}, Andreas Beyer², Dario Riccardo Valenzano¹, Sebastian Grönke¹ and Linda Partridge^{1,3}

Affiliations:

1. Max Planck Institute for Biology of Ageing, Cologne, Germany
2. CECAD Research Centre, Cologne, Germany
3. Institute of Healthy Ageing, University College of London, United Kingdom

3.1 Introduction

Ageing is characterised by a decline in organismal function leading to increased vulnerability to death and development of pathological conditions. These include a profound functional dysregulation of the adaptive immune system (López-Otín et al. 2013; R. A. Miller 1996; Walford 1982), which responds to pathogens by mounting a precise and long-lasting immune memory. In humans and mice, there is a displacement of naïve B cells by antigen-experienced (memory) B cells, resulting in loss of B cell receptor (BCR) repertoire diversity and antigen-specificity (Oh, Lee, and Shin 2019; Dunn-Walters 2016; Weiskopf, Weinberger, and Grubeck-Loebenstein 2009; Dunn-Walters, Banerjee, and Mehr 2003; C. Wang et al. 2014; Hoehn et al. 2019). Age-related immune decline is linked to impaired protection against pathogens and decreased vaccination response, ultimately placing infectious diseases among the leading causes of morbidity and mortality in aged individuals (Wick et al. 2000; Nikolich-Zugich 2005; Ademokun, Wu, and Dunn-Walters 2010; Weiskopf, Weinberger, and Grubeck-Loebenstein 2009).

Morbidity, mortality and impaired functionality in old age can be ameliorated by genetic, environmental and pharmacological interventions (Green et al. 2021; Tyshkovskiy et al. 2019; Fontana, Partridge, and Longo 2010). Dietary Restriction (DR), reduced nutrient intake without malnutrition, is one of the most effective interventions to extend life span and health span in various animal species, including yeast, worms, fruit flies, rodents and non-human primates (Colman et al. 2014; Fontana and Partridge 2015). In humans, short-term DR lowers risk factors for metabolic syndrome and cardiovascular disease (Kraus et al. 2019; Barquissau et

al. 2018), and other age-related pathologies (Fontana and Partridge 2015; Omodei and Fontana 2011; Ikeno et al. 2006). Furthermore, DR can attenuate or reverse some of the age-associated changes in the adaptive immune system in rodents, providing greater resistance to pathogens (R. A. Miller 1996; Messaoudi et al. 2006; Shushimita et al. 2014). DR delays T cell senescence in non-human primates by preserving the naïve T cell pool and T cell receptor repertoire diversity (Messaoudi et al. 2006) and preserves the population of naïve T cells and immature NK cells in aged mice (White et al. 2016). Further, DR increases B cell maturation through a decline in the total B cell population and an increased recirculation of mature B cells in male mice. However, the effect of DR on the BCR repertoire diversity is currently unexplored.

BCRs consist of two heavy chains (IgH), and two light chains (IgL). The heavy chains, which are sufficient to identify B cell clonal relationships (J. Q. Zhou and Kleinstein 2019), have a variable domain encompassed by a combination of *IghV*, *IghD*, and *IghJ* genes, and a constant domain (*IghC*). After antigen identification by the variable domain, *IghC* regions undergo class-switch recombination, where *IghC* isotypes μ (IgM) and δ (IgD) are substituted by either γ , ϵ , or α heavy chains, giving rise to IgG, IgE and IgA isotypes with different effector functions, including opsonization and neutralisation of antigens (Schroeder and Cavacini 2010; Z. Xu et al. 2012). BCR sequencing can inform on the characteristics of the hypervariable loci responsible for antigen-identification and shed light on the different effector functions, by analysing the constant domains coding for immunoglobulin isotypes (Stavnezer, Guikema, and Schrader 2008; Turchaninova et al. 2016; Cook 2000). Indeed, poor health and frailty in mice and humans is associated with the age-dependent decline in BCR diversity, increased clonal expansions, and impaired negative selection of autoreactive B cells and positive selection of high affinity B cells (V. Martin et al. 2015; Gibson et al. 2009; Booth and Toapanta 2021).

Initiation of DR at older ages can improve subsequent health, avoiding the need for long-term DR feeding, potentially of translational relevance to humans (Flatt and Partridge 2018; Redman et al. 2018; Tang et al. 2021). It has been previously shown that DR onset at 16 months of age was sufficient to recapitulate the chronic DR lifespan extension in mice (Drews et al. 2021). However, initiating DR at 20-month-old mice did not extend lifespan (Drews et al. 2021). Several pathological parameters were improved in both groups, and it remains unclear what factors might explain the refractoriness of lifespan to DR initiated at 20 months.

Here, we investigated whether DR delays age-related changes in the BCR that have been reported in mice, and whether it can do so when initiated later in life. We generated a BCR sequence dataset from *ad libitum* fed (AL) and DR mice, and from mice switched from AL to

DR diet at 16 and 20 months of age. To assess systemic immune responses we analysed the spleen, as the major secondary lymphoid organ. To evaluate the relationship between the host and the microbiome directly at mucosal organs, we analysed the ileum. We found that DR delayed the age-associated decline of BCR repertoire diversity in the spleen. Further, the BCR profile of DR mice inversely correlated with morbidity, suggesting that BCR repertoire is associated with increased systemic health. The ileum BCR repertoire underwent only limited changes with age and DR treatment, mainly displaying a higher capacity for antigen binding under chronic DR. Mice subjected to DR starting at 16 months had spleen BCR diversity and clonal expansion rates indistinguishable from those with chronic DR, while mice switched at 20 months of age showed BCR diversity and clonal expansion levels that remained in between the chronic AL and DR, suggesting that these immunological traits contribute to the response of lifespan to DR.

3.2 Results

To investigate how ageing and DR affect BCR repertoire, we sequenced the variable (*IghV*, *IghD*, *IghJ*) region of the BCR (Fig 3.1A) of wild type, female C3B6F1 hybrid mice fed AL or DR (Fig 3.1B). DR feeding was implemented by supplying 40% of the *ad libitum* (AL) food intake (Drews et al. 2021). To address whether any protection of the BCR repertoire can be achieved by DR implemented later in life, we included mice where DR was initiated at 16 (AL_DR16M) or 20 months of age (AL_DR20M) (Fig 3.1B). Total RNA was isolated from the spleen and ileum to capture the systemic or gut-specific profiles, respectively, of five mice per treatment at 5, 20 and 24 months of age (Fig 3.1B). Since sequencing protocols do not preserve Heavy:Light chain pairing, we limited our analysis to BCR-heavy chains, as they are sufficient to identify clonal relationships with high confidence (J. Q. Zhou and Kleinstein 2019). BCR clones from the same naïve B cell ancestor were defined by sequences sharing the same *IghV* and *IghJ* gene, and having the same CDR3 length (Khan et al. 2016; Greiff et al. 2017; Koohy et al. 2018). BCR isotypes were identified by a template-switch adapter in the 5' of the *IghV* variable domain, and isotype-specific primers binding to the *IghC* effector domain (Fig 3.1A) (Turchaninova et al. 2016).

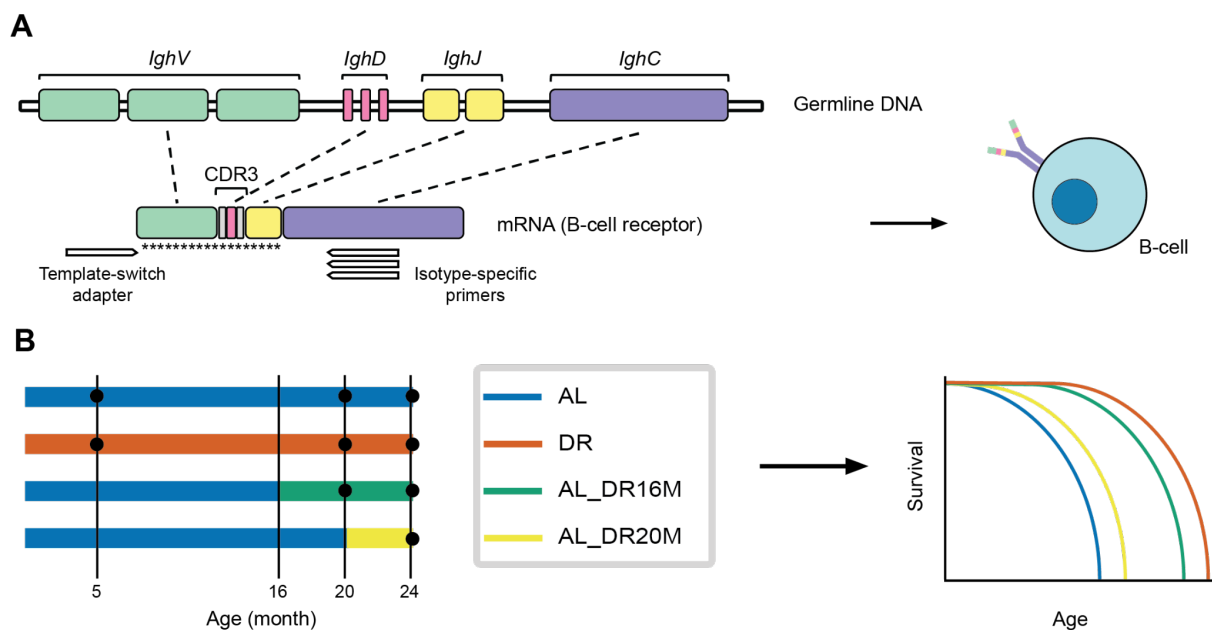


Figure 3.1: A) Schematic of IgH heavy chain gene arrangement of B-cell receptors and location of BCR isotype-specific primers. Asterisks indicate the region modified by somatic hypermutations. **B)** Scheme for DR switch and measurement of lifespans, adapted from (Drews et al. 2021). Black circles indicate time points when spleen and ileum samples were taken. n= 5 mice per treatment.

3.2.1 DR slows the age-associated decline of BCR repertoire diversity in the spleen

We first analysed data from the spleen. Abundances of BCR isotypes were quantified, and the majority of BCRs corresponded to IgM (~61%), a few to IgG (~23%), fewer to IgA (~13%), and yet fewer to IgD and IgE (~3%) (Fig 3.2A) (Le Gallou et al. 2018). No age-dependent differences in relative abundances of IgM, IgA and IgE were detected in AL mice, but there was a significant decline in IgD abundance with age (Fig 3.2A), in line with previous studies in elderly humans (Colonna-Romano et al. 2006). Although the function of IgD is largely unknown, it may be involved in immune self-tolerance (Gutzeit, Chen, and Cerutti 2018; Nguyen 2022), and its decline with age may be associated with increased auto-reactivity. IgD abundance was higher in DR than in AL mice at 5 months and also declined with age, although it remained higher than in AL mice and declined at a slower rate (Fig 3.2A). Therefore, DR not only ameliorated the age-related decline in IgD abundance, but also maintained higher levels of IgD throughout life compared to AL animals, indicating a tighter regulation of immune tolerance under DR.

High BCR within-individual diversity is associated with improved antigen recognition capacity and vaccination response (Dunn-Walters 2016; Ademokun et al. 2011; de Bourcy et al. 2017). Thus, we hypothesised that DR mice would have higher BCR diversity. To measure this, we calculated Hill diversity spectra (Miho et al. 2018; Hill 1973). Clonal richness, i.e. the total number of different BCR clones, was stable in AL mice up to the age of 20 months, and then rapidly declined by 24 months of age (Fig 3.2B). Unexpectedly, DR mice underwent a progressive decline in clonal richness with age (Fig 3.2B), displaying significantly lower richness of B cell clones than AL mice at 20 months of age (Fig 3.2B). However, analysis of the clonal richness of each isotype identified a significantly higher richness of IgE in DR mice at 24 months of age (Sup Fig 3.1A). Therefore, contrary to our hypothesis, DR mice were generally characterised by lower within-mouse richness BCR diversity.

The diversity of the BCR repertoire is not only defined by the number (richness) of clones, but also the relative frequency of the subdivisions of the clonal population. We therefore determined whether DR mice had higher antigen-recognition capacity at old age as reflected by evenness in the size of each B cell clone. To assess both clonal richness and population structure, we evaluated Shannon and Simpson diversity metrics. Shannon diversity is a measure of both clonal richness and population structure, mostly affected by rare clones, while Simpson diversity measures the distribution of the clonal population structure, mostly affected by large clones. AL mice displayed an age-related decline in both Shannon and Simpson

indices (Fig 3.2C, 3.2D), mainly due to a decline in IgM, IgG and IgE isotypes (Sup Fig 3.1B-C). The rare B cell clones of AL mice thus became less abundant with age, and the clonal population structure less uniform. DR mice also experienced an age-dependent decline in Shannon diversity, but to a lesser extent than AL mice (Fig 3.2C). Thus, at 24 months of age, DR mice had higher Shannon diversity than AL mice (Fig 3.2C), suggesting that DR slows the age-related change in the clonal population structure. In contrast to AL mice, Simpson diversity in DR mice was maintained until 20 months of age, with a rapid decline only at 24 months (Fig 3.2D). Therefore, the strongest changes in clonal population structure of DR mice occurred between 20 and 24 months. Similarly, the most striking differences in diversity between AL and DR mice also appeared between 20 and 24 months of age, with DR retaining a more uniform clonal population structure, as indicated by the Shannon diversity. DR mice exhibited a significantly reduced Shannon and Simpson diversity with age in IgM (Sup Fig 3.1B-C), and a less profound loss of IgG Shannon and Simpson diversity with age (Sup Fig 3.1B-C). The ageing BCR repertoire thus showed loss of rare clones, and DR attenuated this change by maintaining a more uniform distribution of large clones.

Figure 3.2: DR slows the age-associated decline of BCR repertoire in the spleen. **A)** Relative abundance of antibody isotypes in the spleen. Significant differences through age (linear regression): IgD (AL p-value = 0.03; DR p-value = 0.002). Significant differences through age and diet (2-way ANOVA): IgD (DR vs AL p-value = 0.03). Significant differences at 5 months of age (Mann-Whitney U test): IgD (DR vs AL p-value = 0.036). Significant differences at 24 months of age (Mann-Whitney U test): IgD (AL_DR16M vs AL p-value = 0.036). **B)** Richness within-individual diversity. Significant differences through age (linear regression): p-value AL = 0.002; p-value DR = 0.000001. Significant differences at 20 months of age (Mann-Whitney U test): DR vs AL p-value = 0.001. Significant differences at 24 months of age (Mann-Whitney U test): AL_DR16M vs AL p-value = 0.0003. **C)** Shannon within-individual diversity. Significant differences through age (linear regression): AL p-value = 0.000001; DR p-value = 0.0002. Significant differences through age and diet (2-way ANOVA): DR vs AL p-value = 0.008. Significant differences at 24 months of age (Mann-Whitney U test): DR vs AL p-value = 0.004; AL_DR16M vs AL p-value = 0.008. **D)** Simpson within-individual diversity. Significant differences through age (linear regression): AL p-value = 0.0000003; DR p-value = 0.03. Significant differences between 20 and 24 months of age (Mann-Whitney U test): DR p-value = 0.036. **E)** Clonal expansion. Significant differences through age (linear regression): AL p-value = 0.00002; DR p-value = 0.02. Significant differences through age and diet (2-way ANOVA): DR vs AL p-value = 0.01. Significant differences at 24 months of age (Mann-Whitney U test): AL_DR16M vs AL p-value = 0.002. Significant differences between 20 and 24 months of age (Mann-Whitney U test): DR p-value = 0.036. **F)** Inter-individual dissimilarity. Significant differences through age (linear regression): AL p-value = 1.0×10^{-17} ; DR p-value = 1.0×10^{-7} . Significant differences through age and diet (2-way ANOVA): DR vs AL p-value = 0.00007. Significant differences at 24 months of age (Mann-Whitney U test): DR vs AL p-value = 0.002, AL vs AL_DR16M p-value = 2.0×10^{-4} , DR vs AL_DR20M p-value = 0.033, and AL_DR16M vs AL_DR20M p-value = 0.005. **G)** Frequency of synonymous SHM. **H)** Frequency of non-synonymous SHM. **I)** Gaussian-fitted CDR3 length distribution per mouse in study. Significant differences in proportion of different CDR3 length distributions at 24 months of age (Fisher's test): DR vs AL p-value = 0.048; AL_DR16M vs AL p-value = 0.011. **B-H)** Lines correspond to mean, and shaded area to 95% confidence intervals. **J)** Relative amount of clones according to their class-switch status. Significant differences through age (linear regression): Post-antigenic (AL p-value = 0.034). Non-significant p-values in Supplementary File 2.

3.2.2 DR attenuates clonal expansions with age in the spleen

To determine whether the age-dependent decrease in within-individual antibody diversity was due to a B cell population skewed towards clonally expanded cells, we calculated clonal expansion as the percentage of the BCR repertoire taken up by the 20 most common clones (P20) (Fig 3.2E). In line with previous work (Gibson et al. 2009; Oh, Lee, and Shin 2019), clonal expansions increased progressively with age in AL mice (Fig 3.2E). This expansion was

most evident in the primary and long-term antigen response isotypes IgM and IgG (Sup Fig 3.1D), suggesting a possible attenuation of memory immune response (Schroeder and Cavacini 2010). Clonal expansions also increased with age in DR mice (Fig 3.2E), but to a significantly lesser extent than in AL animals (Fig 3.2E). At 24 months of age, only ~60% of the total clonal population was occupied by expanded clones in DR mice, while in AL mice it reached ~80% (Fig 3.2E). Further, DR mice maintained a stable rate of clonal expansions in IgM and IgG, only increasing at 24 months of age in IgM (Sup Fig 3.1D). The age-dependent decrease in within-individual diversity was thus associated with a B cell population skewed towards clonally expanded B cells, an effect that was attenuated by DR.

Differences in clonal composition of B cells between individuals are accentuated by the proliferation of different clones in different individuals (Gibson et al. 2009; Weksler and Szabo 2000; Oh, Lee, and Shin 2019; de Bourcy et al. 2017). We therefore hypothesised that there would be higher inter-individual dissimilarity at old than at young age. To quantify dissimilarity, we used the repertoire dissimilarity index (RDI) (Bolen et al. 2017), which calculates differences in *IghV*, *IghD* and *IghJ* gene usage and performs pairwise comparisons between BCR repertoires. Consistent with previous reports in mice and humans (de Bourcy et al. 2017; Gibson et al. 2009; Oh, Lee, and Shin 2019), there was a progressive increase in RDI with age in AL mice (Fig 3.2F). A lesser ageing-associated increase in inter-individual dissimilarity also occurred in DR mice (Fig 3.2F). Isotype-specific analysis revealed that RDI increased with age in all isotypes in AL mice (Sup Fig 3.1E) and in DR mice except for IgA (Fig 3.1E). However, the slope of increasing RDI was significantly reduced under DR in all isotypes except IgE (Sup Fig 3.1E).

IghV and *IghJ* gene usage are largely implicated in the ability of the BCR to bind to antigens, thereby affecting susceptibility to various diseases (Raposo et al. 2014). To determine whether the enhanced antigen recognition capacity of DR mice is further facilitated by selection of different *IghV* or *IghJ* genes than AL, we evaluated *IghV* and *IghJ* usage. In concordance with previous studies (Muggen et al. 2019; Wu et al. 2010; V. Martin et al. 2015), the most commonly used *IghV* gene in AL mice was *IghV1* (Sup Fig 3.2A). In humans, use of the *IghV1* gene family is reduced with age (Ghraichy et al. 2021), and AL mice also showed an age-related decline in the usage of *IghV1*, *IghV3*, *IghV4*, *IghV7*, and *IghV11* (Sup Fig 3.2A) (Ghraichy et al. 2021). *IghV1* was the most commonly used *IghV* gene in DR mice, which showed a decline in usage of *IghV4*, *IghV6*, *IghV7* and *IghV11* with age (Sup Fig 3.2A). However, DR treatment led to a significant increase in the usage of *IghV3*, and *IghV15* compared to AL (Sup Fig 3.2A). There were no differences between AL and DR mice in *IghJ* gene use (Sup Fig 3.2B). DR thus led to changes in *IghV* gene use that may have contributed to the age-related differences in clonal diversity between AL and DR spleen B cells.

3.2.3 DR maintains the somatic hypermutation rate and CDR3 length distribution at old age in the spleen

Clonal diversity is important for efficient antigen recognition (Dunn-Walters 2015), we thus studied whether antigen recognition capacity is affected by ageing and DR. We evaluated the somatic hypermutation (SHM) rate, which is the mechanism for affinity maturation of the BCR repertoire in response to antigen exposure, leading to clonal diversity (Dunn-Walters 2016; Schroeder and Cavacini 2010). The rate of synonymous substitutions indicates neutral evolution, providing a baseline for the nucleotide alteration capacity of the BCR sequence. Non-synonymous substitutions, on the other hand, accumulate during affinity maturation and become fixed under positive selection (Nielsen and Yang 1998). We quantified the frequency of synonymous and non-synonymous mutations in the BCR repertoire. Consistent with previous work (Dunn-Walters 2015), we did not detect any differences in synonymous or non-synonymous SHM rate with age in AL mice (Fig 3.2G-H). Similarly, as previously reported (Hoehn et al. 2019), we did not find age-associated differences for the relative rate of amino acid changing substitutions versus synonymous substitutions or dN/dS ratio (Nielsen and Yang 1998) (Sup Fig 3.2C). We found large dN/dS ratio values (>1), indicating strong positive selection, across all time points in the splenic BCR repertoire of all groups (Sup Fig 3.2C). In contrast, after examining synonymous and non-synonymous SHM rates for each individual isotype, we uncovered an age-associated reduction in IgM synonymous SHM frequency in AL mice (Sup Fig 3.1F), an age-associated increase in IgG synonymous SHM frequency in both AL and DR mice (Sup Fig 3.1F), and an age-associated increase in IgA synonymous and non-synonymous SHMs in DR mice (Sup Fig 3.1F-G). Only the synonymous and non-synonymous SHM rate in IgA was significantly different between AL and DR through age (Sup Fig 3.1F-G), indicating that DR increases the affinity maturation of the IgA repertoire. Taken together, our results point towards a more stable and efficient SHM mechanism under DR treatment, indicating maintained antigen-recognition capacity; where IgA isotype associated with secondary B cell response is predominantly increased.

The length of the hypervariable CDR3 portion of the IgH locus offers valuable insights on antigen binding, selection and preservation of intact immune responses (Schroeder and Cavacini 2010). Increased CDR3 length has been causally associated with autoimmune disorders and old age (Mikocziova, Greiff, and Sollid 2021; C. Wang et al. 2014). We therefore determined whether CDR3 length differs with age and under DR. We found no changes in CDR3 length or standard deviation with age in AL or DR mice (Sup Fig 3.2D). By comparing gaussian distributions, AL mice had an increased proportion of skewed distributions at 24 months of age when compared to DR (Fig 3.2I) and there was higher biological variance

between AL mice, than between DR mice. Similarly, there was a higher proportion of skewed CDR3 regions in 24-month-old AL mice, for both IgG and IgA isotypes, as opposed to the normal distributions of DR mice (Sup Fig 3.1H). Thus, our results suggest that DR mice are less prone to a compromised immune function in old age compared to AL.

Class-switch recombination is the mechanism of diversification by which variable regions of heavy chains are juxtaposed to different constant chains, in order to generate different isotypes and confer different effector functions (Schroeder and Cavacini 2010; Booth and Toapanta 2021). To evaluate the effect of DR on class-switch recombination, clones with only IgM+IgD+SHM- segments were classified as naïve, IgM+IgD+SHM+ as antigen-stimulated, and those with IgM-IgD- where all isotypes had been class-switched, as post-antigenic (C. Wang et al. 2014). Very few post-antigenic BCR clones were found throughout age (Fig 3.2J), which is not surprising given that the spleen is a secondary lymphoid organ, and the mice are not expected to have substantial encounters with potentially challenging/pathogenic antigens based on their housing conditions. The majority of the B cell population consisted of naïve and antigen-stimulated BCR clones (Fig 3.2J). There was a significant loss in the post-antigenic BCR pool in AL mice with age (Fig 3.2J). Conversely, DR mice displayed no differences in naïve, antigen-exposed or post-antigenic clones with age or compared to AL (Fig 3.2J). Thus, these results suggest that ageing might impair the class-switch recombination capacity, while DR did not influence this process.

3.2.4 Midlife onset of DR has more positive effects on the BCR repertoire of the spleen than late-life onset DR

DR onset at 16 months of age (AL_DR16M) leads to a lifespan extension similar to the one observed under a chronic DR diet (Drews et al. 2021) (Fig 3.1B). In contrast, initiating DR at 20 months of age (AL_DR20M) does not lead to lifespan extension, indicating that the critical period of responsiveness to DR treatment lies between 16 and 20 months of age in mice (Drews et al. 2021) (Fig 3.1B). To address whether switching to DR later in life is sufficient to “rejuvenate” the BCR repertoire and recapitulate the immunological characteristics under chronic DR, the midlife (AL_DR16M) and late-onset (AL_DR20M) DR groups were evaluated (Fig 3.1B). To explore whether there are potential functionality alterations between BCR isotypes in AL_DR16M and AL_DR20M groups in comparison to chronic AL and DR groups, we determined the relative abundances of antibody isotypes. IgD abundance in AL_DR16M was significantly higher compared to AL at 24 months of age, recapitulating the DR-specific levels of IgD abundance (Fig 3.2A). In contrast, AL_DR20M mice remained unresponsive to the introduction of the new diet (Fig 3.2A). Therefore, switching to DR as late as 16 months

recapitulated the DR-specific IgD abundance, indicating improved regulation of immune self-tolerance (Gutzeit, Chen, and Cerutti 2018; Nguyen 2022).

Next, we investigated whether DR onset at 16 or 20 months of age recapitulated the increased BCR within-individual diversity of DR mice. Computation of Hill diversity spectra identified significantly higher richness and Shannon diversity in AL_DR16M compared to AL in 24-month-old mice (Fig 3.2B-C). The AL_DR16M group had comparable diversity levels to DR, exhibiting a less dramatic loss in Shannon diversity in old age compared to AL (Fig 3.2C). Conversely, the AL_DR20M Shannon diversity remained in-between AL and DR (Fig 3.2C). Surprisingly, we found a profound increase of IgM and IgE richness in AL_DR16M when compared to DR at 20 months of age (Sup Fig 3.1A). IgD Shannon diversity was also significantly higher in AL_DR16M compared to DR mice at 20 months (Sup Fig 3.1B). In addition, IgM and IgE Shannon and Simpson diversity and IgA Simpson diversity were elevated in AL_DR16M when compared to AL at 24 months of age, indicating an acute primary response (Sup Fig 3.1B-C). Further, AL_DR20M mice displayed a spike in IgE Shannon diversity compared to AL at 24 months (Sup Fig 3.1B). In contrast, IgG Shannon and Simpson diversity in AL_DR20M were consistent with AL, but significantly lower than DR (Sup Fig 3.1B-C). Therefore, DR onset at 16 and 20 months of age mitigated the age-associated decline in BCR within-individual diversity. Although starting DR at 20 months of age did not fully recapitulate the “younger-like” DR diversity, AL_DR16M mice recapitulated the DR diversity via an acute spike in diversity of primary (IgM) and hypersensitivity (IgE) isotypes.

The relative frequency of expanded clones within the antibody repertoire increases with age (Oh, Lee, and Shin 2019; Gibson et al. 2009) and we found that DR reduced the age-dependent clonal expansion rate compared to AL mice (Fig 3.2E). Therefore, we examined whether DR onset at 16 or 20 months of age can reduce the BCR repertoire clonal expansions in old age. There was lower clonal expansion in AL_DR16M compared to AL at 24 months of age (Fig 3.2E). However, AL_DR20M mice remained in-between the AL and DR levels (Fig 3.2E). Thus, DR onset at 16 months of age can reduce the portion of the BCR population occupied by expanded clones.

RDI increased with age at a slower rate in DR compared to AL (Fig 3.2F). Thus, we evaluated whether AL_DR16M mice or AL_DR20M have lower RDI compared to AL. There was a clear separation in two groups: AL and AL_DR20M mice had significantly higher inter-individual dissimilarity than DR and AL_DR16M (Fig 3.2F). This recapitulation of the lower repertoire divergence in DR by AL_DR16M, was already present 4 months after the start of DR, at 20 months (Fig 3.2F). Moreover, AL_DR16M mice experienced a reduction in IgE RDI when compared to AL and DR at 20 months of age (Sup Fig 3.1E), which stabilised to levels similar

to AL and DR 4 months later. At 24 months, RDI of IgA and IgM was lower in AL_DR16M than in AL and DR (Sup Fig 3.1E). Similarly, 24-month-old AL_DR20M mice had reduced IgA and IgM RDI compared to AL (Sup Fig 3.1E). Thus, the effects of DR onset on the repertoire RDI highlighted an initial loss in inter-individual dissimilarity, mainly affecting AL_DR16M mice, consistent with the spike in diversity of IgE, IgA and IgM.

DR affected the different diversification and affinity maturation steps of the BCR development (Fig 3.2E-F, 3.2I, Sup Fig 3.2A). Thus, we evaluated repertoire characteristics of AL_DR16M and AL_DR20M mice. *IghV* and *IghJ* gene usage in AL_DR16M mice was comparable to DR (Sup Fig 3.2A, 3.2B). In line with the findings in DR mice, there were no changes in SHM or class-switch recombination in AL_DR16M or AL_DR20M mice (Fig 3.2G, 3.2H, 3.2J). At 24 months of age, AL_DR16M but not AL_DR20M mice underwent a DR-like reduction in the proportion of different CDR3-length-distributions, which was significantly different from AL (Fig 3.2I). However, the age-dependent skewing of IgA CDR3-length-distribution observed in AL mice was reduced in AL_DR20M mice (Sup Fig 3.1H). On the whole, starting DR as late as 16 months of age reverted the general shift in the CDR3-length-distribution observed during ageing.

In summary, similar to the lifespan reports (Drews et al. 2021) (Fig 3.1B), DR initiation as late as 16 months of age recapitulated the main effects of chronic DR on the BCR dynamics: within-individual diversity, inter-individual dissimilarity, and clonal expansion rate. More specifically, AL_DR16M displayed a profound acute response to DR initiation, generating a spike in IgM and IgE richness, and IgD Shannon diversity at 20-months. While AL_DR16M recapitulated DR-specific levels by 24-months of age, the AL_DR20M group displayed only a partial response, increasing IgE Shannon diversity and reducing the age-dependent skewing of the IgA CDR3-length-distribution.

3.2.5 Effects of DR and ageing on the intestinal BCR repertoire

DR modulates the composition of the gut microbiome in mice and humans (von Schwartzberg et al. 2021; C. Zhang et al. 2013). As mucosal B-cells in the gut are in direct contact with the gut microbiome (Belkaid and Hand 2014; Lindner et al. 2015, 2012; Macpherson et al. 2018), we asked whether DR-induced changes in the microbiome also affect the gut mucosal BCR repertoire. Within the small intestine, the highest accumulation of B-cells is found in the Peyer's patches in the ileum (Donaldson, Shih, and Mabbott 2021). Thus, we measured BCR repertoire dynamics in the ileum dependent on age and DR. Consistent with previous studies (Macpherson et al. 2018; Lindner et al. 2012, 2015), IgA was the predominant isotype in the ileum, accounting for up to 98% of all immunoglobulin isotypes

in young animals (Fig 3.3A). IgM, IgG, IgD, and IgE only accounted for 0.39, 0.33, 0.16 and 0.17% in young mice, respectively (Fig 3.3A). In 20-month-old AL mice, the relative frequencies of IgM and IgG were significantly increased compared to 5-month-old mice, while there was a reduction in IgA (Fig 3.3A). Therefore, in line with previous reports (Macpherson et al. 2018), we observed that in old age, there was an increase in IgM and IgG isotypes at the expense of IgA, which could be important for maintaining homeostasis with the intestinal microbiome.

Next, we investigated whether ageing or DR affected the BCR within-individual diversity in the ileum. Hill diversity spectra analysis of the BCR repertoire revealed an increased richness in DR mice compared to AL at 20 months of age, which was significantly lower than AL in 24-month-old mice (Fig 3.3B). In addition, there was significantly higher IgG richness in DR compared to AL in 24-month-old mice (Sup Fig 3.3A). However, no changes in Shannon or Simpson diversity were detected (Fig 3.3C-D, Sup Fig 3.3B-C). Similarly, the degree of clonal expansion was not significantly changed by age or DR diet (Fig 3.3E, Sup Fig 3.3D). Thus, although we did not observe strong ageing-associated effects on BCR within-individual diversity in the ileum (Fig 3.3B-D), DR mildly increased the diversity of IgG small rare clones (Fig 3.3B). Even in an IgA-dominated organ, IgG has been indirectly implicated in mucosal inflammation and commensal regulation (Castro-Dopico and Clatworthy 2019). Therefore, increased IgG diversity could have implications for enhanced protection against enteropathogens and intestinal inflammation under DR.

To study the effect of age and evaluate whether DR generates a less dissimilar BCR repertoire between individuals, we examined the changes in the ileum RDI. RDI was stable with age in both AL and DR mice (Fig 3.3F). However, there was a significant age-associated decline in the IgM RDI of AL mice, that was mitigated by DR (Sup Fig 3.3E). In addition, RDI of IgD and IgG increased with age in AL mice but decreased in DR mice (Sup Fig 3.3E). Therefore, DR generates a more diverse and less dissimilar ileal BCR repertoire between individuals, with higher chance to bind to known and novel antigens.

Previous studies have shown an age-associated decline in B cell selection processes in the gut, paired with declining SHM rate (Dunn-Walters 2015; McKean et al. 2008). We evaluated whether DR has an effect on class-switch recombination and SHM. As previously reported in humans (Banerjee et al. 2002), the young gut BCR consisted primarily of post-antigenic clones (~73%), some antigen-stimulated clones (~25%) and very few naïve ones (~2%) (Fig 3.3J). There were no differences in the proportions of BCR clones in each class-switch recombination stage with age or under DR (Fig 3.3J). Consistent with previous work (Lindner et al. 2015), the ratio between dN/dS was positive (>1) at all time points indicating positive

selection through age (Sup Fig 3.4C). In contrast, DR mice had significantly higher non-synonymous SHM compared to AL at 24 months of age (Fig 3.3H). Further, we found an age-associated decline in synonymous and non-synonymous SHM in IgM (Sup Fig 3.3F-G). In addition, IgA non-synonymous SHM declined with age in AL (Sup Fig 3.3G), and synonymous IgA SHM increased with age in DR mice (Sup Fig 3.3F). Finally, CDR3 length and variability were also not affected by age or DR (Fig 3.3I, Sup Fig 3.3H). Taken together, DR diversifies the ileal BCR repertoire and increases its affinity maturation by means of SHM of IgM and IgA isotypes.

In summary, age and DR have only minor effects on BCR composition in the ileum. However, SHM rates declined with age in AL mice, and this decline was mitigated by DR. As a peripheral organ, the ileum has more direct exposure to microbial antigens, which induce antibody maturation via SHM and class-switch recombination (Zhao and Elson 2018). Our data imply that DR improves antibody maturation in the ileum through an increased SHM at old age.

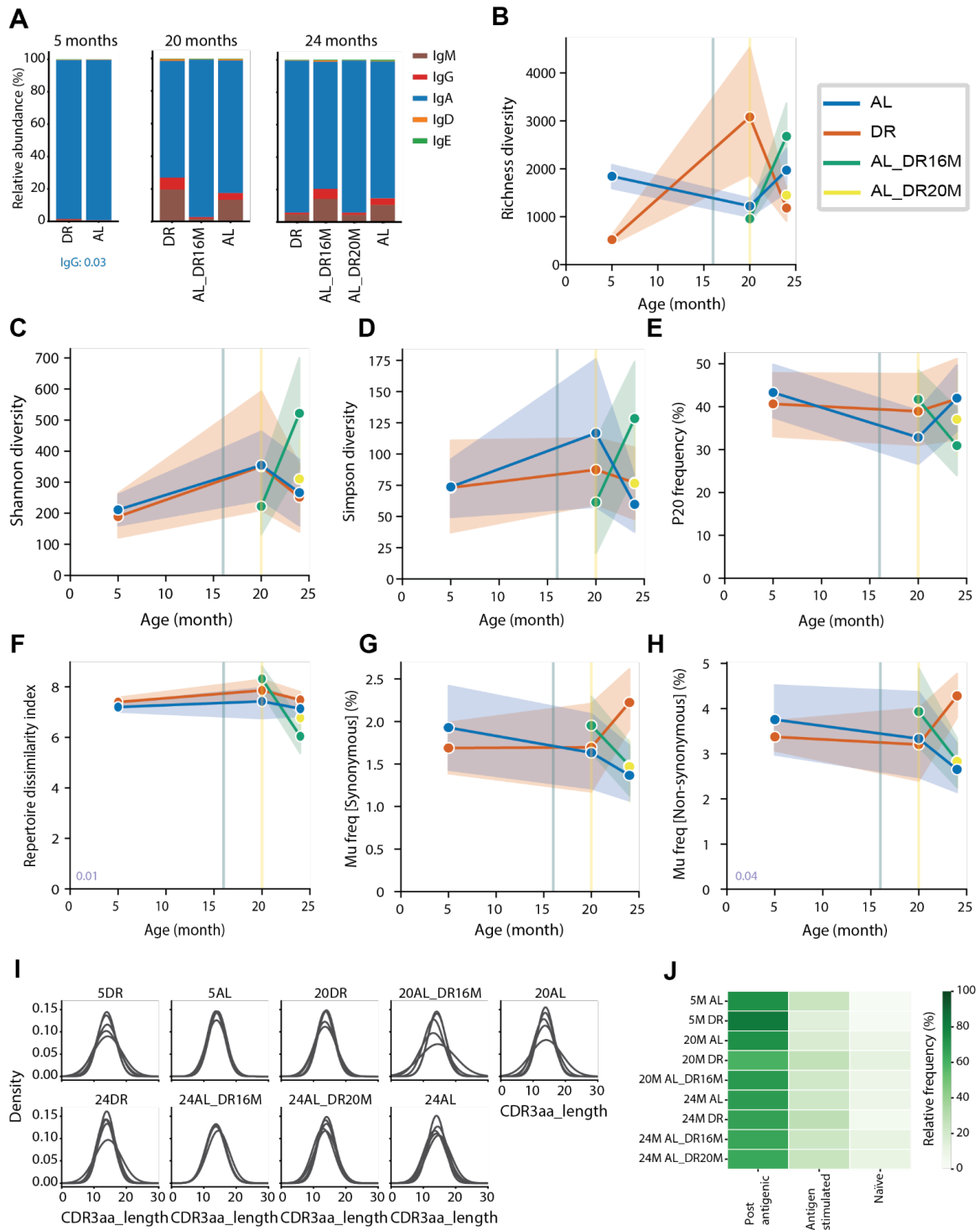


Figure 3.3: DR and ageing have only small effects on the intestinal BCR repertoire **A)** Relative abundance of antibody isotypes in the ileum. Significant differences through age (linear regression): IgG (AL p-value = 0.03). Significant differences between 5 and 20 months of age (Mann-Whitney U test): IgM (AL p-value = 0.036), IgG (AL p-value = 0.036), IgA (AL p-value = 0.024). **B)** Richness within-individual diversity. Significant differences at 20 months of age (Mann-Whitney U test): DR vs AL p-value = 0.002; AL_DR16M vs DR p-value = 7.3×10^{-5} . Significant differences at 24 months of age (Mann-Whitney U test): DR vs AL p-value = 0.01; AL_DR16M vs DR p-value = 0.008. **C)** Shannon within-individual diversity. **D)** Simpson within-individual diversity. **E)** Clonal expansion. **F)** Inter-individual dissimilarity. Significant differences through age and diet (2-way ANOVA): DR vs AL p-value = 0.01. Significant differences at 20 months of age (Mann-Whitney U test): AL_DR16M vs AL p-value = 0.04; AL_DR16M vs DR p-value = 0.009. **G)** Frequency of synonymous SHM. **H)** Frequency of non-synonymous SHM. Significant differences through age and diet (2-way ANOVA): DR vs AL p-value = 0.04. Significant differences at 24 months of age (Mann-Whitney U test): DR vs AL p-value = 0.043; AL_DR16M vs DR p-value = 0.043; AL_DR20M vs DR p-value = 0.043. **I)** Gaussian-fitted CDR3 length distribution per mouse in study. **B-H)** Lines correspond to mean, and shaded area to 95% confidence intervals. **J)** Relative amount of clones according to their class-switch status. Non-significant p-values in Supplementary File 2.

3.2.6 Late-onset DR has no effect on the intestinal BCR repertoire

To address whether the ileum BCR repertoire in the AL_DR16M and AL_DR20M groups recapitulates the slightly improved BCR diversification under chronic DR, we first evaluated the relative abundances of isotypes. No differences in isotype abundances were detected in AL_DR16M or AL_DR20M (Fig 3.3A). By calculating Hill diversity spectra, we found a significantly lower richness in AL_DR16M and AL compared to DR in 20-month-old mice (Fig 3.3B). However, at 24 months of age, AL_DR16M and AL mice exhibited a significantly higher richness than DR (Fig 3.3B), suggesting that the presence of rare clones remained unaffected in AL_DR16M mice. On the other hand, AL_DR20M mice represented an in-between state, with no distinction from either AL or DR (Fig 3.3B). Thus, we did not observe a recapitulation of the DR-like diversification in mice switched to DR late in life. However, we detected an acute response to DR initiation in AL_DR16M through an elevated total number of distinct BCR clones.

We next questioned whether this acute increase in the AL_DR16M diversity translated into other characteristics of the ileal BCR repertoire. No changes in clonal expansion were observed as a response to late DR onset (Fig 3.3E). However, RDI was significantly higher in AL_DR16M 20-month-old mice when compared to AL (Fig 3.3F). Yet, at 24 months of age, AL_DR16M mice had significantly lower dissimilarity than DR mice (Fig 3.3F), indicating a

strong loss of inter-individual dissimilarity in AL_DR16M mice. We found an acute spike in inter-individual dissimilarity of AL_DR16M at 20 months of age in IgA, IgD and IgG, when compared to AL and DR (Sup Fig 3.3E). We further detected a significantly lower IgA, IgM and IgE RDI in AL_DR16M at 24 months compared to AL and DR (Sup Fig 3.3E). These changes in AL_DR16M suggest that the gut BCR repertoire is somewhat responsive to DR initiation at 16 months of age. On the other hand, the IgM RDI of AL_DR20M mice was lower than AL (Sup Fig 3.3E), whereas IgE RDI was lower compared to DR (Sup Fig 3.3E). RDI of AL_DR20M was lower in IgA, and higher in IgG than both AL and DR (Sup Fig 3.3E). Thus, the isotype inter-individual dissimilarity as a response to the introduction of DR diet was highly dependent on the age of DR onset.

To examine whether DR initiation at 16 and 20 months of age recaptured the SHM rate preservation under chronic DR treatment, we evaluated SHM rates in AL_DR16M and AL_DR20M mice. Surprisingly, non-synonymous SHM in 24-month-old mice was significantly lower in AL_DR16M, AL_DR20M and AL compared to DR (Fig 3.3G, 3.3H). This was consistent with SHM findings in IgA (Sup Fig 3.3G), indicating that late-onset of DR did not impact affinity maturation. Finally, CDR3-length-distribution variability of IgD at 20 months was higher in AL_DR16M and AL compared to DR (Sup Fig 3.3H), and significantly decreased in AL_DR16M when compared to both AL and DR at 24 months in IgM (Sup Fig 3.3H).

Taken together, AL_DR16M and AL_DR20M did not recapitulate the DR-like BCR dissimilarity, or SHM rate in the ileum. This refractoriness of response to DR initiation was in line with previous studies in mice and killifish, where diet changes or antibiotics exposure had a minor impact on the gut BCR repertoire (Lindner et al. 2015; Bradshaw et al. 2022). AL_DR16M and AL_DR20M mice manifested little to no effect on the ileum BCR repertoire; they maintained a repertoire similar to chronic AL, even after dietary switch.

3.2.7 The ageing microbiome responds to late-onset DR

The gut microbiome undergoes significant changes with age (Badal et al. 2020) (Chapter 2), primarily reflected in a marked age-dependent decline in within-individual diversity. This decline is accompanied by loss of beneficial bacteria and extensive occupation by commensal and pathogenic bacteria (Nagpal et al. 2018; van der Lugt et al. 2018). Caloric restriction maintains a high abundance of bacteria considered to be beneficial for colonic health (Kok et al. 2018). Having observed mild differences between AL and DR in the ageing ileum BCR repertoire, we questioned whether the microbiome composition was as stable as the ileum BCR repertoire, given the direct contact between ileum and microbiome (Belkaid and Hand 2014; Lindner et al. 2015, 2012; Macpherson et al. 2018). To address this question, we

performed V4-16S rRNA amplicon sequencing of caecal contents. Consistent with our findings in the ileum BCR repertoire (Fig 3.3B-D), we found no difference in microbial within-individual diversity with age or between AL and DR. In contrast, inter-individual dissimilarity in the microbiome, measured using the Unweighted UniFrac diversity index, was significantly higher in AL when compared to DR at 20 and 24 months of age (Fig 3.4).

Given that the microbiome inter-individual dissimilarity increased with age to a larger extent in AL than in DR mice, we next asked whether the caecal microbiome would respond to DR switch at 16 and 20 months of age by converging towards a DR-like microbiome. As opposed to the mild response of the gut BCR repertoire in AL_DR16M and AL_DR20M (Fig 3.3), the gut microbiome of AL_DR16M diverged from the microbiome of AL mice already at 20 months of age (Fig 3.4). These differences persisted up to 24 months, where the inter-individual variability of AL_DR16M and AL_DR20M mice was significantly different from AL (Fig 3.4). Therefore, contrary to the ileum BCR repertoire, the caecal microbiome rapidly responded to the switch from AL to DR, even when initiated at 20 months of age.

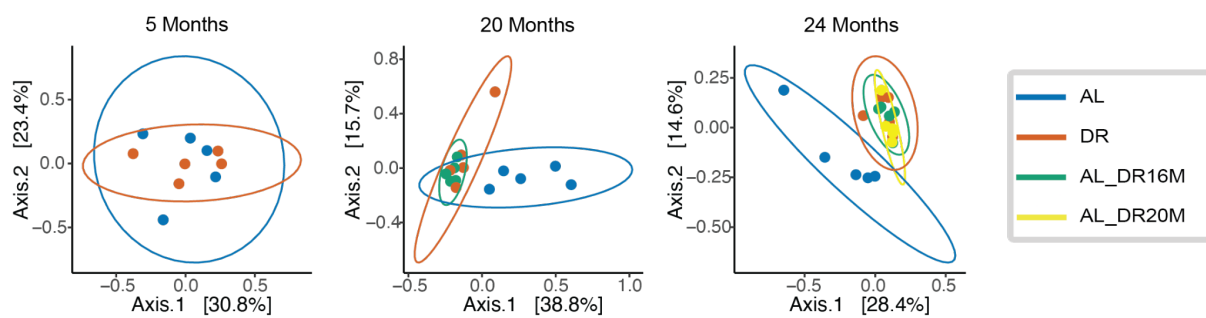


Figure 3.4: The ageing microbiome responds to late-onset DR. Bray-Curtis Principal coordinates analysis; inter-individual dissimilarity. Significant differences at 20 months of age (Mann-Whitney U-test) DR vs AL p-value = 0.009; AL_DR16M vs DR p-value = 0.01. Significant changes at 24 months of age (Mann-Whitney U-test) DR vs AL p-value = 0.01; AL_DR16M vs AL p-value = 0.009; AL_DR20M vs AL p-value = 0.01.

3.2.8 DR-related BCR metrics are associated with healthier phenotypes

Finally, to characterise the observed BCR repertoire dynamics patterns and understand how they are reflected in host health, we tested the correlation between morbidity and BCR metrics, in both the spleen and ileum (Fig 3.5A-B). The ‘macromorbidity index’ developed in the present work was adapted from (Ikeno et al. 2009; Bokov et al. 2011b; Treuting et al. 2008) to encompass the collected macro-pathology of these mice, previously described in detail by Drews et al. 2021. For each mouse, the morbidity index was calculated as the sum of non-

neoplastic pathologies burden, and neoplasia grade. A degree of 1 was assigned to each non-neoplastic pathological finding at dissection, while neoplasia were graded as 0 (absence of tumours), 1 (1 organ affected by tumours), or 2 (2 or more organs affected by tumours, representing metastatic cancer). Different models of morbidity index calculation were tested, yielding similar associations to BCR metrics in all cases (Sup Fig 3.5A-B).

Of all the metrics obtained from the spleen BCR repertoire, clonal expansion (P20), inter-individual dissimilarity (RDI_uniqueness) and mean CDR3 length (cdr3_mu) were positively associated with the macromorbidity index. Shannon and Simpson diversity metrics displayed a negative association (Fig 3.5A), indicating that higher within-individual diversity is associated with healthier mice. Further, we asked which isotypes showed strongest correlation with morbidity, and found that IgM and IgG underpin the strongest association between morbidity and BCR characteristics (Fig 3.5C). With respect to the ileal BCR repertoire metrics, only Simpson diversity was negatively associated with morbidity; high Simpson values were found in healthier mice (Fig 3.5B, Sup Fig 3.5C).

Having found lower clonal expansion and RDI in DR mice, paired with increased Shannon and Simpson diversity (Fig 3.2C-F), our findings suggest that DR might delay the systemic functional decline of the BCR repertoire with age, and be associated younger and healthier BCR repertoire. Similarly, decreased clonal expansion and RDI, and increased Shannon diversity in AL_DR16M mice, might suggest that initiating DR as late as 16 months could rejuvenate the BCR repertoire and be associated with lower morbidity.

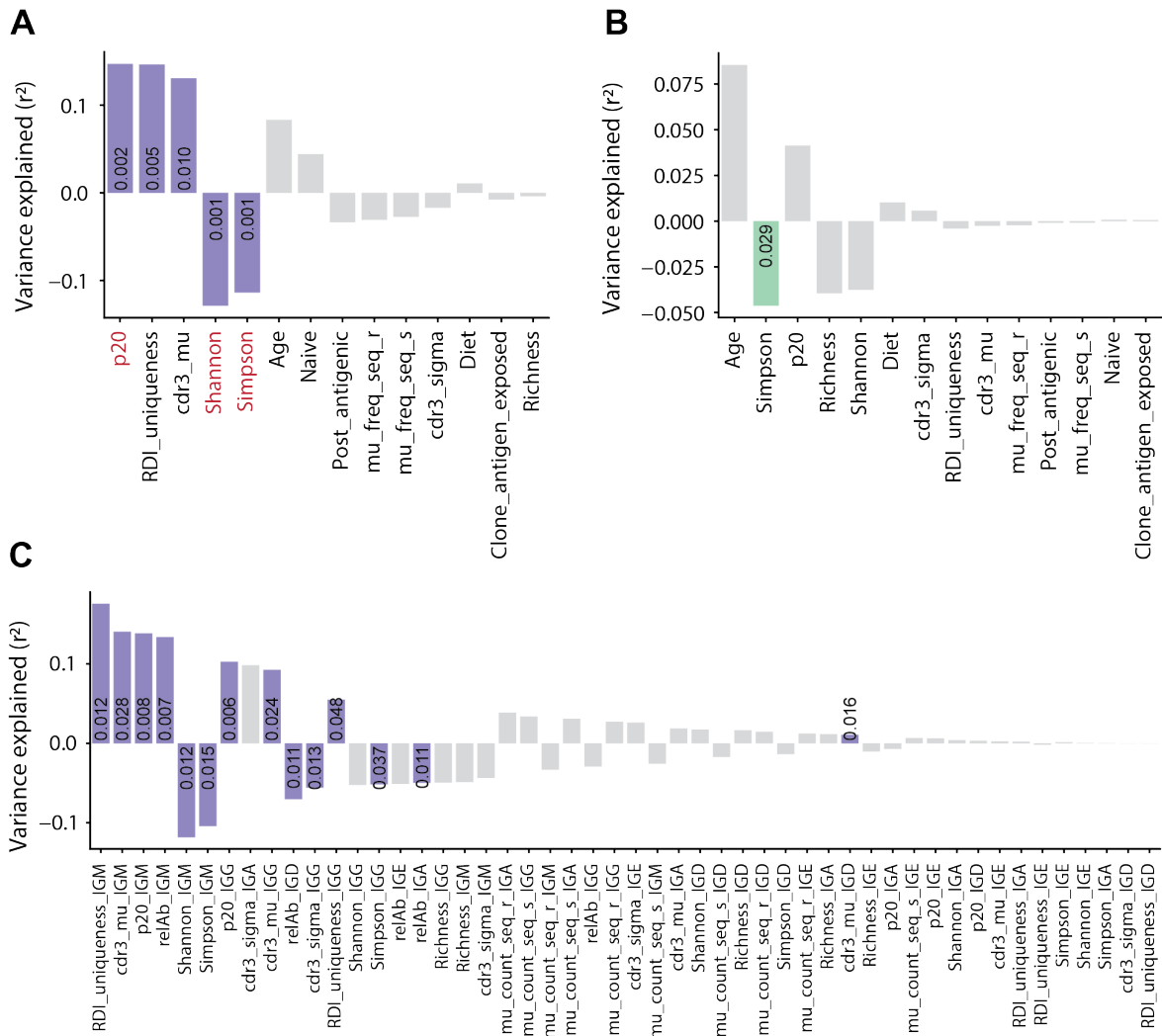


Figure 3.5: DR-associated BCR metrics are associated with healthier phenotypes. Percentage of variance explained in 'macromorbidity index' by **A)** general BCR spleen metrics, **B)** general BCR ileum metrics, **C)** isotype-specific BCR spleen metrics. Coloured bars are spearman p-value < 0.05. Red metrics are Bonferroni corrected p-value < 0.05.

3.3 Discussion

Establishing and maintaining a tight and life-long regulation of immune responses is vital for host homeostasis. The profound impairment of immune function with ageing is well documented (Wick et al. 2000; Nikolich-Zugich 2005; Ademokun, Wu, and Dunn-Walters 2010; Weiskopf, Weinberger, and Grubeck-Loebenstein 2009), and thereby strategies that can ameliorate the age-associated immune dysregulation may be holding a great promise to delay ageing. We asked whether the most powerful anti-ageing intervention known to date (dietary restriction, or DR) has an impact on immune homeostasis, or whether it exerts its function independently from the immune system. Furthermore, DR can beneficially impact host health- and lifespan when started as late as 16 months of age (Drews et al. 2021). To investigate how the B cell receptor (BCR) repertoire changes with age, under chronic DR, and under midlife- and late-life onset of DR diet in the mouse spleen and ileum, we performed BCR sequencing. In addition, we test whether the critical temporal window within which DR beneficially impacts host health- and lifespan is consistent with a remodelling of the BCR repertoire dependent on age of DR onset. To our knowledge, this is the first study to use BCR sequencing to explore the mouse B cell clonal population dynamics with age in response to anti-ageing interventions. Our dataset allowed us to not only investigate the general characteristics of the BCR repertoire in the spleen and ileum, but also the corresponding changes on BCR isotypes. Here, we show for the first time that DR mitigates the ageing of the BCR repertoire in both spleen and ileum. Further, we report a recapitulation of the splenic DR-like BCR repertoire in mice where DR was started at 16 months of age, but not at 20 months. In the current work, we also provide associations of BCR repertoire characteristics to a novel macromorbidity index. We report an association of AL-like BCR repertoire characteristics with high morbidity, and DR-like characteristics with improved health.

The ageing BCR repertoire in the spleen of AL-fed mice followed the classically described pattern in both mice and humans: decreased within-individual diversity, coupled with increased clonal expansion rate and inter-individual dissimilarity (Fig 3.2B-F) (de Bourcy et al. 2017; Gibson et al. 2009; Weksler and Szabo 2000; Nagpal et al. 2018; Booth and Toapanta 2021). On the other hand, although ageing in chronic DR mice was also accompanied by a decline in within-individual BCR variability, increased clonal expansions and inter-individual dissimilarity, these effects were mitigated compared to AL (Fig 3.2C, 3.2E, 3.2F). Importantly, low within-individual diversity, high clonal expansions and high inter-individual dissimilarity correlated with high macromorbidity index. Thereby, the DR-mediated mitigation of the age-associated BCR repertoire dysregulation might, at least partly, contribute to the beneficial effects of DR on mouse health (Fig 3.5A). Furthermore, there is growing evidence that

maintenance of a high BCR diversity translates to enhanced ability to generate robust antibody responses to novel antigens and possibly an enhanced vaccination response at old age (Dunn-Walters 2015; Okawa, Nagai, and Hase 2020). In fact, loss of BCR repertoire diversity in older individuals has been associated with poor vaccination response against pneumococcus and influenza (Ademokun et al. 2011; Tas et al. 2016; de Bourcy et al. 2017). Thus, the observed age-associated decline in within-individual diversity and post-antigenic BCR clones in AL mice (Fig 3.2C, 3.1J), suggests a decrease in high-affinity class-switched isotypes, and might also contribute to the impaired vaccination response in old age (Oh, Lee, and Shin 2019). The amelioration of the ageing splenic BCR dysregulation by DR indicates that DR maintains a healthier, younger-like BCR repertoire. However, a limitation of the current study is the lack of information on the B cell subsets (i.e. marginal, follicular, B-1, etc) encompassing the sequenced cell pool. Future studies performing fluorescence-activated cell sorting should not only investigate the B cell types involved in the DR response, but also causally address whether DR improves vaccination outcomes due to “enrichment” of the BCR repertoire.

Genome variation in the BCR loci is instrumental for mounting adequate immune responses and *IghV* and *IghJ* gene usage have been shown to be largely implicated, thereby affecting susceptibility to various diseases (Raposo et al. 2014). Results from a study in splenocytes showed an age-related increase in *IghV2*, *IghV11*, *IghJ1*, as well as reduction in *IghJ2* gene usage (Holodick et al. 2016). Here, we found a more pronounced decline in *IghV*-gene usage with age in AL compared to DR, especially in *IghV4* (Sup Fig 3.2A-B). Although very little is known about the functional relevance of these changes in ageing, differential *IghV* gene usage has been implicated in age-related diseases, such as rheumatoid arthritis and multiple sclerosis, in both mice and humans (Vencovský et al. 2002; Raposo et al. 2014; Walter et al. 1991). Further, a growing body of evidence is indicative of a role of *IghV* gene usage in polyreactivity, especially in HIV and influenza virus antibody responses; polyreactivity is defined as the ability of an antibody molecule or of a BCR to bind to multiple distinct antigenic targets (Dimitrov et al. 2013). While polyreactivity is thought to dramatically increase with age in mice (Gunti and Notkins 2015), the decline in usage of some *IghV* genes, including the *IghV4* observed in this study, would be indicative of a reduced polyreactivity in our AL mice with age that was attenuated by DR (Sup Fig 3.2A). Increased polyreactivity has beneficial effects, including the diversification of immune repertoires and clearance of defective apoptotic cells, preventing inflammatory responses (Dimitrov et al. 2013). Therefore, we speculate that compared to AL, DR treatment might help retain some levels of polyreactivity and its corresponding benefits for longer periods of time.

During B cell development in the bone marrow, there is preferential removal of B cells expressing BCRs with long CDR3s (Wardemann et al. 2003). Studies in human peripheral blood have associated long CDR3 length with old age and increased autoreactivity, suggesting that there is a selection against BCRs with long CDR3s in the aged immune system (C. Wang et al. 2014). Similarly, in this study long CDR3s correlated with high macromorbidity index (Fig 3.5A). Although the mean CDR3 length was not different between AL and DR (Sup Fig 3.2D), there was increased skewing of CDR3 length production in AL mice, generating BCRs of a smaller length range than both DR and AL_DR16M mice (Fig 3.2I). Even though long CDR3s were found in mice with high macromorbidity, we did not observe a significant reduction under DR anti-ageing intervention. Future studies including higher numbers of mice should evaluate CDR3 lengths and determine whether DR maintains selection against BCRs with long CDR3s, to protect from the ageing-associated increased autoreactivity.

Our results highlight the importance of global splenic BCR repertoire dynamic metrics, such as within-individual variability, inter-individual dissimilarity, clonal expansions and CDR3 length distribution (Fig 3.2C, 3.2E-F) in enhanced health under DR (Fig 3.5A). Moreover, we also uncover intriguing ageing- and DR-associated changes in immunoglobulin isotypes, which have been thus far unexplored in the context of anti-ageing interventions. With respect to ageing-associated changes, we found that IgM, known for their role in the primary immune response as poly-reactive antibodies involved in opsonization of antigens (Schroeder and Cavacini 2010), underwent a decline in within-individual diversity with age in both AL and DR (Sup Fig 3.1B-C). Similarly, IgG, which is involved in long-term protection and neutralisation of toxins and viruses (Schroeder and Cavacini 2010), showed a decline in within-individual diversity with age in AL (Sup Fig 3.1B-C). In line with these results, previous studies have shown an association between age-related decline in IgM and IgG levels and BCR repertoire diversity, with impaired vaccination response (Ademokun et al. 2011; Jiang et al. 2013; Shi et al. 2005). In addition, we found that the low within-individual diversity of both IgM and IgG isotypes was inversely associated with morbidity (Fig 3.5C), suggesting that preservation of IgM and IgG diversity is one of the features of a 'younger', healthier BCR repertoire. Further, regarding DR-associated changes, we observed an amelioration of the ageing-associated increase in IgM clonal expansion rate (Sup Fig 3.1D). Although the implications of this change are unknown, we speculate that DR might offer a tighter regulation of the primary immune response, and thereby the maintenance of IgM clonal expansion rate might be a contributor to DR-mediated beneficial effects. This is corroborated by the fact that high IgM clonal expansion was associated with morbidity (Fig 3.5C). Collectively, although the repertoire trajectories described in this work strictly reflect non-pathogen exposure conditions, as any type of infection is highly unlikely in the current cohort of mice, our results highlight the potential

involvement of IgM and IgG in DR-associated healthspan and lifespan benefits. Nevertheless, in light of the macromorbidity-associated isotype-specific observations, future studies where isotypes are evaluated in the context of healthy ageing are necessary to more comprehensively reveal the implications of these changes on adaptive immune function and DR-associated beneficial effects.

Here, we demonstrate that DR and AL_DR16M mice have “healthier” repertoires than AL and AL_DR20M (Fig 3.5A), especially affecting the splenic within-individual variability, and clonal expansion (Fig 3.2C, 3.2E). The improvement of the immune health in DR and AL_DR16M mice, is the first reported molecular phenotype consistent with the recapitulation of the lifespan extension under DR by AL_DR16M mice (Drews et al. 2021). These findings indicate that the enhanced splenic B cell adaptive immune system of DR mice can be recapitulated in an age-dependent manner, by switching to a DR feeding regime as late as 16 months of age. More specifically, AL_DR16M displayed an increased IgM, IgE and IgA Shannon and Simpson within-individual diversity, recapitulating DR levels (Sup Fig 3.1B-C). IgM spike under AL_DR16M could be indicative of a greater hematopoietic stem cells (HSC) capacity. A previous study on HSCs on chronic and midlife-onset DR mice, showed that chronic DR feeding reduced the loss of repopulating capacity of HSCs observed with age in AL. Furthermore, the onset of DR at 15 months of age improved the hematopoietic regeneration of ageing HSCs (Tao et al. 2020). Thus, an improved regeneration of HSCs would be likely to facilitate the AL_DR16M BCR repertoire responsiveness under dietary switch. Future studies on bone marrow HSCs on midlife- and late-onset DR are necessary to evaluate a possible causal association of an age-of-onset-dependent start of DR with BCR repertoire responsiveness.

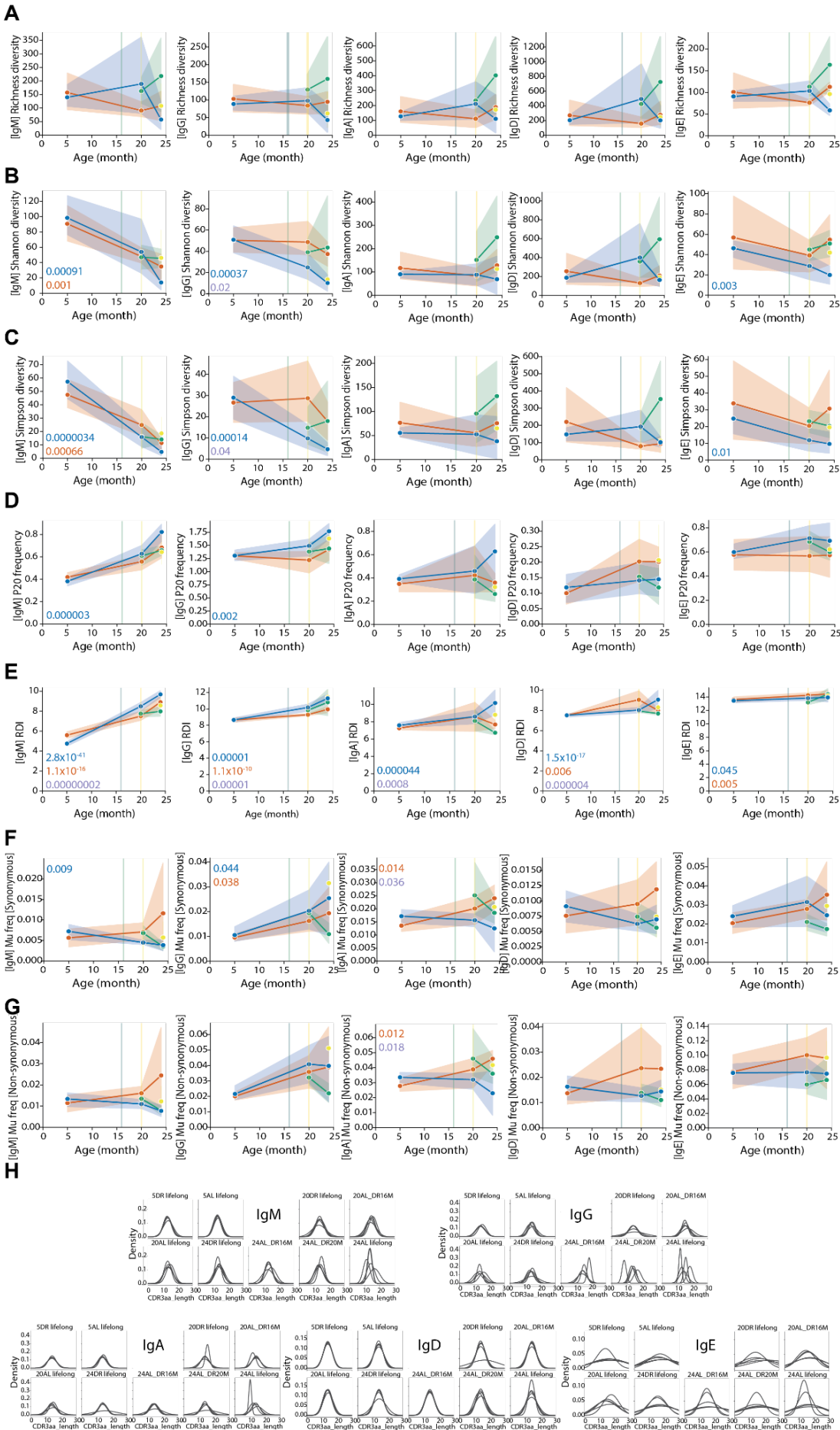
Noteworthy, we found that AL_DR16M respond to DR initiation through an increase in IgE diversity in spleen (Sup Fig 3.1B-C). Although elevated IgE levels are primarily implicated in allergic reactions (Gould and Sutton 2008; Saunders et al. 2019; Schroeder and Cavacini 2010), it is highly unlikely that food or other allergens are contributing to the increased IgE diversity levels after DR onset at 16 months, given the housing conditions and the unchanged chow food composition of our mice. Interestingly, high IgE levels have been previously documented in germ-free or antibiotic-treated mice that are typically characterised by low microbiome diversity, suggesting a regulatory role of the microbiome in controlling systemic IgE levels (Cahenzli et al. 2013). Similarly, a previous study evaluating the longitudinal microbiome characteristics of 50 AL, DR, AL_DR16M and AL_DR20M mice, reported an initial decline in within-individual microbial diversity of AL_DR16M mice before recapitulating diversity levels similar to DR by 18 months of age (Chapter 2). Therefore, the spike in IgE in the AL_DR16M mice might reflect this acute loss of microbial within-individual diversity after

DR onset. Nonetheless, future studies are necessary to confirm and comprehensively assess the changes and potential contributors in IgE responses in the context of dietary switches.

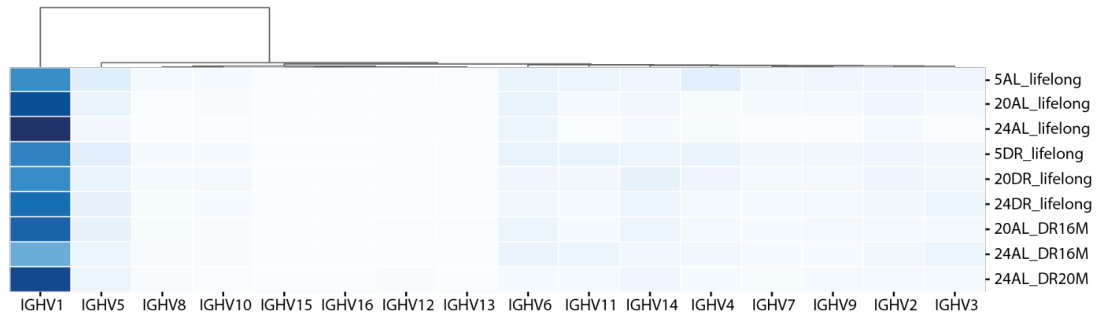
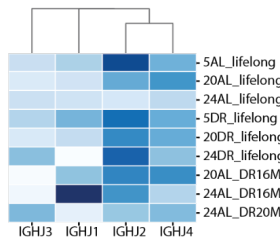
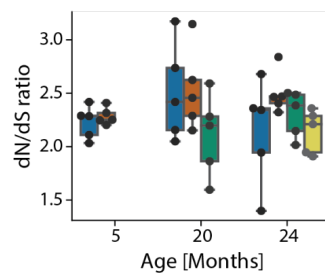
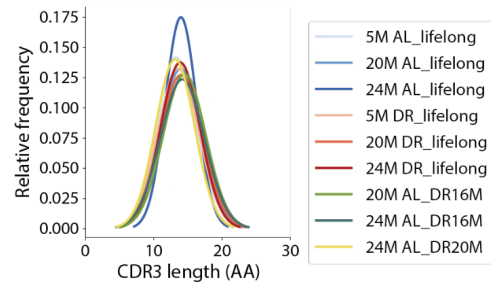
Despite the importance of the gut B cells, and the increasing number of studies examining mucosal antibodies and their interaction with the microbiome (Lindner et al. 2015, 2012; Macpherson et al. 2018; Belkaid and Hand 2014), to the best of our knowledge, the effect of anti-ageing interventions on the gut BCR repertoire are yet to be reported. Here, we show that the ileum BCR repertoire undergoes very few changes with age and under chronic or late onset DR. On the contrary, the microbiome was found to rapidly respond to the switch to DR, even when DR was initiated at 20 months of age (Fig 3.4). In line with other studies where short-term antibiotics, microbiome transfers, or introduction of new diets did not result in changes in the ileum B cell compartment (Bradshaw et al. 2022; Lindner et al. 2015), the switch to DR diet, independently of age-of-onset, did not strongly affect the gut BCR repertoire (Fig 3.3). Nonetheless, the SHM mechanism was found to be highly influenced by both age and diet in the ileum, which is not surprising given the constant microbial antigenic exposure in this organ (Zhao and Elson 2018). More specifically, a declining ageing SHM capacity was observed in AL mice (Fig 3.3G-H), affecting predominantly the IgA isotype (Sup Fig 3.3F-G). Previous analysis of IgA repertoire in human colon and mouse small intestine revealed that neither antibiotic treatment nor diet modulate the IgA clonal composition (Lindner et al. 2015). It was postulated that, to maintain homeostasis through the interaction of the host and its microbiome, the IgA repertoire undergoes diversification of existing memory B cells, instead of generating new B cell clones (Lindner et al. 2015). Elevated SHM in Peyer patches is critical for the generation of a diverse repertoire that can undergo affinity maturation and selection at a later phase (Macpherson et al. 2018). Therefore, the decline in IgA SHM with age we observed under AL feeding may be associated with impaired diversification and affinity maturation capacity, which might ultimately lead to disruption of host-microbiome symbiosis and compromised mucosal defence (Wei et al. 2011; Lindner et al. 2015). On the contrary, DR buffered the age-associated SHM decline observed in the AL mice ileum (Fig 3.3G-H, Sup Fig 3.3F-G), indicating that DR feeding might offer an advantage in preserving diverse mucosal immune responses and gut homeostasis for extended periods.

In conclusion, in this study we not only show mitigation of the age-associated decline in within-individual diversity of the BCR repertoire in the spleen and ileum of mice under DR, correlating with improved mouse health, but also provide the first evidence that the splenic BCR repertoire responds to a mid/late-life start of DR in an age-dependent manner. Our findings highlight the immune responsiveness of the mice where DR was initiated at 16 months of age as one of the contributing factors to extended lifespan.

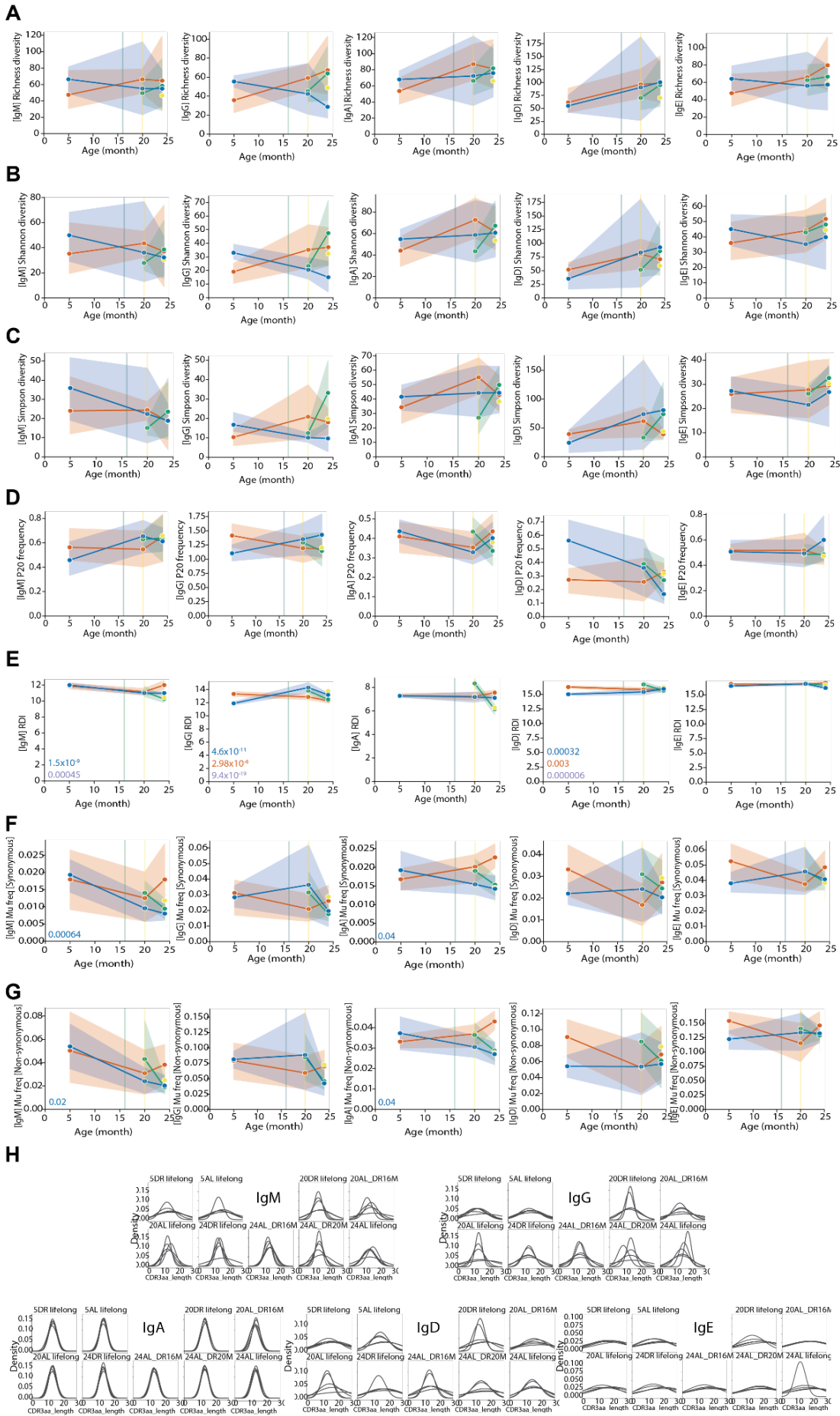
3.4 Supplementary figures



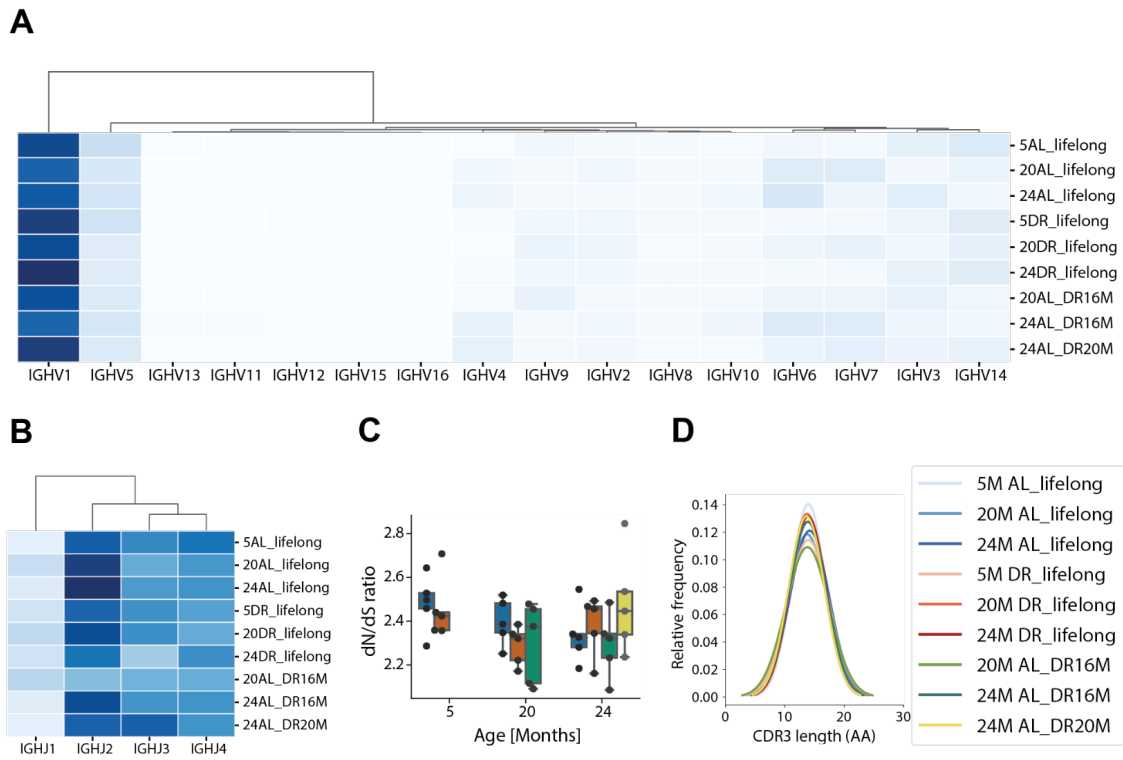
Supplementary figure 3.1: Spleen isotype-specific BCR repertoire metrics. **A)** Richness within-individual diversity. Significant differences at 20 months of age (Mann-Whitney U test): IgM (AL_DR16M vs DR p-value = 0.04), IgE (AL_DR16M vs DR p-value = 0.04). Significant differences at 24 months of age (Mann-Whitney U test): IgE (DR vs AL p-value = 0.005). **B)** Shannon within-individual diversity. Significant differences through age (linear regression): IgM (AL p-value = 0.00091; DR p-value = 0.001), IgG (AL p-value = 0.0004), IgE (AL p-value = 0.003). Significant differences through age and diet (2-way ANOVA): IgG (DR vs AL p-value = 0.02). Significant differences at 20 months of age (Mann-Whitney U test): IgD (AL_DR16M vs DR p-value = 0.02). Significant differences at 24 months of age (Mann-Whitney U test): IgM (AL_DR16M vs DR p-value = 0.04), IgG (AL_DR20M vs DR p-value = 0.01), IgE (AL_DR16M vs DR p-value = 0.002; AL_DR20M vs AL p-value = 0.02). **C)** Simpson within-individual diversity. Significant differences through age (linear regression): IgM (AL p-value = 0.000003; DR p-value = 0.0007), IgG (AL p-value = 0.0001), IgE (AL p-value = 0.01). Significant differences through age and diet (2-way ANOVA): IgG (DR vs AL p-value = 0.04). Significant differences at 24 months of age (Mann-Whitney U test): IgM (AL_DR16M vs AL p-value = 0.02), IgG (AL_DR20M vs DR p-value = 0.02), IgA (AL_DR16M vs AL p-value = 0.03), IgE (AL_DR16M vs AL p-value = 0.04). **D)** Clonal expansion. Significant differences through age (linear regression): IgM (AL p-value = 0.000003), IgG (AL p-value = 0.002). **E)** Inter-individual dissimilarity. Significant differences through age (linear regression): IgM (AL p-value = 2.8×10^{-4} ; DR p-value = 1.1×10^{-16}), IgG (AL p-value = 0.00001; DR p-value = 1.1×10^{-10}), IgA (AL p-value = 0.00004), IgD (AL p-value = 1.5×10^{-17} ; DR p-value = 0.006), IgE (AL p-value = 0.045; DR p-value = 0.005). Significant differences through age and diet (2-way ANOVA): IgM (DR vs AL p-value = 2.0×10^{-8}), IgG (DR vs AL p-value = 0.00001), IgA (DR vs AL p-value = 0.0008), IgD (DR vs AL p-value = 0.000004). Significant differences at 20 months of age (Mann-Whitney U test): IgE (AL_DR16M vs AL p-value = 0.011; AL_DR16M vs DR p-value = 0.00005). Significant differences at 24 months of age (Mann-Whitney U test): IgM (AL_DR16M vs AL p-value = 1.0×10^{-6} ; AL_DR16M vs DR p-value = 0.005; AL_DR20M vs AL p-value = 0.035), IgA (AL_DR16M vs AL p-value = 1.0×10^{-6} ; AL_DR16M vs DR p-value = 0.0005; AL_DR20M vs AL p-value = 0.049). **F)** Frequency of synonymous SHM. Significant differences through age (linear regression): IgM (AL p-value = 0.009), IgG (AL p-value = 0.044; DR p-value = 0.038), IgA (DR p-value = 0.014). Significant differences through age and diet (2-way ANOVA): IgA (DR vs AL p-value = 0.036). **G)** Frequency of non-synonymous SHM. Significant differences through age (linear regression): IgA (DR p-value = 0.012). Significant differences through age and diet (2-way ANOVA): IgA (DR vs AL p-value = 0.018). **H)** CDR3-length distribution Significant differences in CDR3-length distribution variability at 24 months of age (Kolmogorov-Smirnov): IgG (AL vs DR p-value = 0.0061), IgA (AL vs DR p-value = 0.015; AL_DR20M vs AL p-value = 0.024). **A-G)** Blue represents AL, red DR, green AL_DR16M, and yellow AL_DR20M. Lines correspond to mean, and shaded area to 95% confidence intervals.

A**B****C****D**

Supplementary figure 3.2: A) Mean relative *IghV* gene usage in the spleen BCR. Significant changes through age (linear regression): *IghV1* (AL p -value = 0.03), *IghV3* (AL p -value = 8.2×10^{-5}), *IghV4* (AL p -value = 0.001; DR p -value = 0.001), *IghV6* (DR p -value = 0.02), *IghV7* (AL p -value = 0.02; DR p -value = 0.02), and *IghV11* (AL p -value = 0.049; DR p -value = 0.03). Significant changes through age and diet (2-way ANOVA): *IghV3* (DR vs AL p -value = 0.01), *IghV15* (DR vs AL p -value = 0.02). **B)** Mean relative *IghJ* gene usage in the spleen BCR. **A-B)** Darker blue corresponds to higher gene usage, and white to lower. **C)** Ratio of non-synonymous to synonymous mutations in spleen. **D)** CDR3 length gaussian distribution in the spleen.



Supplementary figure 3.3: Ileum isotype-specific BCR repertoire metrics. **A)** Richness within-individual diversity. Significant differences at 24 months of age (Mann-Whitney U test): IgG (p-value DR vs AL = 0.01). **B)** Shannon within-individual diversity. **C)** Simpson within-individual diversity. **D)** Clonal expansion **E)** Inter-individual dissimilarity. Significant differences through age (linear regression): IgM (AL p-value = 1.5×10^{-9}), IgG (AL p-value = 4.6×10^{-11} ; DR p-value = 2.9×10^{-6}), IgD (AL p-value = 0.0003; DR p-value = 0.003). Significant differences through age and diet (2-way ANOVA): IgM (DR vs AL p-value = 0.00045), IgG (DR vs AL p-value = 9.4×10^{-19}), IgD (DR vs AL p-value = 0.000006). Significant differences at 20 months of age (Mann-Whitney U test): IgA (AL_DR16M vs AL p-value = 2.0×10^{-5} ; AL_DR16M vs DR p-value = 5.1×10^{-17}), IgD (AL_DR16M vs AL p-value = 6.7×10^{-4} ; AL_DR16M vs DR p-value = 0.007), IgG (AL_DR16M vs AL p-value = 0.01; AL_DR16M vs DR p-value = 0.00002). Significant differences at 24 months of age (Mann-Whitney U test): IgA (AL_DR16M vs AL p-value = 4.1×10^{-6} ; AL_DR16M vs DR p-value = 2.4×10^{-8} ; AL_DR20M vs AL p-value = 3.12×10^{-8} ; AL_DR20M vs DR p-value = 2.2×10^{-5}), IgM (AL_DR16M vs AL p-value = 0.00018; AL_DR16M vs DR p-value = 6.6×10^{-7} ; AL_DR20M vs AL p-value = 0.00015), IgE (AL_DR16M vs AL p-value = 7.7×10^{-5} ; AL_DR16M vs DR p-value = 0.00013; AL_DR20M vs AL p-value = 0.015), IgG (AL_DR20M vs AL p-value = 0.003; AL_DR20M vs DR p-value = 4.3×10^{-7}). **F)** Frequency of synonymous SHM. Significant differences through age (linear regression): IgM (AL p-value = 0.0006), IgA (AL p-value = 0.04). **G)** Frequency of non-synonymous SHM. Significant differences through age (linear regression): IgM (AL p-value = 0.02), IgA (AL p-value = 0.04). Significant differences at 24 months of age (Mann-Whitney U test): IgA (DR vs AL p-value = 0.024; AL_DR16M vs DR p-value = 0.024; AL_DR20M vs DR p-value = 0.024). **H)** CDR3-length distribution. Significant differences at 20 months of age (Kolmogorov-Smirnov): IgD (DR vs AL p-value = 0.036; AL_DR16M vs DR p-value = 0.036). Significant differences at 24 months of age (Kolmogorov-Smirnov): IgM (DR vs AL p-value = 0.015; AL_DR16M vs DR p-value = 0.015). **A-G)** Blue represents AL, red DR, green AL_DR16M, and yellow AL_DR20M. Lines correspond to mean, and shaded area to 95% confidence intervals.



Supplementary figure 3.4: **A)** Mean relative *IghV* gene usage in the ileum BCR. **B)** Mean relative *IghJ* gene usage in the ileum BCR. **A-B)** Darker blue corresponds to higher gene usage, and white to lower. **C)** Ratio of non-synonymous to synonymous mutations in ileum. **D)** CDR3 length gaussian distribution in the ileum.

4. Appendix: Primers and oligonucleotides

4.1 PCR primers for 16S-Sequencing

Name	Sequence	Source
V4-515F	ACACTCTTTCCCTACACGACGCTCTTCCGATCTGTGYCAGCMGCCGCGGTAA	(Caporaso et al. 2011)
V4-806R	GTGACTGGAGTTCAGACGTGTGCTCTTCCGATCTGGACTACNVGGGTWTCTAAT	(Caporaso et al. 2011)

4.2 Reverse-transcription isotype-specific primers for BCR-Sequencing

Name	Sequence	Source
mIGG12_r1	KKACAGTCACTGAGCTGCT	(Turchaninova et al. 2016)
mIGG3_r1	GTACAGTCACCAAGCTGCT	(Turchaninova et al. 2016)
mIGA_r1	CCAGGTCACATTCATCGTG	(Turchaninova et al. 2016)
mIGM_r1	CTGGATGACTTCAGTGTGT	(Turchaninova et al. 2016)
mIGD_r1	GCCATTTCTCATTTAGAGG	(Turchaninova et al. 2016)
mIGE_r1	G TTCACAGTGCTCATGTTC	(Turchaninova et al. 2016)

4.3 Template-switch oligos for reverse transcription for BCR-Sequencing

Name	Sequence	Source
SmartNNNa	AAGCAGUGGTAUCAACGCAGAGUNNNNUNNNUNNNNUCTTrGrGrGrG	(Turchaninova et al. 2016)

4.4 Primers for first PCR amplification for BCR-Sequencing

Name	Sequence	Source
M1S5	AAGCAGTGGTATCAACGCA	(Turchaninova et al. 2016)
mIGG12_r2	ATTGGGCAGCCCTGATTAGTGGATAGACMGATG	(Turchaninova et al. 2016)
mIGG3_r2	ATTGGGCAGCCCTGATTAAGGGATAGACAGATG	(Turchaninova et al. 2016)
mIGA_r2	ATTGGGCAGCCCTGATTTCAAGTGGGTAGATGGTG	(Turchaninova et al. 2016)
mIGM_r2	ATTGGGCAGCCCTGATTGGGGGAAGACATTTGG	(Turchaninova et al. 2016)
mIGD_r2	ATTGGGCAGCCCTGATTCTCTGAGAGGAGGAAC	(Turchaninova et al. 2016)
mIGE_r2	ATTGGGCAGCCCTGATTAAGGGGTAGAGCTGAG	(Turchaninova et al. 2016)

4.5 Primers for second PCR amplification for BCR-Sequencing

Name	Sequence	Source
M1S	(N)4-6(XXXXX)CAGTGGTATCAACGCAGAG	(Turchaninova et al. 2016)
Z	(N)4-6(XXXXX)ATTGGGCAGCCCTGATT	(Turchaninova et al. 2016)

5. List of figures

Figure 2.1: Experimental design	46
Figure 2.2: Alpha and beta diversity of the microbiome	47
Figure 2.3: Ageing microbiome trends of AL	48
Figure 2.4: Ageing microbiome trends of DR	49
Figure 2.5: Machine learning models for diet and age prediction	51
Figure 2.6: Longitudinally differently abundant bacteria between DR and AL	52
Figure 2.7: PcoA after onset of DR	54
Figure 2.8: Random forest prediction accuracy and PRC of the microbiome	55
Figure 2.9: DR-specific bacteria genera	56
Figure 2.10: Bacteria genera associated with DR-mediated longevity	57
Figure 2.11: Bacteria species associated with microbiome memory or DR-mediated longevity	59
Figure 2.12: Density distribution of mice deaths	60
Figure 2.13: Ageing metabolite trends of AL and DR	62
Figure 2.14: PCoA and PRC of polar and non-polar metabolites	64
Figure 2.15: Longitudinally differently abundant faecal metabolites between diets	65
Figure 2.16: DR-specific or DR-mediated longevity associated faecal metabolites	66
Figure 2.17: Alpha and beta diversity of the Irs1 ^{-/-} and Rapamycin treated microbiomes	68
Figure 2.18: Common differentially regulated bacteria between DR, Irs1 ^{-/-} and Rapamycin	69
Figure 3.1: Experimental design and scheme of IgH heavy chain gene arrangement	86
Figure 3.2: General BCR repertoire characteristics of the spleen	90
Figure 3.3: General BCR repertoire characteristics of the ileum	99
Figure 3.4: The ageing microbiome beta diversity	101
Figure 3.5: Association of BCR metrics with macromorbidity index	103
Supplementary Figure 2.1: Abundance for DR-specific and longevity bacteria genera	77
Supplementary Figure 2.2: Abundance for DR-specific and longevity bacteria species	78
Supplementary Figure 2.3: Metabolites affected by ageing trends in centre-lived and long-lived mice	79
Supplementary Figure 2.4: PRCs of metabolites and microbiome of centre-lived and long-lived mice	80
Supplementary Figure 2.5: Differential abundance of DR-specific or longevity metabolites	80
Supplementary figure 3.1: Spleen isotype-specific BCR repertoire metrics	111
Supplementary figure 3.2: IghV gene usage, dN/dS ratio and CDR3 length in the spleen	112
Supplementary figure 3.3: Ileum isotype-specific BCR repertoire metrics	114
Supplementary figure 3.4: IghV gene usage, dN/dS ratio and CDR3 length in the ileum	115
Supplementary figure 3.5: Association of BCR metrics with alternative morbidity index	116

6. Bibliography

- Abbring, Suzanne, Phillip A. Engen, Ankur Naqib, Stefan J. Green, Johan Garssen, Ali Keshavarzian, and Betty C. A. M. van Esch. 2021. "Raw Milk-Induced Protection against Food Allergic Symptoms in Mice Is Accompanied by Shifts in Microbial Community Structure." *International Journal of Molecular Sciences* 22 (7). <https://doi.org/10.3390/ijms22073417>.
- Ademokun, Alexander, Yu-Chang Wu, and Deborah Dunn-Walters. 2010. "The Ageing B Cell Population: Composition and Function." *Biogerontology* 11 (2): 125–37.
- Ademokun, Alexander, Yu-Chang Wu, Victoria Martin, Rajive Mitra, Ulrich Sack, Helen Baxendale, David Kipling, and Deborah K. Dunn-Walters. 2011. "Vaccination-Induced Changes in Human B-Cell Repertoire and Pneumococcal IgM and IgA Antibody at Different Ages." *Aging Cell* 10 (6): 922–30.
- Altschul, S. F., W. Gish, W. Miller, E. W. Myers, and D. J. Lipman. 1990. "Basic Local Alignment Search Tool." *Journal of Molecular Biology* 215 (3): 403–10.
- Andrews S. (2010). FastQC: a quality control tool for high throughput sequence data. Available online at: <http://www.bioinformatics.babraham.ac.uk/projects/fastqc>
- Anhê, Fernando F., Soumaya Zlitni, Nicole G. Barra, Kevin P. Foley, Mats I. Nilsson, Joshua P. Nederveen, Lauren G. Koch, Steven L. Britton, Mark A. Tarnopolsky, and Jonathan D. Schertzer. 2022. "Life-long Exercise Training and Inherited Aerobic Endurance Capacity Produce Converging Gut Microbiome Signatures in Rodents." *Physiological Reports*. <https://doi.org/10.14814/phy2.15215>.
- Badal, Varsha D., Eleonora D. Vaccariello, Emily R. Murray, Kasey E. Yu, Rob Knight, Dilip V. Jeste, and Tanya T. Nguyen. 2020. "The Gut Microbiome, Aging, and Longevity: A Systematic Review." *Nutrients* 12 (12). <https://doi.org/10.3390/nu12123759>.
- Baghdadi, Maarouf, Tobias Nespital, Andrea Mesaros, Sandra Buschbaum, Martin Purrio, Dominic Withers, Sebastian Grönke, and Linda Partridge. 2022. "Modulation of IIS signalling to improve mammalian health span". (Doctoral dissertation, Universität zu Köln)
- Bakdash, Jonathan Z., and Laura R. Marusich. 2017. "Repeated Measures Correlation." *Frontiers in Psychology* 8 (April): 456.
- Bana, Bianca, and Filipe Cabreiro. 2019. "The Microbiome and Aging." *Annual Review of Genetics* 53 (December): 239–61.
- Banerjee, Monica, Ramit Mehr, Alex Belevsky, Jo Spencer, and Deborah K. Dunn-Walters. 2002. "Age- and Tissue-Specific Differences in Human Germinal Center B Cell Selection Revealed by Analysis of IgVH Gene Hypermutation and Lineage Trees." *European Journal of Immunology*. [https://doi.org/10.1002/1521-4141\(200207\)32:7<1947::aid-immu1947>3.0.co;2-1](https://doi.org/10.1002/1521-4141(200207)32:7<1947::aid-immu1947>3.0.co;2-1).
- Bárcena, Clea, Pedro M. Quirós, Sylvère Durand, Pablo Mayoral, Francisco Rodríguez, Xurde M. Caravia, Guillermo Mariño, et al. 2018. "Methionine Restriction Extends Lifespan in Progeroid Mice and Alters Lipid and Bile Acid Metabolism." *Cell Reports* 24 (9): 2392–2403.
- Bárcena, Clea, Rafael Valdés-Mas, Pablo Mayoral, Cecilia Garabaya, Sylvère Durand, Francisco Rodríguez, María Teresa Fernández-García, et al. 2019. "Healthspan and Lifespan Extension by Fecal Microbiota Transplantation into Progeroid Mice." *Nature Medicine* 25 (8): 1234–42.
- Barquissau, Valentin, Benjamin Léger, Diane Beuzelin, Frédéric Martins, Ez-Zoubir Amri, Didier F. Pisani, Wim H. M. Saris, et al. 2018. "Caloric Restriction and Diet-Induced Weight Loss Do Not Induce Browning of Human Subcutaneous White Adipose Tissue in Women and Men with Obesity." *Cell Reports*. <https://doi.org/10.1016/j.celrep.2017.12.102>.
- Bartley, Jenna M., Xin Zhou, George A. Kuchel, George M. Weinstock, and Laura Haynes. 2017. "Impact of Age, Caloric Restriction, and Influenza Infection on Mouse Gut

- Microbiome: An Exploratory Study of the Role of Age-Related Microbiome Changes on Influenza Responses." *Frontiers in Immunology* 8 (September): 1164.
- Belkaid, Yasmine, and Timothy W. Hand. 2014. "Role of the Microbiota in Immunity and Inflammation." *Cell*. <https://doi.org/10.1016/j.cell.2014.03.011>.
- Beresford-Jones, Benjamin S., Samuel C. Forster, Mark D. Stares, George Notley, Elisa Viciani, Hilary P. Browne, Daniel J. Boehmler, et al. 2022. "The Mouse Gastrointestinal Bacteria Catalogue Enables Translation between the Mouse and Human Gut Microbiotas via Functional Mapping." *Cell Host & Microbe* 30 (1): 124–38.e8.
- Bhattacharai, Yogesh, Si Jie, David R. Linden, Sayak Ghatak, Ruben A. T. Mars, Brianna B. Williams, Meng Pu, et al. 2020. "Bacterially Derived Tryptamine Increases Mucus Release by Activating a Host Receptor in a Mouse Model of Inflammatory Bowel Disease." *iScience*. <https://doi.org/10.1016/j.isci.2020.101798>.
- Bitto, Alessandro, Takashi K. Ito, Victor V. Pineda, Nicolas J. LeTexier, Heather Z. Huang, Elissa Sutlief, Herman Tung, et al. 2016. "Transient Rapamycin Treatment Can Increase Lifespan and Healthspan in Middle-Aged Mice." *eLife* 5 (August). <https://doi.org/10.7554/eLife.16351>.
- Blüher, Matthias, Barbara B. Kahn, and C. Ronald Kahn. 2003. "Extended Longevity in Mice Lacking the Insulin Receptor in Adipose Tissue." *Science* 299 (5606): 572–74.
- Bogatyrev, Said R., Justin C. Rolando, and Rustem F. Ismagilov. 2020. "Self-Reinoculation with Fecal Flora Changes Microbiota Density and Composition Leading to an Altered Bile-Acid Profile in the Mouse Small Intestine." *Microbiome*. <https://doi.org/10.1186/s40168-020-0785-4>.
- Bokov, Alex F., Neha Garg, Yuji Ikeno, Sachin Thakur, Nicolas Musi, Ralph A. DeFronzo, Ning Zhang, et al. 2011a. "Does Reduced IGF-1R Signaling in *Igf1r* $-/-$ Mice Alter Aging?" *PLoS ONE*. <https://doi.org/10.1371/journal.pone.0026891>.
- Bolen, Christopher R., Florian Rubelt, Jason A. Vander Heiden, and Mark M. Davis. 2017. "The Repertoire Dissimilarity Index as a Method to Compare Lymphocyte Receptor Repertoires." *BMC Bioinformatics* 18 (1): 155.
- Bolger, Anthony M., Marc Lohse, and Bjoern Usadel. 2014. "Trimmomatic: A Flexible Trimmer for Illumina Sequence Data." *Bioinformatics*. <https://doi.org/10.1093/bioinformatics/btu170>.
- Booth, Jayaum S., and Franklin R. Toapanta. 2021. "B and T Cell Immunity in Tissues and Across the Ages." *Vaccines*. <https://doi.org/10.3390/vaccines9010024>.
- Bourcy, Charles F. A. de, Cesar J. Lopez Angel, Christopher Vollmers, Cornelia L. Dekker, Mark M. Davis, and Stephen R. Quake. 2017. "Phylogenetic Analysis of the Human Antibody Repertoire Reveals Quantitative Signatures of Immune Senescence and Aging." *Proceedings of the National Academy of Sciences of the United States of America* 114 (5): 1105–10.
- Bradshaw, William John, Michael Poeschla, Aleksandra Placzek, Samuel Kean, and Dario Riccardo Valenzano. 2022. "Extensive Age-Dependent Loss of Antibody Diversity in Naturally Short-Lived Turquoise Killifish." *eLife* 11 (February). <https://doi.org/10.7554/eLife.65117>.
- Bray, J. Roger, J. Roger Bray, and J. T. Curtis. 1957. "An Ordination of the Upland Forest Communities of Southern Wisconsin." *Ecological Monographs*. <https://doi.org/10.2307/1942268>.
- Cahenzli, Julia, Yasmin Köller, Madeleine Wyss, Markus B. Geuking, and Kathy D. McCoy. 2013. "Intestinal Microbial Diversity during Early-Life Colonization Shapes Long-Term IgE Levels." *Cell Host & Microbe* 14 (5): 559–70.
- Callahan, Benjamin J., Paul J. McMurdie, and Susan P. Holmes. 2017. "Exact Sequence Variants Should Replace Operational Taxonomic Units in Marker-Gene Data Analysis." *The ISME Journal* 11 (12): 2639–43.
- Callahan, Benjamin J., Paul J. McMurdie, Michael J. Rosen, Andrew W. Han, Amy Jo A. Johnson, and Susan P. Holmes. 2016. "DADA2: High-Resolution Sample Inference from Illumina Amplicon Data." *Nature Methods* 13 (7): 581–83.
- Camacho, Christiam, George Coulouris, Vahram Avagyan, Ning Ma, Jason Papadopoulos,

- Kevin Bealer, and Thomas L. Madden. 2009. "BLAST+: Architecture and Applications." *BMC Bioinformatics* 10 (December): 421.
- Caporaso, J. Gregory, J. Gregory Caporaso, Christian L. Lauber, William A. Walters, Donna Berg-Lyons, Catherine A. Lozupone, Peter J. Turnbaugh, Noah Fierer, and Rob Knight. 2011. "Global Patterns of 16S rRNA Diversity at a Depth of Millions of Sequences per Sample." *Proceedings of the National Academy of Sciences*. <https://doi.org/10.1073/pnas.1000080107>.
- Castro-Dopico, Tomas, and Menna R. Clatworthy. 2019. "IgG and Fcγ Receptors in Intestinal Immunity and Inflammation." *Frontiers in Immunology* 10 (April): 805.
- Chao, Anne, Nicholas J. Gotelli, T. C. Hsieh, Elizabeth L. Sander, K. H. Ma, Robert K. Colwell, and Aaron M. Ellison. 2014. "Rarefaction and Extrapolation with Hill Numbers: A Framework for Sampling and Estimation in Species Diversity Studies." *Ecological Monographs*. <https://doi.org/10.1890/13-0133.1>.
- Chao, Anne, T. C. Hsieh, Robin L. Chazdon, Robert K. Colwell, and Nicholas J. Gotelli. 2015. "Unveiling the Species-Rank Abundance Distribution by Generalizing the Good-Turing Sample Coverage Theory." *Ecology* 96 (5): 1189–1201.
- Chen, Jing, Chunlan Huang, Jingjing Wang, Hui Zhou, Yingying Lu, Lihong Lou, Junyuan Zheng, et al. 2017. "Dysbiosis of Intestinal Microbiota and Decrease in Paneth Cell Antimicrobial Peptide Level during Acute Necrotizing Pancreatitis in Rats." *PloS One* 12 (4): e0176583.
- Chung, K. W., D. H. Kim, M. H. Park, Y. J. Choi, N. D. Kim, J. Lee, B. P. Yu, and H. Y. Chung. 2013. "Recent Advances in Calorie Restriction Research on Aging." *Experimental Gerontology* 48 (10): 1049–53.
- Colman, Ricki J., T. Mark Beasley, Joseph W. Kemnitz, Sterling C. Johnson, Richard Weindruch, and Rozalyn M. Anderson. 2014. "Caloric Restriction Reduces Age-Related and All-Cause Mortality in Rhesus Monkeys." *Nature Communications* 5 (April): 3557.
- Colonna-Romano, Giuseppina, Alessandra Aquino, Matteo Bulati, Gabriele Di Lorenzo, Florinda Listì, Salvatore Vitello, Domenico Lio, Giuseppina Candore, Gioacchino Clesì, and Calogero Caruso. 2006. "Memory B Cell Subpopulations in the Aged." *Rejuvenation Research* 9 (1): 149–52.
- Cook, Graham. 2000. "Immunobiology: The Immune System in Health and Disease (4th Edn) by C.A. Janeway, P. Travers, M. Walport and J.D. Capra." *Immunology Today*. [https://doi.org/10.1016/s0167-5699\(00\)01613-3](https://doi.org/10.1016/s0167-5699(00)01613-3).
- Dalile, Boushra, Lukas Van Oudenhove, Bram Vervliet, and Kristin Verbeke. 2019. "The Role of Short-Chain Fatty Acids in Microbiota–gut–brain Communication." *Nature Reviews Gastroenterology & Hepatology*. <https://doi.org/10.1038/s41575-019-0157-3>.
- David, Lawrence A., Corinne F. Maurice, Rachel N. Carmody, David B. Gootenberg, Julie E. Button, Benjamin E. Wolfe, Alisha V. Ling, et al. 2014. "Diet Rapidly and Reproducibly Alters the Human Gut Microbiome." *Nature* 505 (7484): 559–63.
- Dhahbi, Joseph M., Hyon-Jeen Kim, Patricia L. Mote, Robert J. Beaver, and Stephen R. Spindler. 2004. "Temporal Linkage between the Phenotypic and Genomic Responses to Caloric Restriction." *Proceedings of the National Academy of Sciences of the United States of America* 101 (15): 5524–29.
- Dimitrov, Jordan D., Cyril Planchais, Lubka T. Roumenina, Tchavdar L. Vassilev, Srinivas V. Kaveri, and Sebastien Lacroix-Desmazes. 2013. "Antibody Polyreactivity in Health and Disease: Statu Variabilis." *Journal of Immunology* 191 (3): 993–99.
- Donaldson, David S., Barbara B. Shih, and Neil A. Mabbott. 2021. "Aging-Related Impairments to M Cells in Peyer's Patches Coincide With Disturbances to Paneth Cells." *Frontiers in Immunology*. <https://doi.org/10.3389/fimmu.2021.761949>.
- Drews, Lisa Franzisca, Carolina Monzó, Andrea Mesaros, Martin Purrio, Ramona Jansen, Oliver Hendrich, Sandra Buschbaum, et al. 2021. "Late-life effects of earlier dietary restriction on lifespan, health span and tissue-specific phenotypes". (Doctoral dissertation, Universität zu Köln). Retrieved from https://kups.ub.uni-koeln.de/61092/1/PhD_thesis_LisaFranziska_Drews_final.pdf
- Dunn-Walters, D. K. 2015. "The Ageing Human B Cell Repertoire: A Failure of Selection?"

- Clinical and Experimental Immunology*. <https://doi.org/10.1111/cei.12700>.
- Dunn-Walters, D. K., M. Banerjee, and R. Mehr. 2003. "Effects of Age on Antibody Affinity Maturation." *Biochemical Society Transactions* 31 (2): 447–48.
- Durazzi, Francesco, Claudia Sala, Gastone Castellani, Gerardo Manfreda, Daniel Remondini, and Alessandra De Cesare. 2021. "Comparison between 16S rRNA and Shotgun Sequencing Data for the Taxonomic Characterization of the Gut Microbiota." *Scientific Reports* 11 (1): 3030.
- Duszka, Kalina, Sandrine Ellero-Simatos, Ghim Siong Ow, Marianne Defernez, Eeswari Paramalingam, Adrian Tett, Shi Ying, et al. 2018. "Complementary Intestinal Mucosa and Microbiota Responses to Caloric Restriction." *Scientific Reports* 8 (1): 11338.
- Dziarski, Roman, Shin Yong Park, Des Raj Kashyap, Scot E. Dowd, and Dipika Gupta. 2016. "Pglyrp-Regulated Gut Microflora *Prevotella Falsenii*, *Parabacteroides Distasonis* and *Bacteroides Eggerthii* Enhance and *Alistipes Finegoldii* Attenuates Colitis in Mice." *PLoS One* 11 (1): e0146162.
- Eisenberg, Tobias, Mahmoud Abdellatif, Sabrina Schroeder, Uwe Primessnig, Slaven Stekovic, Tobias Pendl, Alexandra Harger, et al. 2016. "Cardioprotection and Lifespan Extension by the Natural Polyamine Spermidine." *Nature Medicine* 22 (12): 1428–38.
- Elderman, Marlies, Bruno Sovran, Floor Hugenholtz, Katrine Graversen, Myrte Huijskes, Eva Houtsma, Clara Belzer, et al. 2017. "The Effect of Age on the Intestinal Mucus Thickness, Microbiota Composition and Immunity in Relation to Sex in Mice." *PLoS One* 12 (9): e0184274.
- Ewels, Philip, Måns Magnusson, Sverker Lundin, and Max Källner. 2016. "MultiQC: Summarize Analysis Results for Multiple Tools and Samples in a Single Report." *Bioinformatics*. <https://doi.org/10.1093/bioinformatics/btw354>.
- Fabbiano, Salvatore, Nicolas Suárez-Zamorano, Claire Chevalier, Vladimir Lazarević, Silas Kieser, Dorothée Rigo, Stefano Leo, et al. 2018. "Functional Gut Microbiota Remodeling Contributes to the Caloric Restriction-Induced Metabolic Improvements." *Cell Metabolism* 28 (6): 907–21.e7.
- Flatt, Thomas, and Linda Partridge. 2018. "Horizons in the Evolution of Aging." *BMC Biology* 16 (1): 93.
- Flemer, Burkhardt, Nadia Gaci, Guillaume Borrel, Ian R. Sanderson, Prem P. Chaudhary, William Tottey, Paul W. O'Toole, and Jean-François Brugère. 2017. "Fecal Microbiota Variation across the Lifespan of the Healthy Laboratory Rat." *Gut Microbes* 8 (5): 428–39.
- Fok, Wilson C., Yidong Chen, Alex Bokov, Yiqiang Zhang, Adam B. Salmon, Vivian Diaz, Martin Javors, et al. 2014. "Mice Fed Rapamycin Have an Increase in Lifespan Associated with Major Changes in the Liver Transcriptome." *PLoS One* 9 (1): e83988.
- Fontana, Luigi, and Linda Partridge. 2015. "Promoting Health and Longevity through Diet: From Model Organisms to Humans." *Cell* 161 (1): 106–18.
- Fontana, Luigi, Linda Partridge, and Valter D. Longo. 2010. "Extending Healthy Life Span--from Yeast to Humans." *Science* 328 (5976): 321–26.
- Frampton, James, Kevin G. Murphy, Gary Frost, and Edward S. Chambers. 2020. "Short-Chain Fatty Acids as Potential Regulators of Skeletal Muscle Metabolism and Function." *Nature Metabolism* 2 (9): 840–48.
- Fuentes, Susana, Els van Nood, Sebastian Tims, Ineke Heikamp-de Jong, Cajo J. F. ter Braak, Josbert J. Keller, Erwin G. Zoetendal, and Willem M. de Vos. 2014. "Reset of a Critically Disturbed Microbial Ecosystem: Faecal Transplant in Recurrent *Clostridium Difficile* Infection." *The ISME Journal* 8 (8): 1621–33.
- Gadala-Maria, Daniel, Gur Yaari, Mohamed Uduman, and Steven H. Kleinstein. 2015. "Automated Analysis of High-Throughput B-Cell Sequencing Data Reveals a High Frequency of Novel Immunoglobulin V Gene Segment Alleles." *Proceedings of the National Academy of Sciences of the United States of America* 112 (8): E862–70.
- Galkin, Fedor, Polina Mamoshina, Alex Aliper, Evgeny Putin, Vladimir Moskalev, Vadim N. Gladyshev, and Alex Zhavoronkov. 2020. "Human Gut Microbiome Aging Clock Based on Taxonomic Profiling and Deep Learning." *iScience* 23 (6): 101199.

- Ghosh, Tarini Shankar, Fergus Shanahan, and Paul W. O'Toole. 2022. "The Gut Microbiome as a Modulator of Healthy Ageing." *Nature Reviews. Gastroenterology & Hepatology*, April. <https://doi.org/10.1038/s41575-022-00605-x>.
- Ghraichy, Marie, Valentin von Niederhäusern, Aleksandr Kovaltsuk, Jacob D. Galson, Charlotte M. Deane, and Johannes Trück. 2021. "Different B Cell Subpopulations Show Distinct Patterns in Their IgH Repertoire Metrics." *eLife* 10 (October). <https://doi.org/10.7554/eLife.73111>.
- Gibson, Kate L., Yu-Chang Wu, Yvonne Barnett, Orla Duggan, Robert Vaughan, Elli Kondeatis, Bengt-Olof Nilsson, Anders Wikby, David Kipling, and Deborah K. Dunn-Walters. 2009. "B-Cell Diversity Decreases in Old Age and Is Correlated with Poor Health Status." *Aging Cell* 8 (1): 18–25.
- Giudicelli, Véronique, Denys Chaume, and Marie-Paule Lefranc. 2005. "IMGT/GENE-DB: A Comprehensive Database for Human and Mouse Immunoglobulin and T Cell Receptor Genes." *Nucleic Acids Research* 33: D256–61.
- Goldberg, Alexander A., Vincent R. Richard, Pavlo Kyryakov, Simon D. Bourque, Adam Beach, Michelle T. Burstein, Anastasia Glebov, et al. 2010. "Chemical Genetic Screen Identifies Lithocholic Acid as an Anti-Aging Compound That Extends Yeast Chronological Life Span in a TOR-Independent Manner, by Modulating Housekeeping Longevity Assurance Processes." *Aging*. <https://doi.org/10.18632/aging.100168>.
- Gould, Hannah J., and Brian J. Sutton. 2008. "IgE in Allergy and Asthma Today." *Nature Reviews Immunology*. <https://doi.org/10.1038/nri2273>.
- Granado-Serrano, A. B., M. Martín-Garí, V. Sánchez, M. Riart Solans, R. Berdún, I. A. Ludwig, L. Rubió, E. Vilaprinýó, M. Portero-Otín, and J. C. E. Serrano. 2019. "Faecal Bacterial and Short-Chain Fatty Acids Signature in Hypercholesterolemia." *Scientific Reports* 9 (1): 1772.
- Green, Cara L., Dudley W. Lamming, and Luigi Fontana. 2022. "Molecular Mechanisms of Dietary Restriction Promoting Health and Longevity." *Nature Reviews. Molecular Cell Biology* 23 (1): 56–73.
- Greiff, Victor, Cédric R. Weber, Johannes Palme, Ulrich Bodenhofer, Enkelejda Miho, Ulrike Menzel, and Sai T. Reddy. 2017. "Learning the High-Dimensional Immunogenomic Features That Predict Public and Private Antibody Repertoires." *Journal of Immunology* 199 (8): 2985–97.
- Grönke, Sebastian, David-Francis Clarke, Susan Broughton, T. Daniel Andrews, and Linda Partridge. 2010. "Molecular Evolution and Functional Characterization of Drosophila Insulin-like Peptides." *PLoS Genetics* 6 (2): e1000857.
- Gunti, Sreenivasulu, and Abner Louis Notkins. 2015. "Polyreactive Antibodies: Function and Quantification." *The Journal of Infectious Diseases* 212 Suppl 1 (July): S42–46.
- Gupta, Namita T., Kristofor D. Adams, Adrian W. Briggs, Sonia C. Timberlake, Francois Vigneault, and Steven H. Kleinstein. 2017. "Hierarchical Clustering Can Identify B Cell Clones with High Confidence in Ig Repertoire Sequencing Data." *The Journal of Immunology*. <https://doi.org/10.4049/jimmunol.1601850>.
- Gupta, Namita T., Jason A. Vander Heiden, Mohamed Uduman, Daniel Gadala-Maria, Gur Yaari, and Steven H. Kleinstein. 2015. "Change-O: A Toolkit for Analyzing Large-Scale B Cell Immunoglobulin Repertoire Sequencing Data." *Bioinformatics* 31 (20): 3356–58.
- Gutzeit, Cindy, Kang Chen, and Andrea Cerutti. 2018. "The Enigmatic Function of IgD: Some Answers at Last." *European Journal of Immunology* 48 (7): 1101–13.
- Hahn, Oliver, Lisa F. Drews, An Nguyen, Takashi Tatsuta, Lisonia Gkioni, Oliver Hendrich, Qifeng Zhang, et al. 2019. "A Nutritional Memory Effect Counteracts the Benefits of Dietary Restriction in Old Mice." *Nature Metabolism*. <https://doi.org/10.1038/s42255-019-0121-0>.
- Hao, Yongsheng, Zhanqing Ji, Zhongjian Shen, Youjia Xue, Bo Zhang, Daxin Yu, Tong Liu, et al. 2022. "Increase Dietary Fiber Intake Ameliorates Cecal Morphology and Drives Cecal Species-Specific of Short-Chain Fatty Acids in White Pekin Ducks." *Frontiers in Microbiology* 13 (April): 853797.
- Heiden, Jason A. Vander, Jason A. Vander Heiden, Gur Yaari, Mohamed Uduman, Joel N.

- H. Stern, Kevin C. O'Connor, David A. Hafler, Francois Vigneault, and Steven H. Kleinstein. 2014. "pRESTO: A Toolkit for Processing High-Throughput Sequencing Raw Reads of Lymphocyte Receptor Repertoires." *Bioinformatics*. <https://doi.org/10.1093/bioinformatics/btu138>.
- Hill, M. O. 1973. "Diversity and Evenness: A Unifying Notation and Its Consequences." *Ecology*. <https://doi.org/10.2307/1934352>.
- Hoehn, Kenneth B., Jason A. Vander Heiden, Julian Q. Zhou, Gerton Lunter, Oliver G. Pybus, and Steven H. Kleinstein. 2019. "Repertoire-Wide Phylogenetic Models of B Cell Molecular Evolution Reveal Evolutionary Signatures of Aging and Vaccination." *Proceedings of the National Academy of Sciences of the United States of America* 116 (45): 22664–72.
- Holodick, Nichol E., Teresa Vizconde, Thomas J. Hopkins, and Thomas L. Rothstein. 2016. "Age-Related Decline in Natural IgM Function: Diversification and Selection of the B-1a Cell Pool with Age." *Journal of Immunology* 196 (10): 4348–57.
- Ho, Tin Kam. n.d. "Random Decision Forests." *Proceedings of 3rd International Conference on Document Analysis and Recognition*. <https://doi.org/10.1109/icdar.1995.598994>.
- Ikeno, Yuji, Gene B. Hubbard, Shuko Lee, Lisa A. Cortez, Christie M. Lew, Celeste R. Webb, Darlene E. Berryman, Edward O. List, John J. Kopchick, and Andrzej Bartke. 2009. "Reduced Incidence and Delayed Occurrence of Fatal Neoplastic Diseases in Growth Hormone Receptor/binding Protein Knockout Mice." *The Journals of Gerontology. Series A, Biological Sciences and Medical Sciences* 64 (5): 522–29.
- Ikeno, Yuji, Christie M. Lew, Lisa A. Cortez, Celeste R. Webb, Shuko Lee, and Gene B. Hubbard. 2006. "Do Long-Lived Mutant and Calorie-Restricted Mice Share Common Anti-Aging Mechanisms?--a Pathological Point of View." *Age* 28 (2): 163–71.
- Ishiguro, Edward, Natasha Haskey, and Kristina Campbell. 2018. "Gut Microbiota Throughout the Lifespan." *Gut Microbiota*. <https://doi.org/10.1016/b978-0-12-810541-2.00003-8>.
- Jiang, Ning, Jiankui He, Joshua A. Weinstein, Lolita Penland, Sanae Sasaki, Xiao-Song He, Cornelia L. Dekker, et al. 2013. "Lineage Structure of the Human Antibody Repertoire in Response to Influenza Vaccination." *Science Translational Medicine* 5 (171): 171ra19.
- Juricic, Paula, Yu-Xuan Lu, Thomas Leech, Lisa F. Drews, Jonathan Paulitz, Jiongming Lu, Tobias Nespital, et al. 2022. "Full Geroprotection from Brief Rapamycin Treatment by Persistently Increased Intestinal Autophagy." *bioRxiv*. <https://doi.org/10.1101/2022.04.20.488884>.
- Ke, Shanlin, Sarah J. Mitchell, Michael R. MacArthur, Alice E. Kane, David A. Sinclair, Emily M. Venable, Katia S. Chadaideh, et al. 2021. "Gut Microbiota Predicts Healthy Late-Life Aging in Male Mice." *Nutrients* 13 (9). <https://doi.org/10.3390/nu13093290>.
- Khan, Tarik A., Simon Friedensohn, Arthur R. Gorter de Vries, Jakub Straszewski, Hans-Joachim Ruscheweyh, and Sai T. Reddy. 2016. "Accurate and Predictive Antibody Repertoire Profiling by Molecular Amplification Fingerprinting." *Science Advances* 2 (3): e1501371.
- Kim, Hyun-Jung, Chang Mo Moon, Jihee Lee Kang, and Eun-Mi Park. 2021. "Aging Effects on the Diurnal Patterns of Gut Microbial Composition in Male and Female Mice." *The Korean Journal of Physiology & Pharmacology: Official Journal of the Korean Physiological Society and the Korean Society of Pharmacology* 25 (6): 575–83.
- Kok, Dieuwertje E. G., Fenni Rusli, Benthe van der Lugt, Carolien Lute, Luca Laghi, Stefano Salvioli, Gianfranco Picone, et al. 2018. "Lifelong Calorie Restriction Affects Indicators of Colonic Health in Aging C57Bl/6J Mice." *The Journal of Nutritional Biochemistry* 56 (June): 152–64.
- Kong, Fanli, Yutong Hua, Bo Zeng, Ruihong Ning, Ying Li, and Jiangchao Zhao. 2016. "Gut Microbiota Signatures of Longevity." *Current Biology: CB* 26 (18): R832–33.
- Koohy, Hashem, Daniel J. Bolland, Louise S. Matheson, Stefan Schoenfelder, Claudia Stellato, Andrew Dimond, Csilla Várnai, et al. 2018. "Genome Organization and Chromatin Analysis Identify Transcriptional Downregulation of Insulin-like Growth Factor Signaling as a Hallmark of Aging in Developing B Cells." *Genome Biology* 19 (1): 126.

- Kraus, William E., Manjushri Bhapkar, Kim M. Huffman, Carl F. Pieper, Sai Krupa Das, Leanne M. Redman, Dennis T. Villareal, et al. 2019. "2 Years of Calorie Restriction and Cardiometabolic Risk (CALERIE): Exploratory Outcomes of a Multicentre, Phase 2, Randomised Controlled Trial." *The Lancet. Diabetes & Endocrinology* 7 (9): 673–83.
- Krautkramer, Kimberly A., Jing Fan, and Fredrik Bäckhed. 2021. "Gut Microbial Metabolites as Multi-Kingdom Intermediates." *Nature Reviews. Microbiology* 19 (2): 77–94.
- Langille, Morgan G. I., Conor J. Meehan, Jeremy E. Koenig, Akhilesh S. Dhanani, Robert A. Rose, Susan E. Howlett and Robert G. Beiko. 2014. "Microbial shifts in the aging mouse gut". *Microbiome* <https://doi.org/10.1186/s40168-014-0050-9>
- Le Gallou, Simon, Zhicheng Zhou, Lan-Huong Thai, Remi Fritzen, Alba Verge de Los Aires, Jérôme Mégret, Philipp Yu, et al. 2018. "A Splenic IgM Memory Subset with Antibacterial Specificities Is Sustained from Persistent Mucosal Responses." *The Journal of Experimental Medicine* 215 (8): 2035–53.
- Liang, Jessie Qiaoyi, Tong Li, Geicho Nakatsu, Ying-Xuan Chen, Tung On Yau, Eagle Chu, Sunny Wong, et al. 2020. "A Novel Faecal Marker for the Non-Invasive Diagnosis of Colorectal Adenoma and Cancer." *Gut* 69 (7): 1248–57.
- Lindner, Cornelia, Irene Thomsen, Benjamin Wahl, Milas Ugur, Maya K. Sethi, Michaela Friedrichsen, Anna Smoczek, et al. 2015. "Diversification of Memory B Cells Drives the Continuous Adaptation of Secretory Antibodies to Gut Microbiota." *Nature Immunology* 16 (8): 880–88.
- Lindner, Cornelia, Benjamin Wahl, Lisa Föhse, Sebastian Suerbaum, Andrew J. Macpherson, Immo Prinz, and Oliver Pabst. 2012. "Age, Microbiota, and T Cells Shape Diverse Individual IgA Repertoires in the Intestine." *Journal of Experimental Medicine*. <https://doi.org/10.1084/jem.20111980>.
- López-Lluch, Guillermo, and Plácido Navas. 2016. "Calorie Restriction as an Intervention in Ageing." *The Journal of Physiology*. <https://doi.org/10.1113/jp270543>.
- López-Otín, Carlos, Maria A. Blasco, Linda Partridge, Manuel Serrano, and Guido Kroemer. 2013. "The Hallmarks of Aging." *Cell* 153 (6): 1194–1217.
- Love, Michael I., Wolfgang Huber, and Simon Anders. 2014. "Moderated Estimation of Fold Change and Dispersion for RNA-Seq Data with DESeq2." *Genome Biology* 15 (12): 550.
- Lozupone, Catherine A., Micah Hamady, Scott T. Kelley, and Rob Knight. 2007. "Quantitative and Qualitative β Diversity Measures Lead to Different Insights into Factors That Structure Microbial Communities." *Applied and Environmental Microbiology*. <https://doi.org/10.1128/aem.01996-06>.
- Lozupone, Catherine A., Marcella Li, Thomas B. Campbell, Sonia C. Flores, Derek Linderman, Matthew J. Gebert, Rob Knight, Andrew P. Fontenot, and Brent E. Palmer. 2013. "Alterations in the Gut Microbiota Associated with HIV-1 Infection." *Cell Host & Microbe* 14 (3): 329–39.
- Lugt, Benthe van der, Fenni Rusli, Carolien Lute, Andreas Lamprakis, Ethel Salazar, Mark V. Boekschoten, Guido J. Hooiveld, et al. 2018. "Integrative Analysis of Gut Microbiota Composition, Host Colonic Gene Expression and Intraluminal Metabolites in Aging C57BL/6J Mice." *Aging* 10 (5): 930–50.
- Lu, Jennifer, Florian P. Breitwieser, Peter Thielen, and Steven L. Salzberg. 2017. "Bracken: Estimating Species Abundance in Metagenomics Data." *PeerJ. Computer Science* 3 (e104): e104.
- Macpherson, Andrew J., Bahtiyar Yilmaz, Julien P. Limenitakis, and Stephanie C. Ganal-Vonarburg. 2018. "IgA Function in Relation to the Intestinal Microbiota." *Annual Review of Immunology*. <https://doi.org/10.1146/annurev-immunol-042617-053238>.
- Madeo, Frank, Didac Carmona-Gutierrez, Sebastian J. Hofer, and Guido Kroemer. 2019. "Caloric Restriction Mimetics against Age-Associated Disease: Targets, Mechanisms, and Therapeutic Potential." *Cell Metabolism* 29 (3): 592–610.
- Madeo, Frank, Tobias Eisenberg, Federico Pietrocola, and Guido Kroemer. 2018. "Spermidine in Health and Disease." *Science* 359 (6374). <https://doi.org/10.1126/science.aan2788>.

- Martin, Marcel. 2011. "Cutadapt Removes Adapter Sequences from High-Throughput Sequencing Reads." *EMBnet.journal* 17 (1): 10.
- Martino, Cameron, Liat Shenhav, Clarisse A. Marotz, George Armstrong, Daniel McDonald, Yoshiki Vázquez-Baeza, James T. Morton, et al. 2021. "Context-Aware Dimensionality Reduction Deconvolutes Gut Microbial Community Dynamics." *Nature Biotechnology* 39 (2): 165–68.
- Martin, Victoria, Yu-Chang (bryan) Wu, David Kipling, and Deborah Dunn-Walters. 2015. "Ageing of the B-Cell Repertoire." *Philosophical Transactions of the Royal Society B: Biological Sciences*. <https://doi.org/10.1098/rstb.2014.0237>.
- Maynard, Claire, and David Weinkove. 2018. "The Gut Microbiota and Ageing." *Subcellular Biochemistry*. https://doi.org/10.1007/978-981-13-2835-0_12.
- McKean, David, Konrad Huppi, Michael Bell, Louis Staudt, Walter Gerhard, and Martin Weigert. 2008. "Pillars Article: Generation of Antibody Diversity in the Immune Response of BALB/c Mice to Influenza Virus Hemagglutinin. Proc. Natl. Acad. Sci. USA, 81: 3180-3184, May 1984." *Journal of Immunology* 180 (9): 5765–69.
- McMurdie, Paul J., and Susan Holmes. 2013. "Phyloseq: An R Package for Reproducible Interactive Analysis and Graphics of Microbiome Census Data." *PloS One* 8 (4): e61217.
- Messaoudi, Ilhem, Jessica Warner, Miranda Fischer, Buyng Park, Brenna Hill, Julie Mattison, Mark A. Lane, et al. 2006. "Delay of T Cell Senescence by Caloric Restriction in Aged Long-Lived Nonhuman Primates." *Proceedings of the National Academy of Sciences of the United States of America* 103 (51): 19448–53.
- Miho, Enkelejda, Alexander Yermanos, Cédric R. Weber, Christoph T. Berger, Sai T. Reddy, and Victor Greiff. 2018. "Computational Strategies for Dissecting the High-Dimensional Complexity of Adaptive Immune Repertoires." *Frontiers in Immunology* 9 (February): 224.
- Mikocziova, Ivana, Victor Greiff, and Ludvig M. Sollid. 2021. "Immunoglobulin Germline Gene Variation and Its Impact on Human Disease." *Genes and Immunity* 22 (4): 205–17.
- Miller, R. A. 1996. "The Aging Immune System: Primer and Prospectus." *Science* 273 (5271): 70–74.
- Miller, Richard A., David E. Harrison, Clinton M. Astle, Elizabeth Fernandez, Kevin Flurkey, Melissa Han, Martin A. Javors, et al. 2014. "Rapamycin-Mediated Lifespan Increase in Mice Is Dose and Sex Dependent and Metabolically Distinct from Dietary Restriction." *Aging Cell* 13 (3): 468–77.
- Morrison, Douglas J., and Tom Preston. 2016. "Formation of Short Chain Fatty Acids by the Gut Microbiota and Their Impact on Human Metabolism." *Gut Microbes*. <https://doi.org/10.1080/19490976.2015.1134082>.
- Morselli, Eugenia, Guillermo Mariño, Martin V. Bennetzen, Tobias Eisenberg, Evgenia Megalou, Sabrina Schroeder, Sandra Cabrera, et al. 2011. "Spermidine and Resveratrol Induce Autophagy by Distinct Pathways Converging on the Acetylproteome." *The Journal of Cell Biology* 192 (4): 615–29.
- Muggen, Alice F., Madelon de Jong, Ingrid L. M. Wolvers-Tettero, Martine J. Kallemeijn, Cristina Teodósio, Nikos Darzentas, Ralph Stadhouders, et al. 2019. "The Presence of CLL-Associated Stereotypic B Cell Receptors in the Normal BCR Repertoire from Healthy Individuals Increases with Age." *Immunity & Ageing: I & A* 16 (August): 22.
- Nagpal, Ravinder, Rabina Mainali, Shokouh Ahmadi, Shaohua Wang, Ria Singh, Kylie Kavanagh, Dalane W. Kitzman, Almagul Kushugulova, Francesco Marotta, and Hariom Yadav. 2018. "Gut Microbiome and Aging: Physiological and Mechanistic Insights." *Nutrition and Healthy Aging* 4 (4): 267–85.
- Naradikian, Martin S., Yi Hao, and Michael P. Cancro. 2016. "Age-Associated B Cells: Key Mediators of Both Protective and Autoreactive Humoral Responses." *Immunological Reviews* 269 (1): 118–29.
- Nguyen, Tue Gia. 2022. "The Therapeutic Implications of Activated Immune Responses via the Enigmatic Immunoglobulin D." *International Reviews of Immunology* 41 (2): 107–22.

- Nielsen, Rasmus, and Ziheng Yang. 1998. "Likelihood Models for Detecting Positively Selected Amino Acid Sites and Applications to the HIV-1 Envelope Gene." *Genetics*. <https://doi.org/10.1093/genetics/148.3.929>.
- Nikolich-Zugich, Janko. 2005. "T Cell Aging: Naive but Not Young." *The Journal of Experimental Medicine* 201 (6): 837–40.
- Nouri, Nima, and Steven H. Kleinstein. 2018. "A Spectral Clustering-Based Method for Identifying Clones from High-Throughput B Cell Repertoire Sequencing Data." *Bioinformatics* 34 (13): i341–49.
- Oh, Soo-Jin, Jae Kyung Lee, and Ok Sarah Shin. 2019. "Aging and the Immune System: The Impact of Immunosenescence on Viral Infection, Immunity and Vaccine Immunogenicity." *Immune Network* 19 (6): e37.
- Okawa, Takuma, Motoyoshi Nagai, and Koji Hase. 2020. "Dietary Intervention Impacts Immune Cell Functions and Dynamics by Inducing Metabolic Rewiring." *Frontiers in Immunology* 11: 623989.
- Omodei, Daniela, and Luigi Fontana. 2011. "Calorie Restriction and Prevention of Age-Associated Chronic Disease." *FEBS Letters* 585 (11): 1537–42.
- Ondov, Brian D., Nicholas H. Bergman, and Adam M. Phillippy. 2015. "Krona: Interactive Metagenomic Visualization in a Web Browser." *Encyclopedia of Metagenomics*. https://doi.org/10.1007/978-1-4899-7478-5_802.
- Paliy, O., and V. Shankar. 2016. "Application of Multivariate Statistical Techniques in Microbial Ecology." *Molecular Ecology* 25 (5): 1032–57.
- Peres-Neto, Pedro R., and Donald A. Jackson. 2001. "How Well Do Multivariate Data Sets Match? The Advantages of a Procrustean Superimposition Approach over the Mantel Test." *Oecologia* 129 (2): 169–78.
- Pietrocola, F., S. Lachkar, D. P. Enot, M. Niso-Santano, J. M. Bravo-San Pedro, V. Sica, V. Izzo, et al. 2015. "Spermidine Induces Autophagy by Inhibiting the Acetyltransferase EP300." *Cell Death and Differentiation* 22 (3): 509–16.
- Plubell, Deanna L., Phillip A. Wilmarth, Yuqi Zhao, Alexandra M. Fenton, Jessica Minnier, Ashok P. Reddy, John Klimek, Xia Yang, Larry L. David, and Nathalie Pamir. 2017. "Extended Multiplexing of Tandem Mass Tags (TMT) Labeling Reveals Age and High Fat Diet Specific Proteome Changes in Mouse Epididymal Adipose Tissue." *Molecular & Cellular Proteomics: MCP* 16 (5): 873–90.
- Quast, Christian, Elmar Pruesse, Pelin Yilmaz, Jan Gerken, Timmy Schweer, Pablo Yarza, Jörg Peplies, and Frank Oliver Glöckner. 2013. "The SILVA Ribosomal RNA Gene Database Project: Improved Data Processing and Web-Based Tools." *Nucleic Acids Research* 41: D590–96.
- Raposo, Bruno, Doreen Dobritzsch, Changrong Ge, Diana Ekman, Bingze Xu, Ingrid Lindh, Michael Förster, et al. 2014. "Epitope-Specific Antibody Response Is Controlled by Immunoglobulin V(H) Polymorphisms." *The Journal of Experimental Medicine* 211 (3): 405–11.
- Redman, Leanne M., Steven R. Smith, Jeffrey H. Burton, Corby K. Martin, Dora Il'yasova, and Eric Ravussin. 2018. "Metabolic Slowing and Reduced Oxidative Damage with Sustained Caloric Restriction Support the Rate of Living and Oxidative Damage Theories of Aging." *Cell Metabolism* 27 (4): 805–15.e4.
- Sang, Jianan, Daohua Zhuang, Tao Zhang, Qunfu Wu, Jiangkun Yu, and Zhigang Zhang. 2022. "Convergent and Divergent Age Patterning of Gut Microbiota Diversity in Humans and Nonhuman Primates." *mSystems*, June, e0151221.
- Saunders, Sean P., Erica G. M. Ma, Carlos J. Aranda, and Maria A. Curotto de Lafaille. 2019. "Non-Classical B Cell Memory of Allergic IgE Responses." *Frontiers in Immunology* 10 (April): 715.
- Schroeder, Harry W., Jr, and Lisa Cavacini. 2010. "Structure and Function of Immunoglobulins." *The Journal of Allergy and Clinical Immunology* 125 (2 Suppl 2): S41–52.
- Schwartzberg, Reiner Jumpertz von, Jordan E. Bisanz, Svetlana Lyalina, Peter Spanogiannopoulos, Qi Yan Ang, Jingwei Cai, Sophia Dickmann, et al. 2021. "Caloric

- Restriction Disrupts the Microbiota and Colonization Resistance." *Nature* 595 (7866): 272–77.
- Seabold, Skipper, and Josef Perktold. 2010. "Statsmodels: Econometric and Statistical Modeling with Python." *Proceedings of the 9th Python in Science Conference*. <https://doi.org/10.25080/majora-92bf1922-011>.
- Sekirov, Inna, Shannon L. Russell, L. Caetano M. Antunes, and B. Brett Finlay. 2010. "Gut Microbiota in Health and Disease." *Physiological Reviews* 90 (3): 859–904.
- Selman, Colin, Steven Lingard, Agharul I. Choudhury, Rachel L. Batterham, Marc Claret, Melanie Clements, Faruk Ramadani, et al. 2008. "Evidence for Lifespan Extension and Delayed Age-Related Biomarkers in Insulin Receptor Substrate 1 Null Mice." *FASEB Journal: Official Publication of the Federation of American Societies for Experimental Biology* 22 (3): 807–18.
- Shannon, C. E. 1948. *A mathematical theory of communication*.
- Shannon, Paul, Andrew Markiel, Owen Ozier, Nitin S. Baliga, Jonathan T. Wang, Daniel Ramage, Nada Amin, Benno Schwikowski, and Trey Ideker. 2003. "Cytoscape: A Software Environment for Integrated Models of Biomolecular Interaction Networks." *Genome Research* 13 (11): 2498–2504.
- Shenghua, Piao, Zhu Ziqin, Tan Shuyu, Zhan Huixia, Rong Xianglu, and Guo Jiao. 2020. "An Integrated Fecal Microbiome and Metabolome in the Aged Mice Reveal Anti-Aging Effects from the Intestines and Biochemical Mechanism of FuFang Zhenshu TiaoZhi(FTZ)." *Biomedicine & Pharmacotherapy = Biomedecine & Pharmacotherapie* 121 (January): 109421.
- Shen, Wei, Shuai Le, Yan Li, and Fuquan Hu. 2016. "SeqKit: A Cross-Platform and Ultrafast Toolkit for FASTA/Q File Manipulation." *PLoS One* 11 (10): e0163962.
- Shin, Seung Chul, Sung-Hee Kim, Hyejin You, Boram Kim, Aeri C. Kim, Kyung-Ah Lee, Joo-Heon Yoon, Ji-Hwan Ryu, and Won-Jae Lee. 2011. "Drosophila Microbiome Modulates Host Developmental and Metabolic Homeostasis via Insulin Signaling." *Science* 334 (6056): 670–74.
- Shi, Yuhui, Takashi Yamazaki, Yoshio Okubo, Yoshio Uehara, Kazuo Sugane, and Kazunaga Agematsu. 2005. "Regulation of Aged Humoral Immune Defense against Pneumococcal Bacteria by IgM Memory B Cell." *Journal of Immunology* 175 (5): 3262–67.
- Shushimita, Shushimita Shushimita, Marjolein J. W. de Bruijn, Ron W. F. de Bruin, Jan N. M. IJzermans, Rudi W. Hendriks, and Frank J. M. Dor. 2014. "Dietary Restriction and Fasting Arrest B and T Cell Development and Increase Mature B and T Cell Numbers in Bone Marrow." *PLoS ONE*. <https://doi.org/10.1371/journal.pone.0087772>.
- Simpson, E. H. 1949. "Measurement of Diversity." *Nature*. <https://doi.org/10.1038/163688a0>.
- Smith, Byron J., Richard A. Miller, Aaron C. Ericsson, David C. Harrison, Randy Strong, and Thomas M. Schmidt. 2019. "Changes in the Gut Microbiome and Fermentation Products Concurrent with Enhanced Longevity in Acarbose-Treated Mice." *BMC Microbiology* 19 (1): 130.
- Stadlbauer, Vanessa, Lara Engertsberger, Irina Komarova, Nicole Feldbacher, Bettina Leber, Gerald Pichler, Nicole Fink, et al. 2020. "Dysbiosis, Gut Barrier Dysfunction and Inflammation in Dementia: A Pilot Study." *BMC Geriatrics* 20 (1): 248.
- Stavnezer, Janet, Jeroen E. J. Guikema, and Carol E. Schrader. 2008. "Mechanism and Regulation of Class Switch Recombination." *Annual Review of Immunology* 26: 261–92.
- Stoeva, Magdalena K., Jeewon Garcia-So, Nicholas Justice, Julia Myers, Surabhi Tyagi, Madeleine Nemchek, Paul J. McMurdie, Orville Kolterman, and John Eid. 2021. "Butyrate-Producing Human Gut Symbiont, and Its Role in Health and Disease." *Gut Microbes* 13 (1): 1–28.
- Sung, Chang Mu, Yu-Fei Lin, Kuan-Fu Chen, Huei-Mien Ke, Hao-Yi Huang, Yu-Nong Gong, Wen-Sy Tsai, et al. 2019. "Predicting Clinical Outcomes of Cirrhosis Patients With Hepatic Encephalopathy From the Fecal Microbiome." *Cellular and Molecular Gastroenterology and Hepatology* 8 (2): 301–18.e2.
- Tang, Duo Zhuang, Si Tao, Zhiyang Chen, Ievgen Oleksandrovich Koliesnik, Philip Gerald

- Calmes, Verena Hoerr, Bing Han, et al. 2021. "Correction: Dietary Restriction Improves Repopulation but Impairs Lymphoid Differentiation Capacity of Hematopoietic Stem Cells in Early Aging." *The Journal of Experimental Medicine* 218 (1). <https://doi.org/10.1084/jem.2015110012042020C>.
- Tao, Si, Yiting Wang, Jianying Wu, Ting Zeng, Hui Cui, Zhendong Tao, Lang Lei, et al. 2020. "Long-Term Mid-Onset Dietary Restriction Rejuvenates Hematopoietic Stem Cells and Improves Regeneration Capacity of Total Bone Marrow from Aged Mice." *Aging Cell* 19 (10): e13241.
- Tas, Jeroen M. J., Luka Mesin, Giulia Pasqual, Sasha Targ, Johanne T. Jacobsen, Yasuko M. Mano, Casie S. Chen, et al. 2016. "Visualizing Antibody Affinity Maturation in Germinal Centers." *Science* 351 (6277): 1048–54.
- Thompson, Robert S., Michelle Gaffney, Shelby Hopkins, Tel Kelley, Antonio Gonzalez, Samuel J. Bowers, Martha Hotz Vitaterna, et al. 2021. "Ruminiclostridium 5, Parabacteroides Distasonis, and Bile Acid Profile Are Modulated by Prebiotic Diet and Associate with Facilitated Sleep/clock Realignment after Chronic Disruption of Rhythms." *Brain, Behavior, and Immunity* 97 (October): 150–66.
- Treuting, Piper M., Nancy J. Linford, Sue E. Knoblaugh, M. J. Emond, John F. Morton, George M. Martin, Peter S. Rabinovitch, and Warren C. Ladiges. 2008. "Reduction of Age-Associated Pathology in Old Mice by Overexpression of Catalase in Mitochondria." *The Journals of Gerontology. Series A, Biological Sciences and Medical Sciences* 63 (8): 813–22.
- Turchaninova, M. A., A. Davydov, O. V. Britanova, M. Shugay, V. Bikos, E. S. Egorov, V. I. Kirgizova, et al. 2016. "High-Quality Full-Length Immunoglobulin Profiling with Unique Molecular Barcoding." *Nature Protocols* 11 (9): 1599–1616.
- Tyshkovskiy, A., B. Perinur, A. A. Borodinova, M. V. Gerashchenko, G. P. Ables, M. Garratt, P. Khaitovich, et al. 2019. "Identification and application of gene expression signatures associated with lifespan extension". *Cell Metabolism* 30(3): 573-593.
- Uzal, Francisco A., Mauricio A. Navarro, Jihong Li, John C. Freedman, Archana Shrestha, and Bruce A. McClane. 2018. "Comparative Pathogenesis of Enteric Clostridial Infections in Humans and Animals." *Anaerobe* 53 (October): 11–20.
- Vacca, Mirco, Giuseppe Celano, Francesco Maria Calabrese, Piero Portincasa, Marco Gobbetti, and Maria De Angelis. 2020. "The Controversial Role of Human Gut Lachnospiraceae." *Microorganisms* 8 (4). <https://doi.org/10.3390/microorganisms8040573>.
- Vander Heiden, Jason Anthony, Susanna Marquez, Nishanth Marthandan, Syed Ahmad Chan Bukhari, Christian E. Busse, Brian Corrie, Uri Hershberg, et al. 2018. "AIRR Community Standardized Representations for Annotated Immune Repertoires." *Frontiers in Immunology* 9 (September): 2206.
- Vencovský, J., E. Zďárský, S. P. Moyes, A. Hajeer, S. Ruzicková, Z. Cimburek, W. E. Ollier, R. N. Maini, and R. A. Mageed. 2002. "Polymorphism in the Immunoglobulin VH Gene V1-69 Affects Susceptibility to Rheumatoid Arthritis in Subjects Lacking the HLA-DRB1 Shared Epitope." *Rheumatology* 41 (4): 401–10.
- Vendrig, Nadia J., Lia Hemerik, and Cajo J. F. ter Braak. 2017. "Response Variable Selection in Principal Response Curves Using Permutation Testing." *Aquatic Ecology*. <https://doi.org/10.1007/s10452-016-9604-1>.
- Viltard, Mélanie, Sylvère Durand, Maria Pérez-Lanzón, Fanny Aprahamian, Deborah Lefevre, Christine Leroy, Frank Madeo, Guido Kroemer, and Gérard Friedlander. 2019. "The Metabolomic Signature of Extreme Longevity: Naked Mole Rats versus Mice." *Aging*. <https://doi.org/10.18632/aging.102116>.
- Virtanen, Pauli, Ralf Gommers, Travis E. Oliphant, Matt Haberland, Tyler Reddy, David Cournapeau, Evgeni Burovski, et al. 2020. "SciPy 1.0: Fundamental Algorithms for Scientific Computing in Python." *Nature Methods* 17 (3): 261–72.
- Walford, R. L. 1982. "Studies in Immunogerontology." *Journal of the American Geriatrics Society* 30 (10): 617–25.
- Walter, M. A., W. T. Gibson, G. C. Ebers, and D. W. Cox. 1991. "Susceptibility to Multiple

- Sclerosis Is Associated with the Proximal Immunoglobulin Heavy Chain Variable Region." *The Journal of Clinical Investigation* 87 (4): 1266–73.
- Wang, Chen, Yi Liu, Lan T. Xu, Katherine J. L. Jackson, Krishna M. Roskin, Tho D. Pham, Jonathan Laserson, et al. 2014. "Effects of Aging, Cytomegalovirus Infection, and EBV Infection on Human B Cell Repertoires." *The Journal of Immunology*. <https://doi.org/10.4049/jimmunol.1301384>.
- Wang, Qiong, George M. Garrity, James M. Tiedje, and James R. Cole. 2007. "Naive Bayesian Classifier for Rapid Assignment of rRNA Sequences into the New Bacterial Taxonomy." *Applied and Environmental Microbiology* 73 (16): 5261–67.
- Wang, Yi, Ulrike Naumann, Stephen T. Wright, and David I. Warton. 2012. "Mvabund - an R Package for Model-Based Analysis of Multivariate Abundance Data." *Methods in Ecology and Evolution*. <https://doi.org/10.1111/j.2041-210x.2012.00190.x>.
- Wardemann, Hedda, Sergey Yurasov, Anne Schaefer, James W. Young, Eric Meffre, and Michel C. Nussenzweig. 2003. "Predominant Autoantibody Production by Early Human B Cell Precursors." *Science*. <https://doi.org/10.1126/science.1086907>.
- Waters, Jillian L., and Ruth E. Ley. 2019. "The Human Gut Bacteria Christensenellaceae Are Widespread, Heritable, and Associated with Health." *BMC Biology* 17 (1): 83.
- Wei, Min, Reiko Shinkura, Yasuko Doi, Mikako Maruya, Sidonia Fagarasan, and Tasuku Honjo. 2011. "Mice Carrying a Knock-in Mutation of Aicda Resulting in a Defect in Somatic Hypermutation Have Impaired Gut Homeostasis and Compromised Mucosal Defense." *Nature Immunology*. <https://doi.org/10.1038/ni.1991>.
- Weindruch, Richard, Roy L. Walford, Suzanne Fligiel, and Donald Guthrie. 1986. "The Retardation of Aging in Mice by Dietary Restriction: Longevity, Cancer, Immunity and Lifetime Energy Intake." *The Journal of Nutrition*. <https://doi.org/10.1093/jn/116.4.641>.
- Weiskopf, Daniela, Birgit Weinberger, and Beatrix Grubeck-Loebenstein. 2009. "The Aging of the Immune System." *Transplant International: Official Journal of the European Society for Organ Transplantation* 22 (11): 1041–50.
- Weksler, M. E., and P. Szabo. 2000. "The Effect of Age on the B-Cell Repertoire." *Journal of Clinical Immunology* 20 (4): 240–49.
- White, Matthew J., Charlotte M. Beaver, Martin R. Goodier, Christian Bottomley, Carolyn M. Nielsen, Asia-Sophia F. M. Wolf, Luisa Boldrin, et al. 2016. "Calorie Restriction Attenuates Terminal Differentiation of Immune Cells." *Frontiers in Immunology* 7: 667.
- Wick, G., P. Jansen-Dürr, P. Berger, I. Blasko, and B. Grubeck-Loebenstein. 2000. "Diseases of Aging." *Vaccine* 18 (16): 1567–83.
- Wilmanski, Tomasz, Christian Diener, Noa Rappaport, Sushmita Patwardhan, Jack Wiedrick, Jodi Lapidus, John C. Earls, et al. 2021a. "Gut Microbiome Pattern Reflects Healthy Ageing and Predicts Survival in Humans." *Nature Metabolism* 3 (2): 274–86.
- Wood, Derrick E., Jennifer Lu, and Ben Langmead. 2019. "Improved Metagenomic Analysis with Kraken 2." *Genome Biology* 20 (1): 257.
- Wu, Yu-Chang, David Kipling, Hui Sun Leong, Victoria Martin, Alexander A. Ademokun, and Deborah K. Dunn-Walters. 2010. "High-Throughput Immunoglobulin Repertoire Analysis Distinguishes between Human IgM Memory and Switched Memory B-Cell Populations." *Blood* 116 (7): 1070–78.
- Xu, Jinyu, Jeffrey D. Galley, Michael T. Bailey, Jennifer M. Thomas-Ahner, Steven K. Clinton, and Susan E. Olivo-Marston. 2016. "The Impact of Dietary Energy Intake Early in Life on the Colonic Microbiota of Adult Mice." *Scientific Reports* 6 (January): 19083.
- Xu, Zhenming, Hong Zan, Egest J. Pone, Thach Mai, and Paolo Casali. 2012. "Immunoglobulin Class-Switch DNA Recombination: Induction, Targeting and beyond." *Nature Reviews. Immunology* 12 (7): 517–31.
- Ye, Jian, Ning Ma, Thomas L. Madden, and James M. Ostell. 2013. "IgBLAST: An Immunoglobulin Variable Domain Sequence Analysis Tool." *Nucleic Acids Research* 41: W34–40.
- Yilmaz, Ömer H., Pekka Katajisto, Dudley W. Lamming, Yetis Gültekin, Christian E. Bauer-Rowe, Shomit Sengupta, Kivanc Birsoy, et al. 2012. "mTORC1 in the Paneth Cell Niche Couples Intestinal Stem-Cell Function to Calorie Intake." *Nature* 486 (7404): 490–95.

- Zapata, Heidi J., and Vincent J. Quagliarello. 2015. "The Microbiota and Microbiome in Aging: Potential Implications in Health and Age-Related Diseases." *Journal of the American Geriatrics Society* 63 (4): 776–81.
- Zeng, Ting, Hui Cui, Duo Zhuang Tang, George B. Garside, Yiting Wang, Jianying Wu, Zhendong Tao, Liu Zhang, and Si Tao. 2019. "Short-Term Dietary Restriction in Old Mice Rejuvenates the Aging-Induced Structural Imbalance of Gut Microbiota." *Biogerontology* 20 (6): 837–48.
- Zhang, Chenhong, Shoufeng Li, Liu Yang, Ping Huang, Wenjun Li, Shengyue Wang, Guoping Zhao, et al. 2013. "Structural Modulation of Gut Microbiota in Life-Long Calorie-Restricted Mice." *Nature Communications* 4: 2163.
- Zhang, Yawen, Luyi Chen, Mengjia Hu, John J. Kim, Renbin Lin, Jilei Xu, Lina Fan, et al. 2020. "Dietary Type 2 Resistant Starch Improves Systemic Inflammation and Intestinal Permeability by Modulating Microbiota and Metabolites in Aged Mice on High-Fat Diet." *Aging* 12 (10): 9173–87.
- Zhao, Qing, and Charles O. Elson. 2018. "Adaptive Immune Education by Gut Microbiota Antigens." *Immunology* 154 (1): 28–37.
- Zhou, Julian Q., and Steven H. Kleinstein. 2019. "Cutting Edge: Ig H Chains Are Sufficient to Determine Most B Cell Clonal Relationships." *The Journal of Immunology*. <https://doi.org/10.4049/jimmunol.1900666>.
- Zhou, Y., P. Rychahou, Q. Wang, H. L. Weiss, and B. M. Evers. 2015. "TSC2/mTORC1 Signaling Controls Paneth and Goblet Cell Differentiation in the Intestinal Epithelium." *Cell Death & Disease* 6 (February): e1631.
- Zou, Hui, and Trevor Hastie. 2005. "Regularization and Variable Selection via the Elastic Net." *Journal of the Royal Statistical Society: Series B (Statistical Methodology)*. <https://doi.org/10.1111/j.1467-9868.2005.00503.x>.

Erklärung zur Dissertation
gemäß der Promotionsordnung vom 12. März 2020

***Diese Erklärung muss in der Dissertation enthalten sein.
(This version must be included in the doctoral thesis)***

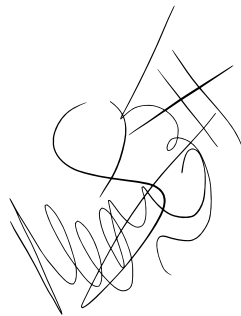
„Hiermit versichere ich an Eides statt, dass ich die vorliegende Dissertation selbstständig und ohne die Benutzung anderer als der angegebenen Hilfsmittel und Literatur angefertigt habe. Alle Stellen, die wörtlich oder sinngemäß aus veröffentlichten und nicht veröffentlichten Werken dem Wortlaut oder dem Sinn nach entnommen wurden, sind als solche kenntlich gemacht. Ich versichere an Eides statt, dass diese Dissertation noch keiner anderen Fakultät oder Universität zur Prüfung vorgelegen hat; dass sie - abgesehen von unten angegebenen Teilpublikationen und eingebundenen Artikeln und Manuskripten - noch nicht veröffentlicht worden ist sowie, dass ich eine Veröffentlichung der Dissertation vor Abschluss der Promotion nicht ohne Genehmigung des Promotionsausschusses vornehmen werde. Die Bestimmungen dieser Ordnung sind mir bekannt. Darüber hinaus erkläre ich hiermit, dass ich die Ordnung zur Sicherung guter wissenschaftlicher Praxis und zum Umgang mit wissenschaftlichem Fehlverhalten der Universität zu Köln gelesen und sie bei der Durchführung der Dissertation zugrundeliegenden Arbeiten und der schriftlich verfassten Dissertation beachtet habe und verpflichte mich hiermit, die dort genannten Vorgaben bei allen wissenschaftlichen Tätigkeiten zu beachten und umzusetzen. Ich versichere, dass die eingereichte elektronische Fassung der eingereichten Druckfassung vollständig entspricht.“

Teilpublikationen:

Monzó C, Gkioni L, Beyer A, Valenzano DR, Grönke S, Partridge L. Dietary restriction mitigates the age-associated decline in mouse B cell receptor repertoire diversity. 2023. Cell Reports. Accepted

Datum, Name und Unterschrift

21 August 2022, Cologne



Erklärung zum Gesuch um Zulassung zur Promotion
gemäß der Promotionsordnung vom 12. März 2020

1. Zugänglichkeit von Daten und Materialien

Die Dissertation beinhaltet die Gewinnung von Primärdaten oder die Analyse solcher Daten oder die Reproduzierbarkeit der in der Dissertation dargestellten Ergebnisse setzt die Verfügbarkeit von Datenanalysen, Versuchsprotokollen oder Probenmaterial voraus.

- Trifft nicht zu
- Trifft zu.

In der Dissertation ist dargelegt wie diese Daten und Materialien gesichert und zugänglich sind (entsprechend den Vorgaben des Fachgebiets beziehungsweise der Betreuerin oder des Betreuers).

2. Frühere Promotionsverfahren

Ich habe bereits einen Dokortitel erworben oder ehrenhalber verliehen bekommen.
Oder: Für mich ist an einer anderen Fakultät oder Universität ein Promotionsverfahren eröffnet worden, aber noch nicht abgeschlossen.
Oder: Ich bin in einem Promotionsverfahren gescheitert.

- Trifft nicht zu
- Zutreffend
Erläuterung:

3. Straftat

Ich bin nicht zu einer vorsätzlichen Straftat verurteilt worden, bei deren Vorbereitung oder Begehung der Status einer Doktorandin oder eines Doktoranden missbraucht wurde.

Ich versichere, alle Angaben wahrheitsgemäß gemacht zu haben.

Datum

21 August 2022

Name

Carolina Monzó Cataluña

Unterschrift

